Technische Universität München
Lehrstuhl für Phytopathologie

Investigation on barley ROP INTERACTIVE PARTNER proteins and their function in barley disease susceptibility

Christopher McCollum

Vollständiger Abdruck der von der TUM School of Life Sciences der Technischen Universität München zur Erlangung des akademischen Grades eines

Doktors der Naturwissenschaften (Dr. rer. nat.)

genehmigten Dissertation

Vorsitzender:	Prof. Dr. Kay H. Schneitz
Prüfer der Dissertation:	1. Prof. Dr. Ralph Hückelhoven
	2. Prof. Dr. Jörg Durner

Die Dissertation wurde am 12.04.2021 bei der Technischen Universität München eingereicht und durch die TUM School of Life Sciences am 02.07.2021 angenommen.

Contents

3-AT	3-amino-1,2,4-triazole
ABA	Abscisic acid
ADP	Adenosine diphosphate
app	Appressorium
At	*Arabidopsis thaliana*
Avr	Avirulence factor
Bd	*Brachypodium distachyon*
Bgh	*Blumeria graminis* f.sp. *hordei*
Bgt	*Blumeria graminis* f.sp. *tritici*
c	Conidium
Ca^{2+}	Calcium ion
cc	coiled-coil
cDNA	complementary DNA
CDS	Coding sequence
CH_3COOK^+	Potassium carbonate
cPCR	colony PCR
cIRF	calculated Instrumental Response Function
CLSM	Confocal Laser Scanning Microscopy
CRISPR	Clustered Regularly Interspaced Short Palindromic Repeats
CSEP	Candidates for secreted effector proteins
Ctr	Control
DAMP	Damage-associated molecular pattern
ddH_2O	double-distilled H_2O
DEPC	Diethyl pyrocarbonate
DHR2	DOCK homology region 2
DNA	Deoxyribonucleic acid
dNTP	Deoxy nucleoside triphosphate
DTT	Dithiothreitol
EB	Extraction buffer
E. coli	*Escherichia coli*
EDTA	Ethylenediaminetetraacetic acid
EHM	Extrahaustorial membrane
ER	Endoplasmatic reticulum
ET	Ethylen
EtOH	Ethanol
ETS	Effector triggered susceptibility
EV	Empty vector
flg22	Flagellin epitope 22
FLIM	Förster Resonance Energy Transfer
f.sp.	forma specialis
G3P	Glycerol 3-phosphate
GEF	Guanosine nucleotide exchange factor
Gb	Giga base pairs
GDI	Guanin dissociation inhibitor
GDP	Guanosine diphosphate

GPCR	G-protein coupled receptor
GTP	Guanosine triphosphate
GTPase	Guanosine triphosphatase
hab	Hours after bombardment
hai	Hours after infection
HCl	Hydrochloric acid
HR	Hypersensitive response
HRP	Horseradish peroxidase
Hv	*Hordeum vulgare*
IP	Immunoprecipitation
JA	Jasmonic acid
LB Agar	Lysogeny broth Agar
LRR	Leucine-rich repeat
LysM	Lysin motif
MAMP	Microbe-associated molecular pattern
MAP	Microtubule-associated protein
Mb	Mega base pairs
MES	2-(*N*-morpholino)-ethanesulfonic acid
MeSA	methyl salicylate
$MgCl_2$	Magnesium chloride
MMT	Million Metric Tons
mRNA	messenger RNA
NaCl	Sodium chloride
NADPH	Nicotinamid adenine dinucleotide phosphate
NaOH	Sodium hydroxide
$(NH_4)_2SO_4$	Diamonium sulfate
NHR	Non-host resistance
NLR	Nucleotide binding leucin-rich repeat receptor
Osj	*Oryza sativa* spp. *japonica*
PAGE	Polyacrylamide gel electrophoresis
PBS	Phosphate-buffered saline
PCR	Polymerase Chain Reaction
PEG	Polyethylene glucol
ph	primary germ tube
Pip	pipenolic acid
PRK	Pollen receptor kinase
PRONE	Plant-specific Rop Nucleotide Exchanger
PRR	Pattern Recognition Receptor
PtdIns(3,5)P_2	Phosphatydilinositol-3,5-bisphosphate
PtdIns(4,5)P_2	Phosphatydilinositol-4,5-bisphosphate
PTI	Pattern triggered immunity
QDO	Quadruple drop-out
RLCK	Receptor-like cytoplasmic kinase
RLP	Receptor-like protein
RNA	Ribonucleic acid
RNAi	RNA interference

ROI	Region of interest
ROS	Reactive oxygen species
SA	Salicylic acid
SAR	Systemic acquired resistance
SD medium	Synthetic drop-out medium
SDS	Sodium dodecyl sulfate
SMC	Subsidiary mother cell
TAE	Tris, Acetic acid, EDTA
TEMED	*N, N, N', N'*-tetraethylmethylenediamine
Tris	Tris(hydroxymethyl) aminomethane
UN	United Nations
USD	US Dollar
USDA	United States Depatment of Agriculture
UV	Ultra violet
WT	Wild-type
Y2H	Yeast-two-hybrid
YPDA	Yeast peptone dextrose adenine

1 Introduction

1.1 Barley, one of the most cultivated cereals

Barley (*Hordeum vulgare*) is one of the major crop plants cultivated in agriculture. *H. vulgare* is an annual grass (Poaceae), which is cultivated in temperate climate around the world. Archaeological studies indicate that barley was already domesticated about 10 000 years ago in the Israel/Jordan area, which was also confirmed by genetic marker studies (Badr et al., 2000). Foraging of barley and other grain plants by hunter and gatherer societies however, seems to go back at least 23 000 years as supported by archaeological studies from the Ohalo II site in Israel (Weiss et al., 2004). In 2018, the global barley production was about 139 million metric tons (MMT) with about 56 MMT of that coming from the European Union. It is the fifth most produced crop world wide behind corn (1123 MMT), wheat (731 MMT), rice (497 MMT), and soybean (360 MMT) (USDA, Foreign Agricultural Service, 2020). About 70% of barley grain is used as animal feed and about 30% is used for malting purposes for example in beer and whiskey, but also used in other foods (UN, Food and Agriculture Organization, 2004).

Barley has been adapted as a model organism for cereal crop plants, since it is a major crop plant, which allows applicability of research in the field and it has a comparatively easy genome structure compared to the economically important wheat, which has a hexaploid genome making genetic research very difficult. The barley genome was sequenced in 2012 and reassembled several times since then (International Barley Genome Sequencing, 2012; Mascher et al., 2017). Barley has at least 25 000 genes in 5Gb of DNA on seven chromosomes. However, due to the low accessibility of monocots by *Agrobacterium tumefaciens* and the long generation time of barley, stable genetic transformation of barley has proven to be very difficult and time-consuming. Just in recent years, especially with the emergence of CRISPR/CAS9, significant progress has been made, but so far the easiest method for gene studies is transient biolistic transformation of single cells with a gene gun (Hiei et al., 2014).

1.2 Plants and their pathogens

Like other organisms, plants are constantly challenged by various microbial pathogens. Diseases can be caused by bacteria, viruses, fungi, or oomycetes. Pathogens take nutrients from host plants causing death of the host or reduced vegetative growth and fruit development. This makes them economically relevant for humans since pathogens can cause major yield losses in crops and other agriculturally important plants. Savary

et al. (2019) estimate an average global annual yield loss between the years 2010 and 2014 on the five major crops, wheat, maize, rice, soybean, and potato of around 21.5%, 22.6%, 30%, 24.4%, and 17.2%, respectively. This was caused by around 137 different pathogens. Crop cultivation on big fields, though required to secure food production for an ever-growing global population, makes it easy for pathogens to spread in vast areas. This is reflected in the market for crop protection, which had a volume of around USD 55 billion in 2019 (Fortune Business Insights, Agriculture Market Research Report, 2020). One of the most well known famines caused by plant pathogens was the Irish potato famine in the mid 19th century. The cause for this famine was the spread of potato late blight during this time in Europe caused by *Phytophthora infestans*, a hemi-biotrophic oomycete. It resulted in the death of millions of people and the emigration of many more, especially in Ireland. Even today, though not causing starvation in Europe anymore, potato late blight still comes with big economic costs due to pest control and yield losses (Haverkort et al., 2008).

Biologically, pathogens are distinguished by their life style, which can be divided into either biotrophic, necrotrophic, or hemi-biotrophic. Necrotrophs actively kill the host during the infection and feed on the content of dead cells. Biotrophs rely on a living host to complete their life cycle and often develop specialized feeding cells, like haustoria. Hemi-biotrophic pathogens start the infection with a biotrophic phase and shift into a necrotrophic phase in later stages of infection. Both, necrotrophy and biotrophy have advantages and disadvantages for pathogens. While biotrophs are closely adapted and very host specific and are therefore restricted, they can feed for a longer period of time from a host. Necrotrophs on the other hand have a rather broad host range, which allows them to be less restricted in their colonization process (Oliver and Ipcho, 2004).

Many pathogens enter the plant through openings, like wounds or stomata, but some pathogens can also penetrate the host cell wall. The bacterium *Pseudomonas syringae* for example, enters the plant through stomata or wounds and colonizes the apoplast (Katagiri et al., 2002). *Colletotrichum sp.*, hemi-biotrophic fungi and causal agents of anthracnose on many plants, penetrate the epidermal cell wall and grow hyphae through host cells (Mendgen and Hahn, 2002).

1.3 The barley powdery mildew fungus

Powdery mildew is a common disease found on thousands of wild plants, but also on different economically important plants. As the name implies, powdery mildew can be identified as a white powder-like cover on plants, especially on leaves (Fig. 1A). Like

many diseases, powdery mildew can also affect crop plants. Studies from greenhouse experiments report up to 25% yield loss from powdery mildew on wheat, but up to 60% yield loss have been reported in the field (Costamilan, 2005; Draz et al., 2019). The causal agent of powdery mildew diseases are biotrophic fungi of the Erysiphales order. For example, *Erysiphe cruciferarum* causes powdery mildew on cabbage and the model plant *Arabidopsis thaliana*, *Erysiphe pisi* on pea, and *Blumeria graminis* on cereals and other grasses. Biotrophic powdery mildew fungi are highly specified to a host, which results in the divergence into different formae speciales (f.sp.). For example *Blumeria graminis* f.sp. *tritici* (*Bgt*) is host specific for wheat (*Triticum aestivum*) but it can not grow on other cereals. *Blumeria graminis* f.sp. *hordei* (*Bgh*) on the other hand is the causal agent of the powdery mildew disease on barley, but it can not infect wheat (Fig. 1A). This specificity likely results in, but is also reinforced by, the strongly reduced genome of powdery mildew fungi, containing a relatively small number of genes. Powdery mildew fungi studied so far seem to have a strongly reduced number of genes with an approximate haploid genome size of about 140Mb but only 6000 genes (Genome of *Bgh*), compared to for example the approximately 5Gb and 25000 genes of barley, or the genome of *Ramularia collo-cygni*, a different barley pathogen with about 11000 genes. Although, the overall genome of the latter is smaller with 32Mb due to fewer repetitive sequences and transposable elements (International Barley Genome Sequencing, 2012; Stam et al., 2018). Many of the missing genes encode enzymes of the primary and secondary metabolism, probably stemming from the biotrophic lifestyle where the host provides most metabolites (Spanu et al., 2010; Wicker et al., 2013). However, the genome of *Blumeria graminis* encodes for a large number of potential effectors, or candidates for secreted effector proteins (CSEP). Effectors, or virulence factors, are secreted proteins, which help the pathogen to manipulate the host (further details on this topic will follow below). *Bgh* has about 500 of these candidates, while in comparison, the phytopathogenic bacterium *Pseudomonas syringae* has about 50, and the rice blast fungus *Magnaporthe oryzae* has about 58 estimated effector candidate genes (Schechter et al., 2006; Mosquera et al., 2009; Pedersen et al., 2012). Though it is not known how many of these candidates actually encode for active effectors, the assumption is that the biotrophic life style of *Bgh* and other powdery mildew fungi requires a high number of effectors in order to control various aspects of the host.

The asexual life cycle of *Bgh* is most relevant for pathogenesis. In the beginning a single haploid spore, the conidium, lands on the plants surface, usually a leaf. Experiments showed that within 60 seconds extracellular material is secreted making the conidium stick to the surface (Carver et al., 1999; Wright et al., 2002). LIPASE1

was shown to be one of the secreted materials by *Bgt*, degrading the host cuticle and releasing long-chain aldehydes (Feng et al., 2009). These long-chain aldehydes are then detected by the fungus, leading to promotion of conidial germination. Especially n-hexacosanal seems to be an important signaling component in this process as shown for *Bgt* and *Bgh* (Zabka et al., 2008; Hansjakob et al., 2010). As a first step in germination, a primary germ tube develops towards the plant surface (Fig. 1B). It penetrates the cuticle but not the cell wall and is assumed to examine the surface (Carver et al., 1999; Edwards, 2002). Thereafter, the appressorial germ tube grows out and differentiates into a hook-like appressorium at its end. From the appressorium the penetration peg penetrates the plant cell wall and establishes the haustorium, about 24 hours after inoculation. The haustorium is the primary site of contact between host and parasite and is utilized for nutrient uptake and the release of virulence factors (O'Connell and Panstruga, 2006; Catanzariti et al., 2007). During this process the host plasma membrane stays intact and hence the host cell stays alive. The host plasma membrane envelopes the haustorium and becomes the extrahaustorial membrane (EHM), which is chemically different from the original plasma membrane. After successful penetration, secondary hyphae grow from the appressorial germ tube on the plant surface. Secondary appressoria and haustoria can be formed from these hyphae. About 7 days after inoculation conidiophores are generated from secondary hyphae and haploid conidia are dispersed by wind.

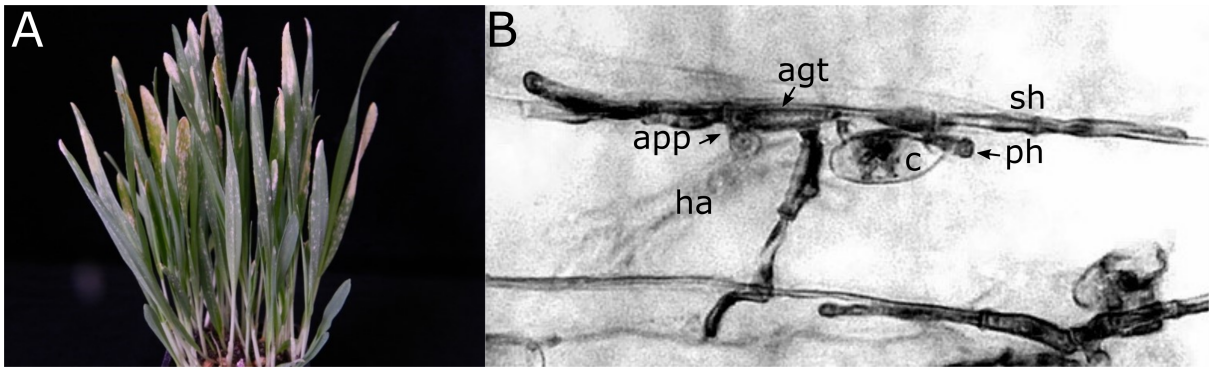

Figure 1: The barley powdery mildew fungus. *Bgh* grows as a powder-like cover on the plants surface (A). In the beginning of the infection a conidia (c) lands on the plant (B). It first establishes a primary germ tube (ph) to make contact with the surface. After that, a appressorial germ tube (agt) with the appressorium (app) develops. The appressorium penetrates an epidermal cell and establishes the haustorium (ha, out of focus) as the main feeding cell. When the haustorium is established, secondary hyphae (sh) are grown from the appressorial germ tube to colonize the plant surface. From secondary hyphae, secondary haustoria can be formed.

1.4 The plant immune system

Unlike animals, plants do not have an adaptive immune system, which means plants solely rely their genetic predispositions for defense against pathogens. All plants have pre-formed defense components, which consist of the cell wall and the cuticle, but also trichomes. Some plants also constitutively produce toxins, so called phytoanticipins. An example are the gluconsinolates of the Brassicaceae, which are constantly synthesized in the plant. Tissue disruption, for example by insect bites, leads to the hydrolyzation of glucosinolates and their biological activation (Mithen, 2001). Early induced defense reactions in plants involve Ca^{2+} influx into the attacked cell, production of reactive oxygen species (ROS), callose depositions for papilla formation, and activation of the mitogen activated protein kinase (MAPK) signaling cascade, which, among other things, results in defense gene expression (Aist, 1976; Bigeard et al., 2015). Later in the interaction, especially if the plant was not immediately successful in fending off the pathogen, a hypersensitive response (HR) in form of programmed cell death can be observed as necrotic lesions on resistant plants. This reaction is supposed to deprive the pathogen of nutrients and prevent further spread. A special part of the defense reaction is phytohormone mediated systemic acquired resistance (SAR), which is supposed to activate priming in distant parts of the plant that have not yet encountered the pathogen. This leads to a faster defense reaction in case of a secondary infection. SAR is dependent on phytohormones like salicylic acid (SA), jasmonic acid (JA), and ethylene (ET) and is mediated by signaling components like methyl salicylate (MeSA), pipecolic acid (Pip) , or glycerol 3-phosphate (G3P) (Singh et al., 2017; Klessig et al., 2018). Whether a population of plants is susceptible to a certain pathogen is dependent on the genetic variety already present in that population. Most plants are resistant to most pathogens. When a plant species is resistant to a specific pathogen it is called non-host resistance (NHR) (Lee et al., 2017). However, a species of plants can contain susceptible subpopulations to a certain pathogen, while others are resistant. Also, a pathogen population can contain virulent strains for a specific plant species, while other strains are not able to infect. Susceptible interactions are considered compatible, while resistant interactions are considered incompatible. This is dependent on the plants ability to recognize the pathogen and block its efforts, but also on the pathogens ability to circumvent defense responses (Nomura et al., 2005).

Two major mechanisms for plants to detect pathogens can be distinguished (Dodds and Rathjen, 2010). The first one is based on surface receptors, so called Pattern Recognition Receptors (PRR), and leads to pattern triggered immunity (PTI). PRRs are part of complexes sitting in the plasma membrane of plant cells and recognize ei-

ther microbe-associated molecular patterns (MAMP) or damage-associated molecular patterns (DAMP). MAMPs are conserved microbe derived structural elements, which are usually essential for the pathogen, while DAMPs are host derived and caused by pathogen induced damage. PRRs can sense these patterns and thereby recognize microbes and potential pathogens nearby. Examples for MAMPs are the conserved amino acid epitope flg22 from flagellin, elf18 from the bacterial elongation factor Tu (EF-Tu), 3-hydroxy fatty acid from bacteria, and chitin oligomers from fungi (Yamada et al., 1993; Felix et al., 1999; Kunze et al., 2004; Kutschera et al., 2019).

PRRs are ligand specific and usually interact with a co-receptor. For example, in *Arabidopsis thaliana* the receptor-like kinase (RLK) FLAGELLIN SENSITIVE 2 (FLS2) binds flg22 through a leucin-rich repeat (LRR) domain (Gómez-Gómez and Boller, 2000). This leads to complex formation with the LRR co-receptor BRASSINOSTEROID INSENSITIVE 1 (BRI1)-ASSOCIATED RECEPTOR KINASE 1 (BAK1) and phosphorylation of both LRR-RLKs. The receptor-like cytoplasmic kinase (RLCK) BOTRYTIS-INDUCED KINASE 1 (BIK1) associates with FLS2 and BAK1. BIK1 gets phosphorylated by BAK1, but subsequently also phosphorylates FLS2 and BAK1 (Chinchilla et al., 2007; Lu et al., 2010; Sun et al., 2013). Activated BIK1 then interacts with and phosphorylates the NADPH oxidase RESPIRATORY BURST OXIDASE HOMOLOG PROTEIN D (RBOHD), which leads to an increase in ROS production. Increase of ROS supports Ca^{2+} influx through an unknown mechanism, which contributes to defense signaling. Ca^{2+} influx also causes a further increase of ROS production by Ca^{2+} binding to calcium dependent protein kinases (CDPK), which then phosphorylate RBOHD generating a positive feedback loop. In a parallel signaling pathway, complex formation of FLS2 and BAK1 induces MAP kinase cascade activation, which ends in activation of WRKY transcription factors and defense gene expression (Asai et al., 2002). For example, MAPK4 is in complex with WRKY33 and MKS1 (MAP KINASE SUBSTRATE 1) under unelicited circumstances. However, if plants are treated with flagellin, MAPK4 gets phosphorylated, which leads to the dissociation of WKRY33 and MKS1. WRKY33 then binds the promotor of *PHYTOALEXIN DEFICIENT 3* (*PAD3*) and induces its expression. PAD3 is involved in the synthesis of the phytoalexin camalexin and WRKY33 mutants have reduced camalexin levels (Qiu et al., 2008).

Chitin, as the most studied fungal elicitor to date, is recognized as *N*-acetylchitooligosaccharide hepta- or octamers (Ito et al., 1997). The receptor was first identified in rice as CHITIN OLIGOSACCHARIDE ELICITOR-BINDING PROTEIN (CEBiP), a receptor-like protein (RLP) without an active kinase domain. CEBiP interacts with its co-receptor CHITIN ELICITOR RECEPTOR KINASE 1 (CERK1) (Kaku et al., 2006; Shimizu et al., 2010). In contrast to the LRR-RLK FLS2, both CEBiP and CERK1

contain lysin motif (LysM) domains. In Arabidopsis, the equivalents are LYSIN MOTIF RECEPTOR KINASE 5 (LYK5) and Arabidopsis CERK1 (Miya et al., 2007; Cao et al., 2014). While CEBiP and LYK5 are the primary chitin binding receptors, CERK1 in both rice and Arabidopsis is required for signal transduction through its respective kinase domain. In Arabidopsis, LYK5 is present as a homodimer in its inactive state. Binding of chitin leads to interaction with CERK1, which triggers the homodimerization of CERK1 and its subsequent phosphorylation. The active signaling complex seems to be a heterotetramer of two LYK5 and two CERK1 proteins (Shimizu et al., 2010; Petutschnig et al., 2010; Liu et al., 2012; Cao et al., 2014). CERK1 can then phosphorylate the RLCK PROBABLE SERINE/THREONINE-PROTEIN KINASE-LIKE 1 (PBL1)-LIKE PROTEIN 27 (PBL27), which in turn phosphorylates MAPKKK5 in the only direct connection between PRRs and MAPK signaling described to date (Shinya et al., 2014; Yamada et al., 2016).

Pathogens can overcome PTI by translocating effector proteins into the host cell. These effectors suppress defense reactions or reprogram the host cell in favor of the pathogen. This is called effector triggered susceptibility (ETS). However, the host can deploy so called R proteins, which is the second major mechanism for pathogen detection by plants. R-proteins either recognize effectors directly, or recognize disturbances of effector targets. Most R-proteins are nucleotide-binding (NB) LRR receptors (NLRs). New research indicates that at least some NLRs assemble in a pentameric ring-like formation upon target recognition, termed resistosome. This was shown for the ZAR1-RKS1-PBL2 complex (Wang et al., 2019) of Arabidopsis, consisting of the NLR HOPZ-ACTIVATED RESISTANCE 1 (ZAR1), and the pseudokinases RESISTANCE RELATED KINASE 1 (RKS1) and PBL1-LIKE PROTEIN 2 (PBL2). In this case the pathogen is not directly, but indirectly detected by the plant. PBL2 is a pseudokinase and acts as a decoy for the *Xanthomonas campestris* effector AvrAC. AvrAC uridylylates members of the VII subfamily of RLCKs, one of which is BIK1 and another one is PBL2. Without PBL2 and ZAR1, introduction of AvrAC would lead to uridylylation of BIK1, which would result in inhibition of immune signaling by inhibiting the kinase activity of BIK1 (Feng et al., 2012). In PBL2 acting as a decoy, it is targeted by AvrAC and gets uridylylated instead of BIK1 (Wang et al., 2015). Uridylylated PBL2 then gets recognized by a preformed complex dimer of ZAR1-RKS1, although only RKS1 interacts with PBL2, resulting in resistosome formation. The resistosome then is thought to get integrated in the plasma membrane where it triggers cell death as part of effector triggered immunity (ETI) (Wang et al., 2019). Interestingly, ZAR1 was originally identified in a reverse genetic screen for Arabidopsis mutants lacking induced immunity by the *Pseudomonas syringiae* effector HopZ1a (Lewis et al., 2010).

HopZ1a is an acetyltransferase that targets tubulin and microtubules, thereby influencing secretion and cell wall-mediated defense (Lee et al., 2012). HopZ1a activates ZAR1-mediated immunity in combination with a different pseudokinase, HopZ-ETI-DEFICIENT 1 (ZED1), which is also targeted by HopZ1a for acetylation, showing how one NLR is able to recognize different effectors (Lewis et al., 2013).

Another example are the *P. syringae* effector AvrRps4 and the *Ralstonia solanacearum* effector PopP2, both of which are recognized by the Arabidopsis toll interleukin 1 receptor (TIR)-NB-LRRs RPS4 (resistance to *Pseudomonas syringae* 4) and RRS1 (resistance to *Ralstonia solanacearum* 1) (Gassmann et al., 1999; Deslandes et al., 2003). RPS4 and RRS1 need to interact with each other via their TIR domain for a functional effector recognition complex. Both AvrRps4 and PopP2 are recognized only by RRS1, but the TIR domain of RPS4 initiates the effector-dependent immune response (Williams et al., 2014; Sarris et al., 2015). Interestingly, RRS1 contains a WRKY sequence and both AvrRps4 and PopP2 interact with this WRKY domain and other defense related WRKY transcription factors. PopP2 additionally has acetyltransferase activity, acetylating lysines and a threonine in the WRKY domain (Tasset et al., 2010). This acetylation was shown to inhibit DNA binding affinity of WRKY domains and it is assumed that RRS1 acts as a decoy for WRKY targeting effectors (Sarris et al., 2015). Interestingly, there are two allels of RRS1 in Arabidopsis. The longer RRS1-R allele in the accessions Nd-1 and Ws-2, and the shorter RRS1-S allele found in Col-0. Both are able to recognize AvrRps4 and get acetylated by PopP2, but only RRS1-R triggers defense response upon PopP2 recognition (Sarris et al., 2015). In order to fulfill its function in defense signaling, the C-terminus and the N-terminal TIR domain of RRS1 need to interact, which frees the TIR domain of RPS4, leading to defense signaling (Williams et al., 2014). In the RRS1 - AvrRps4 interaction, the effector connects the C-terminus and the TIR domain of RRS1 leading to circle generation. In the interaction with PopP2, upon acetylation of the WRKY domain, subsequent phosphorylation of the longer C-terminus of RRS1-R also leads to circle generation, which is not possible in the shorter RRS1-S protein (Guo et al., 2020). Both, RRS1-R and RRS1-S possess DNA binding ability, but it is not clear whether this is also important for their function, or if it is just a side effect from having the WRKY motif. It could be that RRS1 was originally a decoy for the *P. syringae* effector AvrRps4 and possibly a similar effector of Ralstonia, which were supposed to target WRKY transcription factors and interfere with plant defense. Ralstonia then countered with the deployment of PopP2, which acetylated RRS1 to prevent AvrRps4 interaction and possibly the DNA-binding ability. It might be that acetylation of RRS1-S was the original target of PopP2, but through evolution the longer RRS1-R allele appeared in Arabidopsis, now allowing

for the RRS1 - PopP2 interaction to cause defense reactions again. This is speculation and so far no PopP2-like effector has been described in *P. syringae*, and no AvrRps4-like effector has been described in Ralstonia, but it would be a nice example for co-evolution of host and pathogen.

1.5 Susceptibility genes

While one part of pathogen invasion is suppression of host defense by effectors, another layer is the exploitation of native host genes for their own means. These genes are referred to as susceptibility (S) genes or S-factors. In general, these genes fulfill an important role in plant development or provide a different fitness advantage, which prevents the factor from being sorted out by natural selection. Most known S-factors are negative regulators of defense in one way or another, but not all (van Schie and Takken, 2014). One of the most prominent S-factors is the barley gene *MILDEW LOCUS O* (*MLO*). *MLO* is required for penetration success of powdery mildew fungi in barley and a loss of *MLO* leads to broad spectrum durable resistance to almost all powdery mildew fungi (Jørgensen and Mortensen, 1977). *mlo* plants were first discovered by an expedition to Ethiopia in the 1930s and grown on the field in Europe since the 1980s (Jørgensen, 1992), but only in 1997 MLO was identified as a plasma membrane localized protein (Buschges et al., 1997). However, the exact biochemical function of MLO remains elusive. *mlo* mutants form bigger papillae with more H_2O_2 and show spontaneous papilla formation unrelated to defense, suggesting a stronger defense response in *mlo* plants (Stolzenburg et al., 1984; Hückelhoven et al., 2000; Piffanelli et al., 2002). This would make MLO a negative regulator of defense, although this remains questionable since experiments with double mutants of mlo and stress hormone mutants in Arabidopsis did not show spontaneous papilla formation, but remained resistant (Consonni et al., 2006).

Another S-factor is *ENHANCED DISEASE RESISTANCE 1* (*EDR1*), which codes for a MAPKKK that confers susceptibility of *A. thaliana* towards *Erysiphe chicoracearum* (Frye and Innes, 1998; Frye et al., 2001). EDR1 negatively regulates defense gene expression probably by regulating MAP kinase signaling through the E3-ubiquitin ligase KEEP ON GOING (KEG) (Christiansen et al., 2011; Gao et al., 2020). KEG was shown to be phosphorylated in *edr1* mutant plants, which leads to its degradation, indicating that EDR1 prevents KEG from degradation through some unknown mechanism. KEG also ubiquitinates and degrades MKK4 and MKK5 inducing suppression of defense signaling (Zhao et al., 2014; Gao et al., 2020).

RPM1-INTERACTING PROTEIN 4 (RIN4) is a major regulator of PTI and also in-

volved in stomatal regulation (Kim et al., 2005b; Liu et al., 2009) and as such heavily contested in plant – pathogen interactions, specifically in the well studied interaction of *A. thaliana* and *P. syringae*. RIN4 is target of at least four Pseudomonas effectors, namely AvrRps2, AvrB, AvrRpm1, and HopF2, and protected by at least two R-proteins, the NLRs RPS2 and RPM1 (Mackey et al., 2002; Axtell and Staskawicz, 2003; Wilton et al., 2010). Both AvrB and AvrRpm1 trigger the phosphorylation of RIN4 although neither protein has kinase activity (Mackey et al., 2002; Liu et al., 2011). While AvrB acts through the RLCK RPM1-INDUCED KINASE (RIPK), the mechanism for AvrRpm1 is not yet clear. This phosphorylation increases the activity of RIN4, resulting in down-regulation of defense and increased bacterial growth (Liu et al., 2011). Phosphorylation of RIN4 also strengthens its interaction with the H^+ATPases AHA1 and AHA2, in stomata guard cells, resulting in stomatal opening (Liu et al., 2009). The NLR RPM1 seems to guard RIN4 against this manipulation since phosphorylation of RIN4 also leads to ETI and HR through RPM1 (Liu et al., 2011). AvrRps2 is a cystein protease that degrades RIN4 (Axtell and Staskawicz, 2003; Mackey et al., 2003). Although it might seem puzzling why the pathogen would degrade a negative regulator of defense, studies indicate that degradation of RIN4 by AvrRps2 produces two degradation products that also suppress defense responses and actually lead to stronger pathogen growth than the full length protein. The degradation also prevents the activation of RPM1-mediated detection of AvrB and AvrRpm1 (Kim et al., 2005a; Afzal et al., 2011), indicating that degradation of RIN4 might actually be an evolutionary adaptation for the pathogen against host detection. However, the host NLR RPS2 is a guard protein that constitutively interacts with RIN4. Degradation of RIN4 actually leads to its release and activation, triggering ETI and HR (Kunkel et al., 1993; Yu et al., 1993; Axtell and Staskawicz, 2003). The last effector mentioned above also targets RIN4 as yet another adaptation by the pathogen. In an unknown mechanism HopF2 prevents the degradation of RIN4 by AvrRps2 and hence the detection by RPS2 (Wilton et al., 2010). The fight for RIN4 highlights the evolutionary back and forth and is probably exemplary for molecular interactions between pathogen and host.

1.6 Rho of Plants G-proteins

G-proteins are guanosine triphosphatases (GTPases), which convert energy from hydrolyzation of guanosin triphosphate (GTP) into guanosin diphosphate (GDP) for signal transduction while switching between an active and inactive signaling state. Hence, they are often regarded as molecular switches involved in many different cellular processes. G-proteins can be divided into two superfamilies. The trimeric G-proteins

with their α-, β-, and γ-subunits and the small monomeric G-protein of the Ras (rat sarcoma) superfamily. Trimeric G-proteins are plasma membrane associated proteins with the GTPase function contained in the α-subunit. In an inactive GDP-bound state the α-subunit is associated with the β-, and γ-subunits. After signal perception, usually by a G-protein coupled receptor (GPCR), GDP is exchanged for GTP making the α-subunit dissociate from the other subunits and becomes active in signaling (Syrovatkina et al., 2016). Small monomeric G-proteins perform conformational changes when binding to GTP, which allows them to interact with downstream interactors. In general there are five subfamilies in the Ras superfamily, termed Ras, Rho (Ras homolog familiy member), Ran (Ras related nuclear protein), Arf (ADP-ribosylation factor), and Rab (Ras-related in brain). Rab and Arf GTPases are mostly involved in vesicle trafficking. While Rabs are more involved in vesicle targeting, Arfs control coating complexes around vesicles (Schwartz et al., 2007; Jackson and Bouvet, 2014). Ran GTPases control transport in and out of the nucleus and are also involved in spindle assembly in animals (Cavazza and Vernos, 2016). Ras and Rho facilitate most small G-protein mediated signaling processes in animals. Ras G-proteins were originally identified as oncogenes, which are involved in a myriad of cellular processes among other things also the control of other G-proteins (Cox and Der, 2010). Rho are known to control cytoskeletal arrangement and many polarization processes in animals and yeast (Chiou et al., 2017; Jaffe and Hall, 2005; Sit and Manser, 2011).

The Rho subfamily is divided into four groups: Cdc42 (cell division control protein 42), Rac (Ras-related C3 botulinum toxin substrate), the name-giving Rho, and Rop (Rho proteins of plants), which are plant specific and the only Rho found in plants (Engelhardt et al., 2020). As for all G-proteins, the activity of ROPs is tightly regulated by interacting proteins. Guanosine nucleotide exchange factors (GEFs) facilitate the exchange of GDP in the inactive ROP to GTP and activate the G-protein (Fig. 2). RopGEFs can be phosphorylated, either in their plant specific PRONE domain (Plant-specific Rop nucleotide exchanger), or at their C-terminus upon stimulus, which allows them to go from an inhibited state to an active state. This was recently shown for RopGEF12 and the AGC kinase, AGC1.5 in Arabidopsis (Berken et al., 2005; Li et al., 2018). For the sake of completeness it should be mentioned that SPIKE1 is the only described GEF in plants, which does not contain a PRONE domain but instead binds ROPs via its DOCK Homology Region 2 (DHR2) domain (Basu et al., 2008). GEFs themselves can be activated by RLKs, allowing response to extracellular signals. Activated ROPs receive lipid modification, which allows them to localize to membranes. ROPs can be divided into two types, based on the lipid modification they receive when activated, which in turn is dependent on a conserved C-terminal motif. Type I ROPs

are prenylated at the cystein in the conserved CaaL motif (a = aliphatic amino acids) and type II ROPs are *S*-acylated at conserved cystein residues (Engelhardt et al., 2020). This allows ROPs to cycle between membrane and cytosol, depending on their state of activity, like Rho proteins of other organisms. The inactivation of ROPs is mediated by GTPase-activating proteins (GAPs), which catalyze the intrinsic GTPase function of the G-protein (Fig. 2). This leads to the hydrolyzation of GTP to GDP and the inactivation of the G-protein. Guanin nucleotide dissociation inhibitors (GDIs) are another group of ROP regulators that keep Rho/ROPs in an inactive state. GDI bind to inactive ROP-GDP and prevent ROP cycling, while also covering the C-terminal lipid modification of Rho/ROPs to keep them in the cytosol (Dransart et al., 2005).

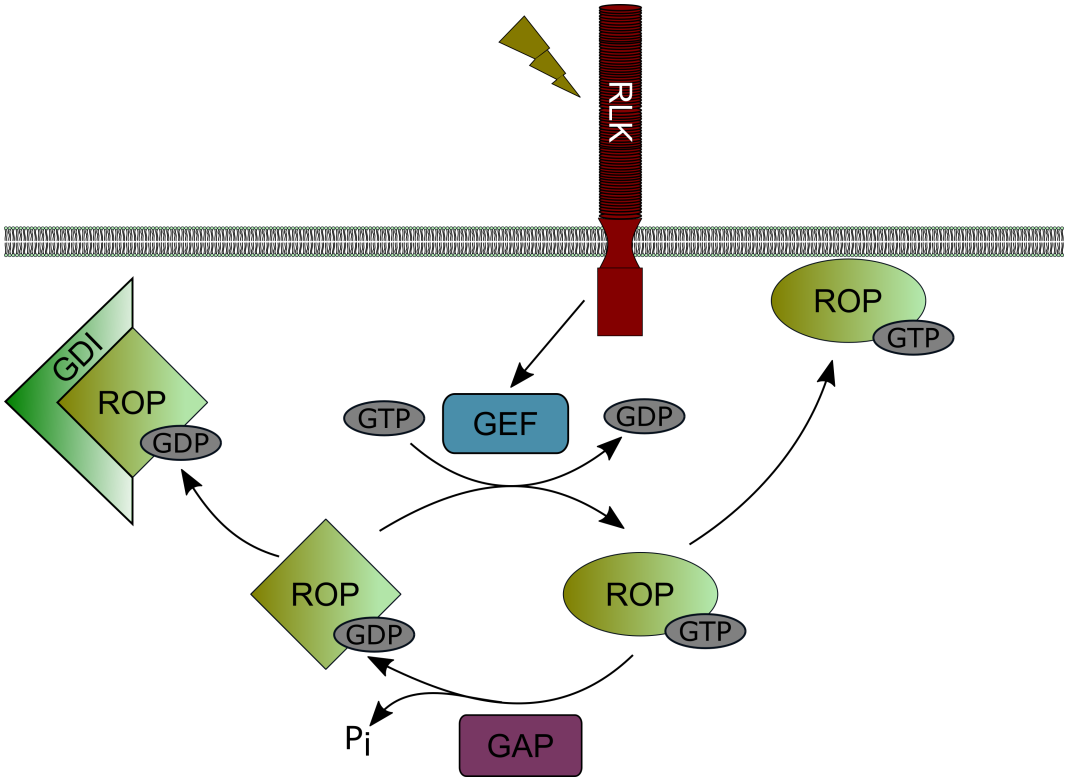

Figure 2: ROP regulation cycle. ROP G-proteins can cycle between in an inactive GDP-bound and an active GTP-bound state. Upon external signal perception, RLKs can activate GEFs. These in turn can activate the ROPs by exchanging GDP ot GTP. Activated ROPs usually receive lipid modifications, which makes them associate to membranes. Inactivation of ROPs is mediated by GAPs, which activate the intrinsic GTPase function of the G-protein, causing the hydrolyzation of GTP. RLK, Receptor-like kinase; GEF, Guanosine nucleotide exchange factor; GAP, GTPase activating protein

There are 11 ROP proteins in *A. thaliana*, 9 in maize (*Zea mays*), 7 in rice (*Oryza sativa*), 9 in tomato (*Solanum lycopersicum*), and 6 ROPs in barley (Schultheiss et al.,

2003; Christensen et al., 2003; Nibau et al., 2006; Feiguelman et al., 2018). They are also often referred to as RAC proteins due to their slightly higher sequence similarity to Rac than any other group of Rho proteins in animals and fungi. As mentioned above, ROPs as well as their Rho counterparts in other organisms regulate mainly, but not exclusively, cell polarization processes. The best studied polarization processes in plants are root hair development and pollen tube elongation. Root hair development requires polarization of a single root cell, the trichoblasts, and the outgrowth of root hairs from these cells. This increases the surface area of the root and improves nutrient uptake and anchorage to the soil (Mendrinna and Persson, 2015). ROP2 is essential for this process in Arabidopsis (Jones et al., 2002), but there is evidence that other ROPs are involved as well and possibly fulfill redundant functions. At least ROP4 and ROP6 also influence root hair formation (Molendijk et al., 2001). The RLK FERONIA was shown to interact with RopGEF1, which probably activates ROP2 (Duan et al., 2010). ROP2 controls ROS production in the root hair tip via the NADPH-Oxidase RBOHC (Jones et al., 2007). RopGEF1 and ROP2 also control Ca^{2+} accumulation in the root hair. This is initiated by $[Ca^{2+}]_{cyt}$-ASSOCIATED PROTEIN KINASE 1 (CAP1), an RLK belonging to the same subfamily as FERONIA. CAP1 interacts with RopGEF1 and knock-out of *CAP1* results in an impaired Ca^{2+} gradient. Both ROS and Ca^{2+} gradients are important features of polarized growth (Bai et al., 2014; Huang et al., 2019). ROP2 also influences microtubule organization in root hairs via the ARMADILLO REPEAT KINESIN 1 (ARK1) (Yang et al., 2007) and influences lipid composition by interacting with the PHOSPHATIDYLINOSITOL 4-PHOSPHATE 5-KINASE 3 (PIP5K3) at root hair tips, controlling the production of phosphatidylinositol-4,5-bisphosphate (PtdIns(4,5)P_2) in the root tip. On the other hand ROP10 interacts with FORMATION OF APLOID AND BINUCLEATE CELLS 1 (FAB1) to produce PtdIns(3,5)P_2 at the root hair shank (Hirano et al., 2018).

During sexual reproduction of flowering plants, a pollen grain with the male gametophyte lands on the flower pistile. The pollen creates the pollen tube as a confined rapid outgrowth from the pollen, to deliver the male gametophytes to the ovule with the female gametophyte (Cameron and Geitmann, 2018). During this process the ovule emits small peptides called LUREs that attract the pollen tube (Okuda et al., 2009; Takeuchi and Higashiyama, 2012). These peptides are recognized by pollen receptor kinases (PRKs), which are transmembrane RLKs (Muschietti et al., 1998; Chang et al., 2013; Takeuchi and Higashiyama, 2016). Although silencing of PRK2 influences tip localized ROS accumulation in pollen, there appears to be a strong redundancy in the function of PRKs since only triple mutants had any effect on pollen tube growth in Arabidopsis (Zhang et al., 2008; Chang et al., 2013). These PRKs form a com-

plex with RopGEFs and ROP proteins and can activate RopGEFs by phosphorylation, which in turn leads to the activation of ROPs (Kaothien et al., 2005; Gu et al., 2006; Zhang and McCormick, 2007). In Arabidopsis ROP1, was shown to be the primary player in pollen tube polarization and growth although at least two more ROPs (ROP3, ROP5) were identified in pollen (Li et al., 1999). There appears to be a strong redundancy in RopGEF function as well, because similar to PRKs, only quadruple mutants of RopGEF1, 9, 12, and 14 influenced tube growth in studies by Chang et al. (2013). In pollen tubes, ROPs regulate exocytosis, probably by controlling actin dynamics, but also calcium signaling and membrane lipid composition (Li et al., 1999; Kost et al., 1999; Fu et al., 2001; Gu et al., 2005; Lee et al., 2008).

Besides pollen tube and root hair polarization, ROPs are involved in a variety of processes like cell shape, stomata opening and xylem cell development (Fu et al., 2005; Hong et al., 2015; Oda and Fukuda, 2012).

1.6.1 Downstream interactors of ROPs

ROPs can interact with different downstream interactors to fulfill different functions. Direct interaction with ROP GTPases in plants appears so be mainly mediated by two distinct classes of plant specific scaffold proteins. The first class contains a CRIB domain (Cdc42/Rac-interactive binding), which is a well described Rho interacting domain from other organisms (Pirone et al., 2001). However, these ROP-interactive CRIB-motif containing proteins (RICs) are only described in plants and contain no conserved domains outside of the CRIB domain. There are 11 RICs in *A. thaliana* and at least 8 in barley (Wu et al., 2001; Engelhardt et al., 2019). The second class are plant specific ROP interactive partners (RIPs), also known as interactor of constitutively active ROPs (ICR). Five RIP proteins are described in *A. thaliana* and are characterized by their ROP interacting QWRKAA motif and a motif at the N-terminus (Lavy et al., 2007; Li et al., 2008).

These interactors seem to connect ROPs with downstream executors, although only very few of these executors are known. RIC7 interacts with ROP2 in Arabidopsis to negatively regulate light induced stomata opening. Here RIC7 interacts with the exocyst subunit Exo70B1 and probably inhibits its function (Hong et al., 2015). ROP6 promotes microtubule ordering in pavement cells through RIC1, which was shown to interact with the p60 subunit of katanin. Katanin severs microtubule branching points for microtubule paralellization (Fu et al., 2009; Lin et al., 2013). ROP2 on the other hand inhibits RIC1, but promotes actin assembly by interacting with RIC4 in pavement cells. The downstream executors in this process are not yet known, but in tobacco pollen tubes RAC1 is involved in the phosphorylation of ACTIN-DEPOLYMERIZATION

FACTOR 1 (ADF1), decreasing its ability to depolymerize actin (Chen et al., 2003; Fu et al., 2005). A similar mechanism could be involved in actin organization in Arabidopsis pavement cells and pollen tubes. In the latter, ROP1 interacts with RIC4 to promote actin assembly and with RIC3 to promote actin disassembly by influencing tip localized Ca^{2+} accumulation. In a different report, RIC1 was shown to cap cortical actin filaments in pollen tube tips in the presence of Ca^{2+} (Zhou et al., 2015). However, whether there is a connection to RIC3 and if the same ROP is involved in this pathway is not yet known. By influencing the actin cytoskeleton though, ROP1 regulates vesicle trafficking to the pollen tube tip, an important process in tip growth (Wu et al., 2001; Gu et al., 2005; Lee et al., 2008).

Of the five RIP proteins in *A. thaliana*, so far only two have been assigned a function. RIP1/ICR1 marks pollen germination sites, can interact with ROP1 in pollen tubes, and localizes to the plasma membrane of the pollen tube tip (Li et al., 2008). RIP1/ICR1 is also involved in auxin distribution in roots, by interacting with the Sec3a subunit of the exocyst complex (Lavy et al., 2007). This influences the polar localization of PINFORMED (PIN) auxin transporters (Hazak et al., 2010). The exact interacting ROP is not yet known, but an independent study shows that auxin distribution in Arabidopsis roots is dependent on ROP3 and ROP6 (Huang et al., 2014). ROP6 is activated by the RopGEF SPIKE1 (SPK1) and also interacts also with RIC1, but this seems to be necessary to maintain auxin induced polar PIN2 localization (Lin et al., 2012). RIP1 also interacts with the Ca^{2+}-binding protein Ca^{2+}-DEPENDENT MODULATOR OF ICR1 (CMI1), to regulate auxin response in a calcium-dependent manner (Hazak et al., 2019). *cmi1* mutants have shorter roots, which is also displayed by the *rip1* knock-out phenotype (Lavy et al., 2007). *rip1* plants additionally lost interdigitation of epidermal pavement cells, similar to what was observed for ROP4 knock-out plants with additional ROP2 silencing by RNA interference (RNAi) (Fu et al., 2005). This indicates that RIP1 is involved in several different developmental processes.

RIP3, also known as MIDD1 (MICROTUBULE DEPLETION DOMAIN 1), is involved in xylem cell development. During xylem cell differentiation, the cell wall is partly reinforced by a secondary cell wall. After programmed cell death, the cell wall remains as a sieve like structure (Fukuda, 1996; Zhong and Ye, 2015). For secondary cell wall formation microtubules are essential since they control the localization of the cellulose synthase complex (CESA). Local microtubule depletion leads to a lack of secondary cell wall at this position. A complex of ROP11, RIP3/MIDD1, and the microtubule depolymerizing kinesin KINESIN13A is responsible for the generation of these microtubule depleted zones. While the complex is restricted by the microtubule localized IQ67 DOMAIN 13 (IQD13), the ROP11-RIP3-KIN13A complex localizes to microtubule

plus-ends and destructs them (Mucha et al., 2010; Oda et al., 2010; Oda and Fukuda, 2012, 2013; Sugiyama et al., 2017).

All these different interactions highlight how ROPs can interact with different downstream interactors to fulfill a specific function. For example ROP2 interacts with RIC7 in stomata opening, but with RIC1, RIC3, and RIC4 in pollen tubes. Specific downstream interactors can also interact with different ROPs. For example RIC1 interacts with ROP6 to organize microtubules during pavement cell formation, but was also shown to be suppressed by interaction with ROP2 in salt stress conditions, where it acts in microtubule recovery (Fu et al., 2005; Li et al., 2017). ROP signaling can be further diversified by the interaction with different downstream executors, for example RIP1 interacts with Sec3a, but also with CMI1 (Lavy et al., 2007; Hazak et al., 2019). All this indicates strongly that ROP signaling can be very flexible and can generate very different outcomes depending on the interaction partners that find each other.

1.6.2 ROPs in host – pathogen interactions

To date, only a few connections between ROPs and pathogenesis are known in plants. It was reported that Arabidopsis ROP6 is involved in preinvasive defense against powdery mildew. Expression of dominant negative (DN) ROP6 enhanced resistance against the adapted pathogen *Golovinomyces orontii*. This coincided with constitutively increased levels of SA in these plants. Curiously, the same study found that expression of DN ROP6 reduces resistance to the non-adapted powdery mildew *Blumeria graminis* (Poraty-Gavra et al., 2013). Rice (*Oryza sativa*) RAC1 is involved in PTI and ETI against the rice blast fungus *Magnaporthe grisea* (Ono et al., 2001; Kawano et al., 2010). OsRAC1 acts downstream of the chitin receptor OsCeBiP and OsCERK1. Upon chitin perception, OsRopGEF1 is phosphorylated by OsCERK1, which leads to its activation. OsRopGEF1 then activates OsRAC1, causing an increase in defense gene expression, enhanced production of phytoalexins, and ROS production by interacting with the NAPDH-Oxidase RBOHB (Ono et al., 2001; Wong et al., 2007; Akamatsu et al., 2013). OsRAC1 also induces programmed cell death by interacting with the NLR PIT. Here OsRAC1 interacts with a different immune complex to promote cell death (Kawano et al., 2010; Akamatsu et al., 2020).

There are some cases of symbiotic interactions where ROPs are involved. In the interaction of legumes with nitrogen-fixing rhizobia, the bacteria interact with root hairs of the host plant. During this interaction a bacterium is entrapped by the root hair and subsequently an infection thread is established as an invagination of the root hair towards the root cell. Here, a nodule is formed as an accommodation for the symbiotic bacteria (Wang et al., 2012). ROP10 of *Medicago trunculata* is involved in this process.

MtROP10 is upregulated in response to rhizobia and change in expression or activity of MtROP10 resulted in aberrant infections (Lei et al., 2015). A similar part is played by ROP6 of *Lotus japonicus*. Recently it was shown that LjROP6 interacts with the NODULATION FACTOR RECEPTOR 5 (NFR5) and the GEF SPK1. Although the infection itself was not affected by LjROP6 or LjSPK1, the formation of the infection thread was diminished in the respective knock-out plants (Ke et al., 2012; Liu et al., 2020).

Rho G-proteins are well known targets for pathogens in humans and other organisms. Many bacterial toxins modify Rho proteins by glycosylation, ADP-ribosylation, deamidation, or adenylation and thereby influencing their activity. Other bacterial factors mimic GEFs and GAPs and influencing Rho activity in this way (Popoff, 2014; Aktories, 2015). The *Clostridium botulinum* C3 toxin for example ADP-ribosylates RhoA, RhoB, and RhoC in humans causing reduced activation by GEFs and stronger affinity to GDI, thereby removing it from the activation cycle in an inactive state (Aktories et al., 1989; Chardin et al., 1989; Barth et al., 1999; Genth et al., 2003). This leads to the depolymerization of actin (Chardin et al., 1989).

Salmonella enterica serotype Typhimurium is a cell invading bacterium causing gastroenteritis in humans and other mammals, and its manipulation of Rho signaling provides an excellent example of G-proteins being utilized as susceptibility factors by a pathogen (Hume et al., 2017). In the process of cell invasion Salmonella exploits host Rho signaling by deploying several effector proteins. SopE and SopE2 mimic GEF proteins and activate Rac and Cdc42 signaling in the host cell, causing rearrangement of the actin cytoskeleton and membrane ruffling, which is necessary for bacterial uptake (Stender et al., 2000; Hardt et al., 1998; Friebel et al., 2001). IQGAP1, a scaffold protein with an inactive GAP domain, plays an integral part in this, by connecting Rho signaling to MAPK signaling, the actin nucleating Arp2/3 (actin-related protein 2/3), and the Arp2/3 activator N-WASP (Wiskott–Aldrich syndrome protein) (Kim et al., 2011). Additionally, SopE promotes Caspase1 activation via Rac1 and Cdc42 causing inflammatory response in the gut. This probably helps Salmonella to compete with intestinal microbiota (Stecher et al., 2007; Muller et al., 2009). SptP is another Salmonella effector that acts as a GAP to switch off G-protein signaling after successful invasion (Fu and Galan, 1999).

ROPs have essential roles in plant development and signaling and as in other organisms should provide a convenient point of attack for pathogens. In this context it would be surprising if ROP G-proteins would not be targeted by pathogens more frequently than it is currently known.

1.7 The susceptibility factor RACB

The barley protein RACB is another ROP involved in plant – pathogen interactions. It was found to be a susceptibility factor in the interaction of barley and the barley powdery mildew fungus *Hordeum vulgare* f.sp. *hordei* (*Bgh*) (Schultheiss et al., 2002, 2003). RACB is expressed in the epidermis of barley leaves and is one of six ROPs identified in barley. It belongs to the class I of ROPs with the CaaL (CSIL, in case of RACB) domain for prenylation (Schultheiss et al., 2003). RACB also contains a conserved cysteine residue (C158), which was found in activated AtROP6 to be *S*-acylated (Sorek et al., 2017). This may be important for the membrane localization of activated RACB. Transient knock-down of *RACB*, as well as stable knock-down in transgenic barley renders plants less susceptible to *Bgh*, while over-expression increases susceptibility (Pathuri et al., 2008; Hoefle et al., 2011). RACB seems to be involved in several developmental processes. RACB RNAi plants do not develop root hairs and stomata subsidiary cell development is impaired. Both processes require single cell polarization (Hoefle et al., 2011; Scheler et al., 2016). RACB appears to have no influence on early PTI like ROS production or MAPK signaling. RACB influences penetration resistance however, probably by influencing single cell polarization during fungal attack. Nuclear movement is a common response of plants to pathogen attacks and in developmental processes (Griffis et al., 2014). Movement of the nucleus to the site of attack was slower in RACB RNAi plants compared to the wild-type. Established haustoria in RACB RNAi plants are also smaller on average, possibly resulting from a lack of transport of components for haustorial accommodation, both processes indicating impaired polarization (Hoefle et al., 2011; Scheler et al., 2016). Recently, it was shown that the RACB homolog RAC6 of wheat (*T. aestivum*) is also a susceptibility factor in the interaction of wheat with the wheat stripe rust fungus *Puccinia striiformis* f.sp. *tritici*. TaRAC6 negatively influences cell death and ROS production showing its influence on defense reactions (Zhang et al., 2020). However, this was not observed for RACB (Pathuri et al., 2008; Scheler et al., 2016).

RACB is target of at least one fungal effector. ROP-INTERACTIVE PEPTIDE 1 (ROPIP1) is secreted from the haustorium to the host cell where it can interact with RACB (Nottensteiner et al., 2018). ROPIP1 and RACB interact at microtubules and ROPIP1 negatively influences microtubule stability. MICROTUBULE-ASSOCIATED ROP-GTPASE ACTIVATING PROTEIN 1 (MAGAP1) is a microtubule associated Rop-GAP that interacts with RACB at the plasma membrane and at microtubules (Hoefle et al., 2011). Expression of MAGAP1 decreases the susceptibility of barley to *Bgh*, likely countering the RACB effect. ROP G-proteins are known to interact with different downstream interactors. RIC171 was shown to interact with RACB and over-

expression influences the penetration rate in favor of *Bgh*. RACB and RIC171 interact at the cell periphery in barley epidermal cells and RIC171 localizes to the site of fungal attack (Schultheiss et al., 2008). However, an exact mechanism for RACB-RIC171 signaling has not yet been shown.

ROP-BINDING-KINASE 1 (RBK1) is another interactor of RACB. RBK1 gets activated by RACB and seems to be involved in a control mechanism via the type II S-phase kinase 1-associated (SKP1)-like protein, which is part of the SKP1-cullin 1-F-box (SCF)-E3 ubiquitin ligase complex. RBK1 is upregulated upon pathogen attack and silencing of RBK1 or SKP1-like increases the abundance of RACB (Huesmann et al., 2012; Reiner et al., 2015). This might provide a mechanism for the plant to control the susceptibility factor RACB.

1.8 Objectives

RACB is an essential component in susceptibility signaling during the interaction of barley and *Bgh*. Since the exact mechanism of RACB signaling remains elusive, the aim of this work was to identify and characterize ROP INTERACTIVE PARTNER (RIP) proteins as potential downstream interactors of RACB in barley. Therefore, RIP proteins were to be isolated and tested for their interaction with RACB in yeast and *in planta*. All RIP proteins were also tested for their influence on the penetration rate of *Bgh* and investigated for their potential role in RACB susceptibility signaling. The hope is, by fully understanding the RACB signaling pathway, to learn more about plant – pathogen interactions in general. This may further open new ways in genetic crop protection by breeding or gene technology.

2 Materials and Methods

2.1 Biological material

Barley (*Hordeum vulgare*) cultivar Golden Promise was used for all experiments. Plants were grown in a climate chamber (Conviron, Winnipeg, Canada) under long day conditions with a 16h/8h day/night cycle. Relative humidity was set at 65% and light intensity at 150µM s^{-1} m^{-2}. Temperature was at 18℃ day and night. Plants were grown on Einheitserde® Classic, CL-ED73 (Einheitserdewerke, Werkverband e.V., Sinntal-Altengronau) soil.

Blumeria graminis f.sp. *hordei* race A6 (*Bgh*) was propagated on barley plants under the conditions described above. Spores were dispersed on 7 day old barley plants. From there, freshly developed spores were used for inoculation experiments.

2.2 RNA isolation from barley

In order to obtain the coding sequences (CDS) of genes of interest, RNA needed to be isolated from barley. Therefore, a TRIzol®-based (Thermo Fisher Scientific, Waltham, Massachusetts, USA) method was used. Primary leaves from 7 days old barley plants were harvested, frozen in liquid nitrogen and ground to a powder. Then the ground material was put in a reaction tube, TRIzol was added and the mixture was thoroughly vortexed. Afterwards, the mixture was centrifuged at 12000g for 10min at 4℃, before the supernatant was moved to a new tube and 200µl chloroform were added. The mixture was shaken for 15sec, and after incubation at room temperature for 10min the samples were centrifuged again for 15min at 12000g and 4℃. Subsequently, the upper liquid layer was moved to a fresh reaction tube and mixed with 500µl isopropanol, before it was incubated again at room temperature for 10min. After another centrifugation step at 12000g for 10min at 4℃, the supernatant was removed and the pellet was washed with 1ml of 70% EtOH. After a last centrifugation step at 7500g for 5min at 4℃, the supernatant was again removed and the remaining pellet was dried. The dry pellet was then solved in 20-50µl DEPC (diethyl pyrocarbonate) treated water at 60℃ on the shaker.

2.3 Evaluation of nucleotide concentrations

The concentration of RNA, cDNA and DNA samples was measured using the Nanodrop® ND-1000 spectrophotometer (PEQLAB Biotechnologie GmbH, Erlangen, Germany) at 260nm wavelength. A 260/280 ratio between 1.8 and 2.2 was considered as

clean.

2.4 cDNA synthesis

For the reverse transcription of RNA (section 2.2) into cDNA, the QuantiTect® Reverse Transcription Kit (Qiagen, Hilden, Germany) was used. Reverse transcription was performed according to the manufacturer's instructions. For each reaction 1µg of RNA was used. In a first step contamination with genomic DNA was removed by adding 2µl of gDNA Wipeout buffer to the RNA and RNase-free water was added as well to a total volume of 14µl. The mix was then incubated for 5min at 42℃. After incubation 1µl of primer mix (random primer) and 1µl of Reverse Transcriptase were added together with 5µl of 5x RT-buffer. The mix was again incubated for 30min at 42℃ before the reaction was stopped at 95℃ for 5min.

2.5 Polymerase chain reaction

Different DNA polymerases were used in this work. Phusion DNA-Polymerase (Thermo Fisher Scientific, Waltham, Massachusetts, USA) was used for most PCR reactions due to its low error rate. In some cases, Herculase II Fusion DNA polymerase (Agilent, Santa Clara, California, USA) was used to amplify genes of interest from cDNA. For semiquantitative PCR (section 2.5.1), Taq Polymerase (SupraTherm^{TM} Taq polymerase, Genecraft, Münster, Germany) was used. Annealing temperature and elongation time were adjusted based on the respective template. As standard, PCR was run for 32 cycles. Components of the reaction mix and standard programs were as follows:

Reaction mix Phusion:

Components	**Amount for 1 reaction**
5x GC Buffer	10µl
dNTPs (10mM)	1µl
Primer forward (10pmol/µl)	2.5µl
Primer reverse (10pmol/µl)	2.5µl
Phusion DNA polymerase	0.5µl
DNA template	0.01 - 2µg
ddH_2O	add 50µl

Program Phusion:

Temperature	**Time**
98℃	30sec
98℃	10sec
X℃	10sec
72℃	Xsec
72℃	8min

Reaction mix Herculase:

Components	Amount for 1 reaction
5x Buffer	10µl
dNTPs (100mM)	0.5µl
Primer forward (10pmol/µl)	1.25µl
Primer reverse (10µmol/µl)	1.25µl
DNA template	0.01 - 0.5µg
Herculase DNA polymerase	1µl
ddH_20	add 50µl

Program Herculase:

Temperature	Time
95℃	1min
95℃	20sec
X℃	20sec
68℃	Xsec
68℃	4min

Reaction mix Taq:

Components	Amount for 1 reaction
10x Buffer	2µl
dNTPs (10mM)	0.4µl
Primer forward (10pmol/µl)	0.4µl
Primer reverse (10pmol/µl)	0.4µl
Taq DNA polymerase	0.2µl
cDNA template	2µl 1:10
ddH_2O	add 20µl

Program Taq:

Temperature	Time
95℃	5min
95℃	30sec
X℃	30sec
72℃	Xsec
72℃	3min

2.5.1 Semiquantitative PCR

To determine transcript levels *in planta*, semiquantitative PCR (sqPCR) with a Taq polymerase (SupraTherm^{TM} Taq polymerase, Genecraft, Münster, Germany) (section 2.5) was performed. Therefore, 7 day old barley leaves where inoculated with *Bgh*. Samples where taken 24 hours later from inoculated leaves, and uninoculated leaves, or roots as control. Additionally, epidermal strips where taken from inoculated as well as uninoculated leaves. Afterwards, RNA was extracted from the samples (section 2.2). For sqPCR the generated cDNA (section 2.4) was diluted 1:10 and 2µl of cDNA was used for the PCR (section 2.5). *HvUBC* (*UBIQUITIN-CONJUGATING ENZYME E2*, HORVU3Hr1G080790) was used as control. The PCR was run for 34 cycles using the following forward (fwd) and reverse (rev) primer pairs and annealing temperatures:

Gene of interest	Primer(fwd/rev)	Annealing Temperature
RIPa	5'-GCCAAGACAAGGAATGGCTC-3'/ 5'-GAGAGCTTCATGGGTGACCT-3'	59℃
RIPb	5'-TGGTGGCTTTGGCAGTCCGT-3'/ 5'-AAGCGCCATCCGCAAGTGCT-3'	59℃
RIPc	5'-TGCACCTCAAGACCACGG-3'/ 5'-CTTCTTGAGCTCGTCCTGCA-3'	59℃
CARI	5'-GCGAGGAGGAGCTACATACA-3'/ 5'-TGTCTTTGCGCTCTTGTCTG-3'	59℃
UBC	5'-TCTCGTCCCTGAGATTGCCCACAT-3'/ 5'-TTTCTCGGGACAGCAACACAATCTTCT-3'	59℃

2.6 Restriction digest

Restriction enzymes were obtained from Thermo Fisher Scientific (Waltham, Massachusetts, USA). Digestion was performed at the recommended temperature for one hour in case of control digests and over night for cloning purposes (section 2.9.1). For the latter, the digest was stopped afterwards at the recommended temperature. For control digests, at least 500ng DNA was digested in a 20µl reaction, while for cloning purposes at least 1000ng DNA were digested in a 50µl reaction.

2.7 Agarose gel electrophoresis

In order to display DNA amplicons or show DNA fragments from restriction digests, I performed agarose gel electrophoresis. Here, DNA is separated by size in a agarose polymer matrix. Under electrical current negatively charged DNA travels along the electrical field to the anode of a gel electrophoresis chamber. Ethidium bromide was used to detect DNA under UV light. The voltage was set between 100V and 120V and for most applications a 0.8% (w/v) agarose concentration was used. As a running buffer 1x TAE buffer was used with components as follows:

Components	Amount (1l)	Concentration
Tris base	4.84g	40mM
Na_2 EDTA (pH 8.0)	2ml	6mM
Acetic acid	1.142ml	20mM
H_2O	add 1l	

2.8 Gel extraction

Amplified PCR products or restriction enzyme digested inserts for classical cloning were purified by agarose gel extraction. Therefore, the Macherey-Nagel (Düren, Germany) NucleoSpin® Gel and PCR Clean-up kit was used following the manufacturer's instructions. The washing step was performed twice and the extracted DNA was solved in 20µl ddH_2O.

2.9 Cloning procedures

The various plasmids used in this work required different cloning methods (section 2.21). In most cases genes of interest were introduced into target plasmids by classical cloning (section 2.9.1), but silencing constructs as well as some fusions to fluorophores were obtained by using the gateway cloning system (section 2.9.2).

2.9.1 Classical cloning

In classical cloning, restriction enzymes are applied to create matching single strand overlaps on inserts and plasmids, which are then used to fuse the insert into the plasmid by ligation. Therefore, in a first step inserts were amplified with primers introducing specific restriction sites at the 5'- and the 3'- end of the inserts (see Table 2). Afterwards, the amplified inserts were purified using agarose gel extraction (section 2.8). In a second step, the insert, as well as the target plasmid, were both digested over night with restriction enzymes corresponding to the introduced restriction sites (section 2.6). To get rid of phosphate residues on the loose ends of the digested plasmid, 1.5µl FastAP alkaline phosphatase (Thermo Fisher Scientific, Waltham, Massachusetts, USA) was added to a 50µl digest solution. To ligate the insert into the target plasmid, both were mixed in a 3:1 ratio, with approximately 50ng of plasmid added together with T4 DNA Ligase (Thermo Fisher Scientific, Waltham, Massachusetts, USA). Standard Ligation mix was set up as follows:

Component	Amount for 1 reaction
10x Ligase Buffer	1µl
Target plasmid	50ng
Insert	Xng
T4 DNA Ligase	0.5µl
ddH_2O	add 10µl

The ligation mix was incubated at 4℃ over night. Afterwards, the assembled plasmid was transformed into *Escherichia coli* (*E. coli*) Dh5α (section 2.10) for plasmid proliferation. After one day of bacterial growth in a 3ml culture, plasmids were extracted again (section 2.11). To identify positive clones, a control digest was performed using suitable restriction enzymes (section 2.6).

2.9.2 Gateway cloning

For gateway cloning, inserts were amplified using primers introducing attB attachment sites. In a two-step PCR reaction, first specific primers were used to amplify the inserts and making them compatible for the second primer pair, GATE_R and GATE_F (see below), introducing the attachment sites. For both PCR reactions Phusion polymerase was used (section 2.5), applying a special touchdown PCR program (see below). After each PCR reaction, the inserts were purified by gel extraction (section 2.8). The insert containing the attB attachment sites was then introduced into the pDONR223 entry vector with the corresponding attP attachment sites, allowing for BP clonase reaction using the Gateway BP Clonase^{TM} II (Invitrogen, Carlsbad, California, USA). For this reaction, insert and plasmid were mixed in a 3:1 molecular ratio with 50ng of pDONR223 used. Clonase reaction took place at 25℃ over night. Afterwards, plasmids were transformed into *E. coli* DH5α (section 2.10). The plasmid was extracted again from an overnight culture of successfully transformed *E. coli* (section 2.11). From the pDONR223, inserts were introduced into the target plasmid using LR-clonase reaction with Gateway LR Clonase^{TM} II (Invitrogen). Plasmids were mixed in a 1:1 ratio and the clonase reaction took place over night at 25℃. Afterwards, the assembled plasmid was transformed into *E. coli* (section 2.10) for plasmid proliferation. After one day of bacterial growth in a 3ml culture, plasmids where extracted again (section 2.11). To identify positive clones, a control digest was performed, using suitable restriction enzymes (section 2.6).

Primer	Sequence
GATE_F	5'-GGGACAAGTTTGTACAAAAAAGCAGGCTCA-3'
GATE_R	5'-GGGGACCACTTTGTACAAGAAAGCTGGGTC-3'

Touch-down PCR:

Temperature	Time	
98℃	30sec	
98℃	10sec	
62℃	10sec	Δ-1℃
72℃	Xsec	10 cycles
98℃	10sec	
52℃	10sec	
72℃	Xsec	22 cycles
72℃	8min	

2.10 Transformation of *E. coli*

Chemically competent *Escherichia coli* (*E. coli*) strain K-12 Dh5α (fhuA2 Δ(argF-lacZ)U169 phoA glnV44 Φ80 Δ(lacZ)M15 gyrA96 recA1 relA1 endA1 thi-1 hsdR17) (Clontech, Mountain View, USA) was used for plasmid proliferation. Therefore, frozen *E. coli* were thawed on ice. Then, about 50-100µl *E. coli* were added to 10µl ligation reaction mixture (section 2.9.1) or 5µl clonase reaction mixture (section 2.9.2) and incubated on ice for 30 minutes. Afterwards, heat shock was performed at 42℃ for 45 seconds and the cells were incubated at 37℃ for 1 hour and finally plated on LB Agar plates containing the appropriate antibiotics (see below).

LB medium:

Components	Amount (1l)
Peptone	10g
NaCl	10g
Yeast extract	5g
Agar	15g

Added antibiotics:

Antibiotic	Concentration
Ampicillin	100mg/l
Kanamycin	50mg/l
Streptomycin	50mg/l

2.11 Plasmid extraction

Plasmids were extracted from *E. coli* DH5α using the NucleoSpin® Plasmid Kit from Macherey-Nagel (Düren, Germany) following the manufacturer's instructions for small scale plasmid extraction from between 2 and 5ml overnight culture. For large scale plasmid extractions used for biolistic transformation experiments (section 2.13), plasmids were extracted from 100ml overnight culture with the NucleoBond® Xtra Midi/Maxi Kit from Macherey-Nagel following the manufacturer's instructions.

For quick plasmid extractions to test transformed *E. coli*, a different protocol was used, based on Birnboim and Doly (1979). For that, 2ml of over-night culture were centrifuged for 1min at 13000rpm. The supernatant was discarded and the pellet was solved in 100µl buffer P1 (see below). Thereafter, 200µl buffer P2 (see below) were added and after brief mixture, the solution was incubated at room temperature for 5min to lyse the cells. The reaction was stopped adding 150µl buffer P3 (see below) and 2 drops of chloroform for phase separation. After briefly mixing, the sample was centrifuged for 10min at 13000rpm. Afterwards, the supernatant was discarded again and the pellet was washed, adding 100µl 70% EtOH, and centrifuged again for 10min at 13000rpm. The supernatant was then discarded again and the pellet was dried, before it was finally solved in 20µl ddH_2O.

Buffer P1:

Components	**Concentration**
Tris-HCl, pH 8.0	50mM
EDTA	50mM
Sucrose	15%
RNase A	10mg/ml

Buffer P2:

Components	**Concentration**
NaOH	0.2M
SDS	1%

Buffer P3:

Components	**Amount**
5M $CH_3COO\ K^+$	60% (3M)
ddH_2O	28.5%
Acetic acid	11.5%
	pH 5.2

2.12 Site directed mutagenesis

Several mutations were introduced into *HvRIPb* for domain function analyses. Here, Pfu polymerase (Promega, Madison, Wisconsin, USA) was used to amplify plasmids containing the gene of interest with primers (see below) introducing single or double nucleotide exchanges. After PCR, the plasmids were digested with DpnI, which is specific for methylated DNA and should therefore spare newly amplified plasmid but eliminate the original unmutated plasmid. In the end, the new plasmids were transformed into *E. coli* again (section 2.10) and amplified. From there, the plasmids were extracted again (section 2.11) and analyzed by sequencing. The Pfu polymerase reaction mix and PCR program were as follows:

Reaction mix Pfu:

Components	Amount for 1 reaction
10x Buffer	5µl
dNTPs (10mM)	1µl
Primer forward (10pmol/µl)	1µl
Primer reverse (10pmol/µl)	1µl
Pfu DNA polymerase	1µl
Plasmid template	5-20ng
ddH_2O	add 50µl

Program Pfu:

Temperature	Time	
95℃	5min	
95℃	1min	
55℃	30sec	
72℃	5min	15 cycle
72℃	8min	

Mutation	Primer Sequence fwd/rev
Q540L/ W541G	5'-GCGCCGGCTGCGCGTGCAGTCCGACCTGGGGCGCAAGGCTGCAGAGGCCGCCG-3'/ 5'-CGGCGGCCTCTGCAGCCTTGCGCCCCAGGTCGGACTGCACGCGCAGCCGGCGC-3'
E86Q	5'-CTAAGGTCAACCAGCTCCAAGATCAGCTGAAGAAGACCAAGGAACAGTTG-3'/ 5'-CAACTGTTCCTTGGTCTTCTTCAGCTGATCTTGGAGCTGGTTGACCTTAG-3'
D85N/ E86Q	5'-CCAGCTCCAAAATCAGCTGAAGAAGACCAAGGAACAGTTGAGTGCATCAG-3'/ 5'-TCTTCAGCTGATTTTGGAGCTGGTTGACCTTAGAGTCCAGCTCAGTTAGC-3'

2.13 Transient transformation of barley

Transient transformation of barley plants was performed using a BIO-RAD particle delivery system PDS-1000/He (Hercules, California, USA) in accordance with Schweizer et al. (1999). The first leaf from 7 day old barley plants was detached and put on 0.8% Water-Agar. 1µm Gold particles were coated with plasmids coding for genes

of interest, markers, or transformation markers. Therefore, 1µg of plasmid and 0.5µg of plasmid coding the transformation marker, were added to 11µl of gold particles (27.5mg/ml) for each shot. The resulting volume was doubled by adding 2.5mM $CaCl_2$ and subsequently 3µl of 2mg/ml protamine (Sigma-Aldrich, St.Louis, USA). After incubation for 30 min, gold particles were sedimented by centrifugation and washed twice, once with 70% EtOH and once with 100% EtOH. After each washing step, the supernatant was discarded and finally the coated gold particles were solved in 6µl 100% EtOH per shot. The gold particles were then pipetted on a macrocarrier and shot at 900psi onto the detached barley leaves in about 25In Hg vacuum.

2.14 Infection assays

For infection assays, 7 days old barley plants were transiently transformed by particle bombardment (section 2.13). Over-expression was achieved by introducing genes of interest into pGY1 vectors (see Table 1), containing the CaMV35S promotor. Transformed leaves were inoculated with *Bgh* 24 hours after bombardment. Knock-down of genes was achieved by transient induced gene silencing (TIGS), based on (Douchkov et al., 2005). For this, about 250bp to 600bp of the coding sequence of the gene of interest were introduced into the pIPKTA30N vectors (see Table 1), which resulted in double strand RNA formation and hence in RNA interference (RNAi). In contrast to over-expression, transformed leaves were inoculated with *Bgh* 48 hours after bombardment. For both over-expression and silencing, the penetration rate into the transformed cells was determined by fluorescence microscopy, 24 hours after inoculation. The penetration rate was calculated as the amount of penetrated cells, containing an established haustorium, among all attacked cells.

2.15 Confocal Laser Scanning Microscopy

For confocal laser scanning microscopy (CLSM), other than FLIM (section 2.15.5), a Leica TCS SP5 system was used (Leica, Microsystems, Wetzlar, Germany). Transiently transformed barley cells, were analyzed 24 to 48 hours after bombardment. The top half of each cell was scanned in xyz acquisition mode as z-stacks. For detection of GFP, YFP, and CFP an argon laser was used at 20% power. For detection of mCherry and RFP a DPSS 561nm laser was used. The scanning speed was 400Hz and a HCX PL APO lambda blue 20.0x0.7 IMM UV objective was used for image acquisition. The pinhole was set at 60µm diameter. Standard excitation wavelength and detector settings were as follows:

Fluorophore	Excitation (nm)	Detection range (nm)
CFP	456	465-500
GFP	488	500-550
YFP	514	525-550
mCherry/RFP	561	570-610

2.15.1 Ratiometric Bimolecular Flourescence Complementation

To test interactions *in planta*, Bimolecular Fluorescence Complementation (BiFC) was performed. Therefore, genes of interest were cloned into plasmids coding for N- or C-terminal split YFP constructs (nYFP or cYFP) (section 2.9.1, see Table 1). Plasmids carrying the constructs were co-transformed into barley epidermal leaves (section 2.13). In BiFC, two interacting proteins, each fused to one respective split YFP truncation, should bring the two halves of YFP close enough together to reconstitute the fluorophore so that YFP signal can be restored. Additionally, a plasmid expressing cytosolic mCherry was also co-expressed as a transformation control and reference for the YFP signal. Images were taken 24 to 48 hours post bombardment. Throughout each experiment microscope settings were kept constant and the same settings were used for the control as well as for the interaction of interest. Signal (Mean Fluorescence Intensity, MFI) was measured in at least 20 cells in single planes over a linear region of interest (ROI) using the LAS X software from Leica (version 3.7.0.20979, Wetzlar, Germany). The average ratio between restored YFP and mCherry signal for each construct was calculated from the YFP/mCherry ratio of each individual cell.

2.15.2 Evaluation of microtubule to cytosol signal ratio

In order to determine microtubule to cytosol signal ratios, images of 10 different cells from different experiments where analyzed. For each cell, cytosolic signals were measured as MFI at cytosolic strands at three different positions using the Leica LAS X software (version 3.7.0.20979, Wetzlar, Germany). Measurements were conducted similar for microtubule signals. In the end the average microtubule signal was normalized to the average cytosolic signal for each cell. Over all, the average ratio of cytosol and microtubules was calculated for each construct.

2.15.3 Measurement of RNAi-efficiency

In order to evaluate efficiencies of RNAi constructs, I measured silencing efficiency as the reduction of fluorescence signal from the flourophore-tagged protein of interest in presence of the RNAi construct. Therefore, I transformed single epidermal cells of barley leaves with the respective RNAi constructs (section 2.13, see Table 1), and co-expressed the respective fluorophore-tagged proteins of interest and a transformation marker, which also served as internal reference. As control, I expressed the fluorophore tagged protein of interest together with the empty RNAi plasmid (pIPKTA30N) and a transformation marker. Images were taken 24 hours after bombardment with the Leica TCS SP5 microscope (section 2.15) as z-stacks of xy optical sections of the upper half of the cell. Images of at least 30 cells were taken for each construct. The ImageJ software was used to measure fluorescence intensities over the whole cell as gray scales. The ratio between fluorophore and marker signal intensity was calculated for each cell and in the end for each construct the average ratio was calculated.

2.15.4 Evaluation of Protein expression levels

To compare relative expression levels, YFP tagged fusion proteins of RIPb, RIPbCC1, RIPbVaCC2, and RIPbCC2 were transiently co-expressed with mCherry as a transformation marker and internal reference in barley epidermal cells (section 2.13). 24 hours after bombardment the upper half of at least 30 transformed cells were imaged as z-stacks of XY optical sections using the Leica TCS SP5 microscope (section 2.15). The ImageJ software was used to measure fluorescence intensities over the whole cell as gray scales. The ratio between YFP and mCherry signal intensity was calculated for each cell and in the end the average ratio was calculated for each construct.

2.15.5 Fluorescence lifetime imaging

Another way to test protein – protein interactions is fluorescence lifetime imaging (FLIM) via time correlated single photon counting (TCSPC). The principle of FLIM is based on Förster resonance energy transfer (FRET), the energy transfer between two fluorophores. Here, I used the FLIM pairs meGFP and mCherry, which were tagged to the proteins of interest by Gateway cloning (section 2.9.2, see Table 1). If the donor meGFP is excited, its electrons are elevated to a higher energetic stage. After excitation the electrons return to their original energetic state, which leads to a release of excess energy as fluorescence. In presence of the acceptor mCherry, the return to the original energetic state happens faster due to energy transfer from meGFP to mCherry.

This difference in meGFP lifetime can be measured by using a pulsed laser system and a single photon detector. FLIM was performed with the Olympus FV3000 (Olympus, Shinjuku, Tokio, Japan) system linked to a PicoQuant FCS/FLIM-FRET/rapidFLIM kit, consisting of a 485 nm (LDH-D-C-485) pulsed laser, two TCSPC modules (TimeHarp 260 PICO Dual, TimeHarp 260 NANO Dual), and two PMA hybrid 40 detectors (PicoQuanT, Berlin, Germany).

FLIM was measured in the cell periphery of transformed single epidermal barley cells (section 2.13), 48 hours after bombardment. For each cell at least 500 photons were counted per pixel and at least 15 cells per experiment were analyzed. The laser pulse frequency was 40Mhz and detection had a resolution of 25ps. The 60x immersion objective on the Olympus FV3000 was used for analyzing fluorescence.

The data were processed with the Symphotime64 software by Picoquant via n-exponential reconvolution, a fitting with n=3 degrees of freedom and a calculated instrumental response function (cIRF).

2.16 Yeast-two-hybrid

Yeast (*Saccharomyces cerevisiae*) strain AH109 (Clontech, Mountain View, California, USA) Genotype MATa, trp1-901, leu2-3, 112, ura3-52, his3-200, gal4Δ, gal80Δ, LYS2::GAL1$_{UAS}$-GAL1$_{TATA}$-HIS3, MEL1, GAL2$_{UAS}$-GAL2$_{TATA}$-ADE2, URA3::MEL1$_{UAS}$-MEL1$_{TATA}$-lacZ was used for protein – protein interaction studies in yeast. Yeast was propagated on plates with YPDA medium (see below) and grown in an liquid overnight culture (YPDA) for transformation. Yeast cells were transformed with either pGADT7 as prey, or pGBKT7 as bait vectors containing the genes of interest as inserts (see Table 1). The small-scale LiAc yeast transformation procedure was used based on the manufacturer's instructions in the Yeast Protocols Handbook protocol V.E. (Clontech, Mountain View, California, USA). For selection of transformed cells, yeast was streaked on synthetic dropout (SD) agar plates lacking leucine and tryptophan (SD-Leu-Trp; see below). After 3-4 days, growing colonies were collected and streaked on sector plates also containing SD-Leu-Trp agar. After another 3-4 days, yeast was taken from the sector plates, solved in water, and every sample was then set to the same optical density measured at a wavelength of 600nm. Finally, 7µl of transformed yeast was dropped out on SD plates lacking leucine, tryptophan, adenine and histidine (Quadruple drop-out, QDO; see below) for the selection of interactions and additionally on SD-Leu-Trp as growth control. Optionally, 3-amino-1,2,4-triazole (3-AT) was added to the medium to eliminate unspecific interactions caused by a leaking HIS3 reporter gene.

Components SD	Amount (1l)
Yeast nitrogen base without amino acids	1.7g
Glucose	20g
$(NH_4)_2SO_4$	5g
Amino acid mixture	see below
(Agar)	(20g)
H_2O	add 1l
pH 5.8	

Components YPDA	Amount (1l)
Yeast extract	10g
Peptone	20g
Glucose	20g
Adenine	30mg
(Agar)	(20g)
H_2O	add 1l

List of amino acids in the amino acid mixture:

Amino acids	Abbreviation	Amount (1l)
L-Adenine hemisulfate	Ade	20mg
L-Arginine HCl	Arg	20mg
L-Histidine HCl mono hydrate	His	20mg
L-Isoleucine	Ile	30mg
L-Leucine	Leu	100mg
L-Lysine HCl	Lys	30mg
L-Methionine	Met	20mg
L-Phenylalanine	Phe	50mg
L-Threonine	Thr	200mg
L-Tryptophane	Trp	20mg
L-Tyrosine	Tyr	30mg
L-Uracil	Ura	20mg
L-Valin	Val	150mg

2.17 Yeast-two-hybrid screening for downstream interactors

To screen for potential interaction partners of proteins of interest, a yeast screening was performed using a barley cDNA library previously constructed according to the Matchmaker^{TM} Library Construction & Screening Kits User Manual (section IX, X, XII, Clontech, Mountain View, California, USA). The library was cloned into the pGADT7 prey plasmid and transformed into the AH109 yeast strain. In order to conduct a yeast mating experiment, bringing together bait and prey plasmids, the gene of interest needed to be cloned into the pGBKT7 (section 2.9.1, see Table 1) and transformed into the Y187 yeast strain using the method described in 2.16. Successfully transformed

cells were selected using SD plates lacking Trp (section 2.16).

Transformed cells were grown in a 50ml overnight culture in SD liquid medium without Trp. On the following day, 500ml of 2x YPDA medium (section 2.16) were inoculated with 10^9 cells of the overnight culture and combined with 10^9 cells of the cDNA library. Additionally, 45ml of 2x YPDA medium, containing (50µg/ml) kanamycin was added. The mating was conducted over night on the shaker at around 50rpm at 30℃.

One day later, the culture was checked for remaining zygotes. If none could be found, the culture was centrifuged at 1000rpm for 10min before the pellet was solved in 0.5x YPDA medium (section 2.16). The cells were then centrifuged again at 1000rpm for 10min and subsequently solved again in 10ml 0.5x YPDA medium. In the end, yeast was streaked on QDO plates and additionally on SD-Leu, SD-Trp, and SD-Leu-Trp plates as control (section 2.16).

2.17.1 Plasmid extraction from yeast and identification of interactors

Grown yeast colonies were picked from QDO plates (section 2.17) and streaked onto QDO sector plates again for proliferation. From there, cells were transferred into reaction tubes. Plasmids were isolated from yeast, using lyticase, which is able to break up the cell wall of yeast cells. 15µl of lyticase solution consisting of lyticase buffer (1.2M sorbitol, 0.1M Tris base, pH 7.6) and 5U lyticase (Sigma-Aldrich, St.Louis, Missouri, USA) were added to the yeast cells followed by 30min incubation at 37℃ and another 30min incubation at 95℃. In the end, the solution was quickly spun down and frozen at -20℃. After defreezing, 2µl were used for a colony PCR (cPCR) using primers 313 and 310 (see below) and Taq polymerase (SupraTherm^{TM} Taq polymerase, Genecraft, Münster, Germany) (see below). Positive clones were then sent for sequencing.

cPCR reaction mix:

Components Taq	Amount for 1 reaction
10x Buffer	5µl
dNTPs (10mM)	1µl
Primer 313 (10pmol/µl)	1µl
Primer 310 (10pmol/µl)	1µl
Taq DNA polymerase	0.5µl
Plasmid extraction	2µl
ddH_2O	39.5µl

Program cPCR:

Temperature	Time	
94℃	5min	
94℃	30sec	
55℃	30sec	
72℃	2min	36 cycles
72℃	3min	

Primer	Sequence
Primer 313	5'-CTATTCGATGATGAAGATACCCCACCAAACC–3'
Primer 310	5'-TGGCGAAGAAGTCCAAA-3'

2.18 Protoplast generation and transformation

Protoplast isolation and transfection from barley epidermal leaves was adapted from Zhang et al. (2011). In a first step, the lower epidermis was removed from 7 to 10 days old barley leaves. The rest of the leaves without the epidermis was floated on digestion solution (see below) in a petri-dish for 4 hours in the dark with occasional gentle rotation.

Digestion solution:

Components	Concentration
Mannitol	0.45M
Gamborgs B5	3.16mg/ml
MES pH 5.7	10mM
$CaCl_2$	10mM
Cellulase onozuka R10	0.5%
Macerozyme R10	0.5%
Driselase	0.5%

After the incubation, an equal volume of W5 buffer (see below) was added to the digestion, and the mix was then gently shaken for 10sec. Subsequently, all protoplasts were washed from the petri-dish into a tube using W5 buffer. The protoplasts were then filtered through 100µm nylon meshes.

W5 buffer:

Components	Concentration
NaCl	154mM
$CaCl_2$	125mM
KCl	5mM
MES pH 5.7	10mM

After washing, the protoplast solution was gently centrifuged at 1000rpm for 3min in a swinging bucket. The supernatant was discarded and the pellet was washed again

with W5 solution. Afterwards, the supernatant was discarded again and the protoplasts were solved in MMG (see below) at a concentration of 2x10^6 cells/ml. The cells were checked under the microscope for viability.

MMG:

Components	Concentration
Mannitol	0.4M
$MgCl_2$	15mM
MES pH 5.7	2mM

Protoplasts were transformed using a polyethylene glycol (PEG) based protocol. In the beginning 50µg (25µg for markers) of plasmids were added to 1ml protoplasts, before 1.1ml of PEG solution (see below) was added and the mixture was incubated at room temperature in the dark for 20min. Then 4.4ml of W5 solution was added and the resulting solution was mixed by slowly inverting the tube. Afterwards, the protoplasts were centrifuged at room temperature for 3min at 1000rpm and then resolved in 1ml WI buffer (see below). The protoplasts were finally incubated in the dark for 6 to 16 hours.

PEG solution:

Components	Concentration
PEG 4000	40% (w/v)
Mannitol	0.2M
$CaCl_2$	0.1M

WI buffer:

Components	Concentration
Mannitol	0.5M
KCl	20mM
MES pH 5.7	4mM

2.18.1 Protein isolation from protoplasts and immunoprecipitation

Proteins were isolated from protoplasts and enriched by immunoprecipitation (IP) for determination of protein levels. Therefore, protoplasts were centrifuged at 1000rpm for 3min and solved in 200µl Extraction Buffer (EB, see below). The samples were then quickly frozen in liquid nitrogen and then vortexed for 15sec after thawing. After centrifugation for 10min at 10000rpm at 4℃, the supernatant was transferred into a new reaction tube. Meanwhile, 10µl anti-GFP beads were prepared (GFP-Trap® Magnetic Agarose, ChromoTek, Planegg, Germany). Beads were washed three times with 450µl of EB. After each washing step, beads were separated from buffer with a magnetic rack.

The extracted proteins were added to the magnetic beads and the whole solution was incubated for 50min under steady rotation at 4℃. Afterwards, the beads were again separated from the solution with a magnetic rack and washed three times with wash buffer (WB, see below). The beads were then solved in 50µl 2x SDS buffer and boiled for 10min at 95℃.

GTEN:

Components	Concentration
Glycerol	10%
Tris base pH 7.5	25mM
EDTA	1mM
NaCl	150mM

Extraction buffer:

Components	Concentration
DTT	10mM
1x protease inhibitor cocktail	
Nonidet P40	1%
PMSF	1mM
GTEN	add

Wash buffer:

Components	Concentration
1x protease inhibitor cocktail	
PMSF	1mM
GTEN	add

2.19 Protein isolation from Yeast

For whole protein extraction from yeast a protocol based on Kushnirov (2000) was used. Colonies were picked from sector plates (section 2.16) and grown over night in SD-Leu-Trp medium. On the next day, 4ml of the over night culture were collected and centrifuged at 13000rpm for 1min. The supernatant was discarded and the pellet solved in 100µl of ddH_2O. Afterwards, 100µl of 0.2M NaOH were added and after vortexing, the samples were incubated for 10min at room temperature for cell lysis. Then the lysate was centrifuged again at 4000rpm for 5min at 4℃. In the end, the supernatant was discarded and the pellet was solved in 37.5µl of ddH_2O and 12.5µl 4x SDS buffer. Samples were subsequently cooked for 3min at 95℃ for protein denaturation. Before western blot the samples were quickly centrifuged at 4000rpm for 30sec.

2.20 SDS-PAGE and western blot

Isolated proteins from yeast or IP were separated by polyacrylamide gel electrophoresis (PAGE) and detected by western blotting (Laemmli, 1970). The acrylamide gel consisted of a 5% stacking gel (680µl/ml gel H_2O, 166µl/ml 30% acrylamide, 126µl/ml 1M Tris-HCl pH 6.8, 10µl/ml % SDS, 10µl/ml 10% ammonium persulfate, 1µl/ml TEMED (*N, N, N', N'* tetraethylmethylenediamine)) and a 12% resolving gel (330µl/ml H_2O, 400µl/ml 30% acrylamide, 250µl/ml 1.5M Tris base pH 8.8, 10µl/ml 10% SDS, 10µl/ml ammonium persulfate, 0.4µl/ml TEMED). Next to the samples, 4.5µl of PageRuler Plus Prestained Protein Ladder (Thermo Fisher Scientific, Waltham, Massachusetts, USA) was put on the gel in order to determine protein sizes. The gels run between 80V and 120V, until sufficient protein separation was achieved in a Mini Protean III Cell system (Bio-Rad, Hercules, California, USA). As running buffer 1x Laemmli buffer (10g/l Tris base, 14.4g/l glycine, 0.1g/l SDS, pH 8.3) was used.

Proteins were then transferred onto a methanol activated PVDF membrane (Bio-RAD, Hercules, California, USA) in a Biometra Fastblot B43 system (Biometra, Göttingen, Germany) at a current of 5mA/cm^2. The membrane was sandwiched in two layers of blotting paper (Whatman GB005) on each side, soaked in transfer buffer (25mM Tris base, 192mM Glycine, 10% methanol). After blotting, the membrane was stained with Ponceau S if necessary and subsequently washed in distilled water. In a next step, free binding sites were blocked with 5% (w/v) dry milk powder in PBS-T buffer (50mM Tris base, 150mM NaCl, pH 6.7, 0.05% Tween20) for one hour at room temperature while shaking (3D shaker). After one hour, the blocking solution was discarded and the primary antibody (see below) was applied to the membrane. Therefore, the antibody was solved in 5% dry milk powder in PBS-T buffer. The membrane floated in the antibody solution for one hour while shaking at room temperature. Afterwards, the antibody solution was discarded and the membrane was washed three times in PBS-T buffer for 10min. The secondary antibody, coupled to a horseradish peroxidase (HRP), was applied like the primary antibody at a concentration of 1:5000. After shaking for one hour the antibody solution was again discarded and the membrane was washed in PBS-T buffer 5 times for 5min. If no secondary antibody was required (HA, see below), the membrane was directly washed 5 times for 5min in PBS-T buffer after the primary antibody. As HRP substrate, HCL Pico Plus (Thermo Fisher Scientific, Waltham, Massachusetts, USA) was used and detection was performed with a CCD Camera system Fusion-SL4 (Vilber Lourmat, Marne la Valée, France) and the FusionCapt Advance Solo 4 (version 16.06) software.

List of antibodies:

Primary Antibody	**Dilution**	**Secondary Antibody**
c-Myc 9E10, sc-40 (1)	1:500	m-IgG$_\kappa$ BP-HRP, sc-516102 (1)
anti-GFP B-2, sc-9996 (1)	1:1000	m-IgG$_\kappa$ BP-HRP, sc-516102 (1)
anti-HA-HRP SF10 (2)	1:2000	not requiered

(1) Santa Cruz Biotechnology, Dallas, Texas, USA

(2) Sigma-Aldrich, St.Louis, Missouri, USA

2.21 Plasmid used in this thesis

Different plasmids were used in this work suitable for distinct experiments. Overexpression of genes of interest was achieved with the pGY1 plasmid (Schweizer et al., 1999) containing a CaMV35S promotor. Next to the classic pGY1 version, a modified pGY1 plasmid was used containing a Gateway cassette for Gateway cloning (Hückelhoven lab). Fluorescence tags were introduced with modified pGY1 plasmids containing either a GFP tag (Schultheiss et al., 2003) YFP tag (Hoefle and Hückelhoven, 2014), a CFP tag (Nottensteiner et al., 2018) or an RFP tag (Hoefle et al., 2011). Additionally, pGY1 versions containing the meGFP or mCherry as well as 5' and 3' Gateway cassettes for N- and C-terminal fusions, respectively (Hückelhoven lab), were used mainly for FLIM (section 2.15.5). For silencing, the pIPKTA38 plasmid was used as an entry vector into the pIPKTA30N vector (Douchkov et al., 2005) for double stranded RNA transcription. The yeast plasmids were acquired from Clontech (Mountain View, California, USA) as mentioned in section 2.16. For BiFC, (section 2.15.1) the pUC-Spyne and pUC-Spyce plasmids were used introducing N- or C-terminal split YFP fusions (Walter et al., 2004; Waadt et al., 2008). For Gateway cloning, other than cloning of the silencing plasmids, the pDONR223 was used as entry vector (section 2.9.2).

The following table (Table 1) lists plasmids used in this work, the respective cloning method, restriction sites used for classical cloning and references. If the respective plasmid has not yet been published but was also not created by me, reference is given as "Hückelhoven lab". pGY1, pUC, pGADT7, and pIPKTA30N plasmids were selected for ampicillin resistance. pGBKT7 and pIPKTA38 were selected for kanamycin resistance. pDONR223 was selected for streptomycin resistance (section 2.10).

Table 1: List of Plasmids

Plasmid	Cloning procedure	Restriction sites/ GW cloning method	Reference
Over-expression			
pGY1-Ripa	classic	XbaI	Hückelhoven lab
pGY1-Ripb	classic	XbaI/SalI	this work
pGY1-Ripc	classic	XbaI/PstI	this work
pGY1-Car1	classic	XbaI/SalI	this work
pGY1-Costars	classic	XbaI/SalI	this work
pGY1-RipbCC1	classic	XbaI/SalI	this work
pGY1-RipbCC1Va	Gateway	LR	this work
pGY1-RipbVa	classic	XbaI/SalI	this work
pGY1-RipbVaCC2	classic	XbaI/SalI	this work
pGY1-RipbCC2	classic	XbaI/SalI	this work
pGY1-RipaCC2	Gateway	LR	this work
pGY1-RACB WT			Schultheiss et al. (2003)
pGY1-CA RACB			Schultheiss et al. (2003)
pGY1-DN RACB			Schultheiss et al. (2003)
pGY1-RAC1 WT			Schultheiss et al. (2003)
pGY1-CA RAC1			Schultheiss et al. (2003)
pGY1-DN RAC1			Schultheiss et al. (2003)
pGY1-RFP-MAGAP1-Cter			(Hoefle et al., 2011)
Silencing			
pIPKTA30N-Ripa	Gateway	LR	this work
pIPKTA30N-Ripb	Gateway	LR	this work
pIPKTA30N-Ripc	Gateway	LR	this work
pIPKTA30N-δ-COP	Gateway	LR	this work
pIPKTA30N-Synaptotagmin-7	Gateway	LR	this work
pIPKTA30N-Costars	Gateway	LR	this work
Fluorescence tag			
pGY1-YFP-Ripa	classic	XbaI	Hückelhoven lab
pGY1-YFP-Ripb	classic	XbaI/SalI	this work
pGY1-YFP-Ripc	classic	XbaI/PstI	this work
pGY1-GFP-Ripb	classic	XbaI/SalI	this work
pGY1-YFP-RipbCC1	classic	XbaI/SalI	this work
pGY1-RipbCC1-meGFP	Gateway	LR	this work
pGY1-YFP-RipbCC1Va	classic	XbaI/SalI	this work

Plasmid	Cloning procedure	Restriction sites/ GW cloning method	Reference
pGY1-YFP-RipbVa	classic	XbaI/SalI	this work
pGY1-YFP-RipbVaCC2	classic	XbaI/SalI	this work
pGY1-YFP-RipbCC2	classic	XbaI/SalI	this work
pGY1-RipaCC1-meGFP	Gateway	LR	this work
pGY1-meGFP-RipaCC2	Gateway	LR	this work
pGY1-RipcCC1-meGFP	Gateway	LR	this work
pGY1-meGFP-RipcCC2	Gateway	LR	this work
pGY1-CFP-CA RACB	classic		Nottensteiner et al. (2018)
pGY1-CFP-RACB WT	classic		Nottensteiner et al. (2018)
pGY1-RFP-MAGAP1-Cter	classic		Hoefle et al. (2011)
pGY1-YFP-CAR1	classic	XbaI/SalI	this work
pm-rk			(Nelson et al., 2007)
Yeast Transformation			
pGADT7-Ripa	classic	Nde/BamHI	Hückelhoven lab
pGADT7-Ripb	classic	EcoRI/BamHI	this work
pGADT7-Ripc	classic	EcoRI/BamHI	this work
pGBKT7-Ripb	classic	EcoRI/BamHI	this work
pGBKT7-RACB WT	classic		Hoefle et al. (2011)
pGBKT7-CA RACB	classic		Hoefle et al. (2011)
pGBKT7-DN RACB	classic		Hoefle et al. (2011)
pGBKT7-RAC1 WT	classic		Hückelhoven lab
pGBKT7-CA RAC1	classic		Hückelhoven lab
pGBKT7-DN RAC1	classic		Hückelhoven lab
pGBKT7-Kin13A1	classic	NcoI/BamHI	this work
pGBKT7-Kin13A1-Cter	classic	NcoI/BamHI	this work
pGBKT7-Kin13A2	classic	NcoI/BamHI	this work
pGBKT7-Kin13A2-Cter	classic	NcoI/BamHI	this work
pGADT7-RipbCC1	classic	EcoRI/BamHI	this work
pGADT7-RipbCC1Va	classic	EcoRI/BamHI	this work
pGADT7-RipbVa	classic	EcoRI/BamHI	this work
pGADT7-RipbVaCC2	classic	EcoRI/BamHI	this work
pGADT7-RipbCC2	classic	EcoRI/BamHI	this work
Bimolecular Fluorescence Complementation			
pUC-Spyne(R)173-Ripa	classic		Hückelhoven lab
pUC-Spyne(R)173-Ripb	classic	SpeI/SalI	this work
pUC-Spyne(R)173-Ripc	classic	SpeI/BamHI	this work

Plasmid	Cloning procedure	Restriction sites/ GW cloning method	Reference
pUC-Spyce-CA RACB	classic		Schultheiss et al. (2008)
pUC-Spyce-DN RACB	classic		Schultheiss et al. (2008)
pUC-Spyce(MR)-Ripb	classic	SpeI/SalI	this work
pUC-Spyne(R)173-CAR1	classic	SpeI/SalI	this work
pUC-MAGAP1-Spyce(M)	classic	XbaI/SalI	Hückelhoven lab
Entry Vectors			
pDONR223-RipaCC2	Gateway	BP	this work
pDONR223-Ripb	Gateway	BP	this work
pDONR223-RipcCC2	Gateway	BP	this work
pDONR223-RipbCC1Va	Gateway	BP	this work
pIPKTA38-Ripa	classic	SalI/XbaI	Hückelhoven lab
pIPKTA38-Ripb	classic	SmaI	this work
pIPKTA38-Ripc	classic	SalI/XbaI	this work
pIPKTA38-δ-COP	classic	SmaI	this work
pIPKTA38-Synaptotagmin-7	classic	SmaI	this work
pIPKTA38-Costars	classic	SmaI	this work

2.22 Primers

The following list (Table 2) contains all primers used for cloning plasmids mentioned in Table 1. The table contains the gene of interest, which was amplified with the respective primers as well as the introduced restriction sites for classical cloning (underlined) or attachment sites for Gateway cloning, and the primer sequence. Introduced restriction sites are underlined in the sequence. If no restriction site was introduced or no restriction site was used during the cloning procedure (i.e. blunt end cloning), only the fusion sites (5' or 3') is given.

Table 2: List of Primers

Gene	Restriction site	Sequence
RIPa	XbaI (5')	TCTAGAATATGCAGACAGCCAAGACAAG
RIPa	XbaI (3')	TCTAGATCATTTCTTCCACATTCCACTG
RIPa	NdeI (5')	ACATATGCAGACAGCCAAGACAAGG
RIPa	BamHI (3')	TGGATCCTCATTTCTTCCACATTCCACTG
RIPa (RNAi)	XbaI (5')	ATCTAGAAGTCCCAGCTCTCGCAGCTGCAAG

Gene	Restriction site	Sequence
RlPa (RNAi)	SalI (3')	TGTCGACGTCTCCGCCACCTCCTCCTCGA
RlPaCC2	attB (5')	GCAGGCTCAATGCAGGACGACGCGAGAACG
RlPaCC2	attB (3')	GAAAGCTGGGTCTCATCATTTCTTCCACATTCCACTG
RlPb	XbaI (5')	TCTAGATATGCAGAACTCAAAAACC
RlPb	SalI (3')	AGTCGACCGGTCTCATGAGCT
RlPb	SpeI (5')	TACTAGTTTCATGCAGAACTCAAAAACCAGTAG
RlPb	EcoRI (5')	AGAATTCATGCAGAACTCAAAAACCAGTAG
RlPb	BamHI (3')	TGGATCCGGTCTCATGAGCTTCTTCAC
RlPbCC1	BamHI (3')	TGGATCCTCAGAGATTGACAAGCTGGCAC
RlPbCC1	SalI (3')	TGTCGACTCAGAGATTGACAAGCTGGCA
RlPbVa	EcoRI (5')	AGAATTCTCAGCAGCAGAGGAGTCC
RlPbVa	XbaI (5')	ATCTAGATATGTCAGCAGCAGAGGAGTCC
RlPbVa	BamHI (3')	TGGATCCTCATTCGCTCAGCCCGTCTG
RlPbVa	SalI (3')	TGTCGACTCATTCGCTCAGCCCGTCTG
RlPbCC2	EcoRI (5')	AGAATTCGAAATGCAGCCGGAGC
RlPbCC2	XbaI (5')	ATCTAGACGAAATGCAGCCGGAGC
RlPb	attB (5')	GCAGGCTCAGGAATGCAGAACTCAAAAACCAGTAG
RlPb	attB (3')	GAAAGCTGGGTCTCAGGTCTCATGAGCTTCTTCAC
RlPbCC1Va	attB (3')	GAAAGCTGGGTCCTCATTCGCTCAGCCCGTCTG
RlPb (RNAi)	(5')	ATCTAGACAGAGGCACGAAGGTGCCAAGCAC
RlPb (RNAi)	(3')	TGTCGACCTTCAGGCATTCTTGCAACCGGGC
RlPc	XbaI (5')	TCTAGATATGCCGAGATCCAG
RlPc	PstI (3')	TCTGCAGTCACCTTCACTTGTTGCCC
RlPc	EcoRI (5')	AGAATTCATGCCGAGATCCAGGGGGTC
RlPc	BamHI (3')	TGGATCCGGTTGTTGTCAGTCACCTTCAC
RlPc	SpeI (5')	TACTAGTGATATGCCGAGATCCAGG
RlPc	attB (5')	GCAGGCTCAGGAATGCCGAGATCCAGGGG
RlPc $\triangle$stop	attB (3')	GAAAGCTGGGTCTCCCTTGTTGCCCTTCTTCTTCC
RlPcCC2	attB (3')	GAAAGCTGGGTCTCAACCTTCACTTGTTGCCCT
RlPcCC2	attB (5')	GCAGGCTCAGAAATGGAGAGCCCGGAG
RlPc (RNAi)	XbaI (5')	ATCTAGAAGGGAACAGCTCGTGTCTGCGGAG
RlPc (RNAi)	SalI (3')	TGTCGACGAGCTCCGCATTGTCGGCCGTGA
CARI	XbaI (5')	ATCTAGAGAGGAGCTACATACATACAAG
CARI	SalI (3')	TGTCGACGTCACTTGGCGTCGGCTTCG
CARI	SpeI (5')	AACTAGTAGATCCGTCCATCAGAGGATG
CARI	attB (5')	GCAGGCTCACATCAGAGGATGGAAGACGGG

Gene	Restriction site	Sequence
CARI	attB (3')	GAAAGCTGGGTCTCCCTTGGCGTCGGCTTCG
COSTARS (RNAi)	(5')	TCGGAGAAGAAACCGGCGAG
COSTARS (RNAi)	(3')	AGACTTGCCGGTGTTGCAAA
COSTARS	XbaI (5')	ATCTAGAGAAACCGGCGAGG
COSTARS	SalI (3')	TGTCGACTCAAGCATCAGCCACCG
SYT7 (RNAi)	(5')	GAGATGGGCGTAGTCAGCAC
SYT7 (RNAi)	(3')	ACCCGTAGGCCTTTGCAACA
δ-*COP* (RNAi)	(5')	TGCTGGCCATCGGTATCTGGA
δ-*COP* (RNAi)	(3')	GCCACTAACAAGAAACGGCAGT
KINESIN13A1	NcoI (5')	ACCATGGAGATGGCGCGGTGGCTGCA
KINESIN13A1	BamHI (3')	AGGATCCAGCGGGCATGCGCTCCT
KINESIN13A1-Cter	NcoI (5')	ACCATGGAAGAGCAGCCCACTGGACAGA
KINESIN13A2	NcoI (5')	ACCATGGatATGAACGCGAGCGGGCGCC
KINESIN13A2	BamHI (3')	AGGATCCGCGGGcatgcTCAAGGGCACT
KINESIN13A2-Cter	NcoI (5')	ACCATGGTGGCTGCTGCACCTTTACGA

2.23 Bioinformatics

Genes of interest were identified using the IPK Barley Blast Server (https://webblast.ipk-gatersleben.de/barley_ibsc/) with the 2016 genome annotation (Mascher et al., 2017). General sequence comparisons were performed with BLAST on NCBI (https://blast.ncbi.nlm.nih.gov/Blast.cgi). Secondary structure analyses were performed with the Simple Modular Architecture Research Tool (SMART, http://smart.embl-heidelberg.de/). For sequence searches in rice, the Sequence (BLAST) Tool was used on the Rice Genome Annotation Project website (http://rice.plantbiology.msu.edu/index.shtml). Protein and DNA alignments were created with Clustal Omega (https://www.ebi.ac.uk/Tools/msa/clustalo/) in Jalview v2.11.0 (Waterhouse et al., 2009) and phylogenetic trees were designed with PhyML v3.0 (http://www.atgc-montpellier.fr/phyml/; Guindon et al. (2010)) in SeaView v4 (http://doua.prabi.fr/software/seaview; Gouy et al. (2009)).

3 Results

3.1 Identification of RIP proteins in barley

BLAST searches identified three genes coding for ROP INTERACTIVE PARTNER (RIP) proteins in the barley genome (2016 assembly, Mascher et al. (2017)). Predicted RIP proteins contain a C-terminal QWRKAA motif and a QDEL motif at the N-terminus, both of which were described previously for RIP proteins of *A. thaliana* (Lavy et al., 2007). Although the first glutamate in the QEEL motif of Arabidopsis RIPs was exchanged to an aspartate (QDEL) in barley, the similar chemical properties of both amino acids may not result in a change in functionality. Since there were no clear orthologies between the previously described Arabidopsis RIPs and the identified barley RIPs, we named them RIPa (HORVU3Hr1G087430), RIPb (HORVU1Hr1G012460) and RIPc (HORVU3Hr1G072880). Over all, HvRIPs share little sequence similarity outside of the QWRKAA and QDEL motifs (Fig. 3A, $\sim$30%). Additionally, all RIPs have a lysine-rich C-terminus. Data from Li et al. (2008) show that C-terminal lysine residues are important for membrane localization of AtRIP1 (At1g17140). In order to get an overview of the protein family, I ran extended BLAST searches for RIP proteins in the monocots rice (*Oryza sativa* ssp. *japonica*) and *Brachypodium distachyon*. In both species, like in barley, I identified three RIP proteins (*Osj*: LOC_Os01g61760.2, LOC_Os05g03120.1, OsJ_03509; *Bd*: BRADI_2g54177v3, BRADI_2g50317v3, BRADI_2g37920v3).

Alignment of the amino acid sequences of RIPs from barley, rice, Brachypodium, and Arabidopsis (Supp. Fig. S1), support the phylogenetic tree in Fig. 3B. All three RIP proteins from barley share a branch with each one RIP protein from rice and Brachypodium, which points to a possible conserved functionality between monocot RIPs. On the other hand, RIP proteins from Arabidopsis are located on separate branches of the phylogenetic tree. AtRIP2 (At2g37080), AtRIP3 (At3g53350), and AtRIP5 (At5g60210) seem to be closer in their sequence to barley RIPa and RIPb and their respective orthologs from rice and Brachypodium, while AtRIP1 (At1g17140) and AtRIP4 (At1g78430) seem to be closer related to the RIPc branch. However, no clear orthology is presented between Arabidopsis and monocot RIPs.

Analysis of transcript abundance by semiquantitative PCR (sqPCR) showed that barley *RIPb* and *RIPc* are both transcribed in whole leaves and epidermal strips of barley leaves (Fig. 3C), with *RIPb* showing consistently higher transcription. Only a very faint band of *RIPa* was observed in leaves and the epidermis in particular. Each lane of *RIPa* also displays a light band below the 100bp mark of the ladder. These might be the unprocessed primers. *RIPa* transcript was however detected in barley roots

(Supp. Fig. S2). When challenged with *Bgh*, transcription levels of *RIP* genes did not change in an observable manner. I used the housekeeping gene *Ubiquitin-conjucating enzyme E2* (*HvUbc*) as control, which also showed no change in transcription levels in inoculated plants, compared to non-inoculated.

3.2 RIPs show distinct intracellular localization patterns

The intracellular localization of proteins can give hints about their function within the cell. Therefore, I transiently expressed YFP and GFP fusion proteins of HvRIPs in single epidermal cells of barley leaves by biolistic transformation and imaged these proteins by confocal laser scanning microscopy (CLSM). The fusion proteins are all expressed with an CaMV35S promotor and are visible under the confocal microscope after several hours. Additionally, cytosolic mCherry was expressed as a marker. All RIPs show specific localization patterns. YFP-RIPa localizes to the cytosol as well as agglomerates, visible as speckles close to the cell periphery (Fig. 4A, left hand panel). These agglomerates were more or less stationary, which indicates that these are most likely not vesicles. YFP-RIPb localizes mostly to the cytosol, but also to a lesser degree to the cell periphery (presumably the plasma membrane) and linear threads, resembling microtubules (Fig. 4A, center panel). RIPc localizes to the cytosol, but also to what seem to be microtubules, similar to RIPb (Fig. 4A, right hand panel). However, I observed the microtubule localization only when RIPc was expressed with a C-terminal tag in barley. An N-terminal tag resulted exclusively in cytosolic localization, indicating that the tag might interfere with the microtubule localization. The position of the tag had no influence on the localization of RIPa and RIPb.

To further analyze the localization of RIPb, I co-expressed specific intracellular markers with YFP-RIPb. In order to identify the threads, I co-expressed the microtubule marker RFP-MAGAP1-Cter, as well as free CFP as a cytosolic marker (Fig. 4B). RFP-MAGAP1-Cter comprises the C-terminal 165 amino acids of MAGAP1, but was shown to have no effect on fungal penetration success. It was thus considered a microtubule marker that does not interfere with ROP signaling (Hoefle et al., 2011). The signal profile over a linear region of interest (ROI) of a single XY section of the z-stack (Fig. 4C) supports the notion that RIPb localizes to microtubules since the YFP profile shares signal peaks with the microtubule marker. These peaks do not appear in the profile of cytosolic CFP (Fig. 4C, graphs at right hand side). In order to test whether the localization of YFP-RIPb in the cell periphery coincides with plasma membrane, the plasma membrane marker pm-rk was co-expressed (Nelson et al., 2007; Weis et al., 2013). Both YFP-RIPb and the mCherry-tagged pm-rk show some

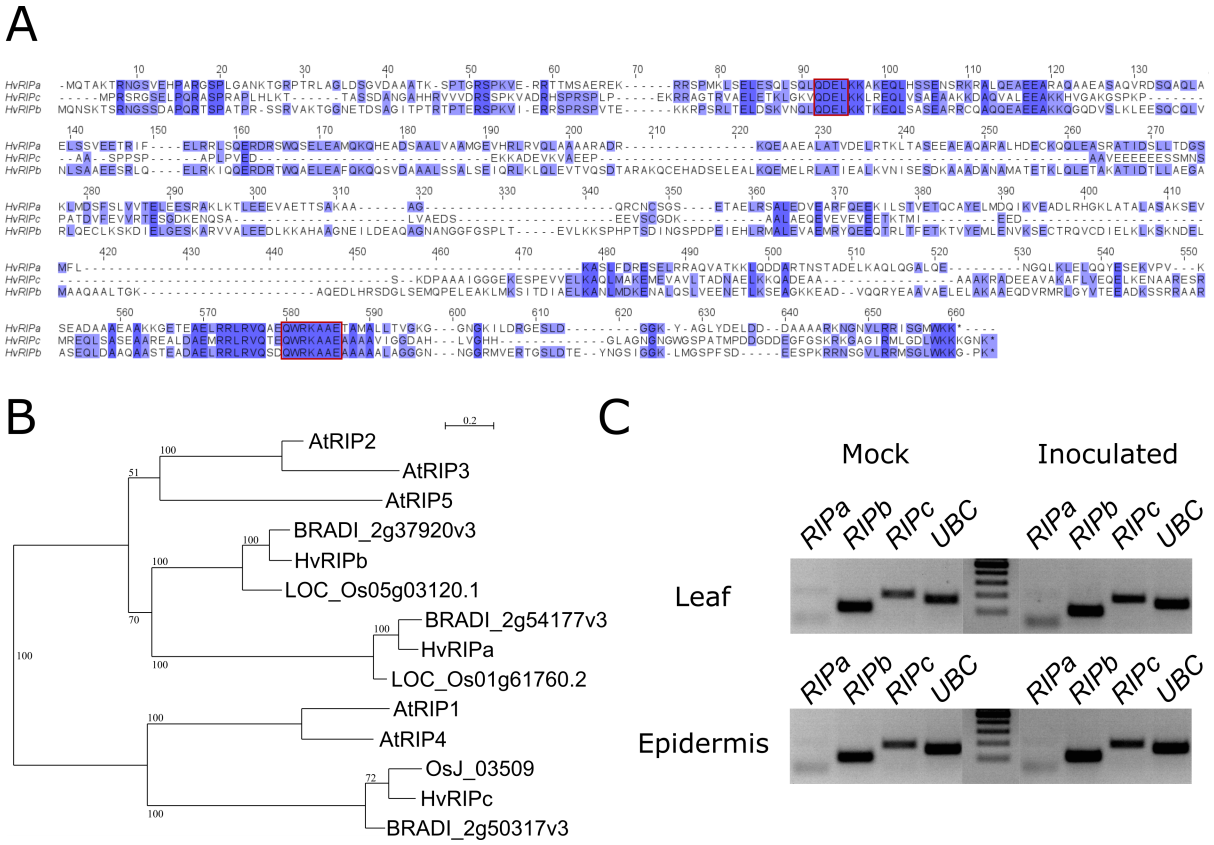

Figure 3: Phylogenetic analysis and expression of barley RIP proteins. Alignment of amino acid sequences of RIP proteins from barley (HvRIPa, HvRIPb, HvRIPc) (A). The red rectangles mark the conserved QDEL and QWRKAA motifs. B) shows the phylogenetic relation between the three barley RIPs, the five RIPs from Arabidopsis (AtRIP1, AtRIP2, AtRIP3, AtRIP4, AtRIP5), three identified rice RIPs (LOC_Os01g61760.2, LOC_Os05g03120.1, OsJ_03509) as well as three identified RIPs from Brachipodium (BRADI_2g54177v3, BRADI_2g50317v3, BRADI_2g37920v3). Semiquantitative PCR (C) of barley *RIP* transcripts in whole leaves and the epidermis of barley leaves in samples inoculated or not inoculated with *Bgh*. As a control, the constitutively expressed housekeeping gene *HvUBC* was used. Same amounts of cDNA were used for sqPCR reactions and an identical amount of PCR product was used for electrophoretic separation. Expected amplicon sizes are 209bp for *RIPa*, 109bp for *RIPb*, 188bp for *RIPc*, and 156bp for *UBC*. The lowest band of the ladder corresponds to 100bp, the second lowest band corresponds to 200bp.

co-localization though it is not complete. Measurements over a linear ROI confirm, that the YFP-RIPb signal co-localizes with pm-rk but extends further into the cytosol (S5A, experiments by Dr. Stefan Engelhardt).

3.3 RIPs can interact with barley RACB

After identifying RIPs in barley, I examined them for their interaction with ROP G-proteins. All RIP proteins contain the QWRKAA motif in their sequence, which is reported to be necessary for ROP interaction (Lavy et al., 2007). Since I was interested in downstream interactors of the susceptibility factor RACB, I tested the interaction of RIPa, RIPb, and RIPc with the typeI ROP RACB in yeast-two-hybrid. Additionally, I tested the interaction with the typeII ROP RAC1 to account for interaction specificity (Fig. 5). Next to the wild-type versions of the G-proteins, I also tested the interaction with the constitutively activated (CA) variants (RACB-G15V, RAC1-G23V) and the dominant negative (DN) variants (RACB-T20N, RAC1-T28N). The mutations in the CA variants prevent the hydrolysis of GTP, which keeps the G-protein in an activated signaling state, while the mutations in DN variants prevent the release of GDP and therefore keep the protein in an inactive signaling state. Since active ROPs get modified by prenylation (type I) and palmitoylation (type II) at their very C-terminus for membrane localization (Lavy et al., 2002), the sequences of all ROP variants used in the yeast-two-hybrid were stopped right before the respective motif (RACB-$\triangle$CSIL; RAC1-$\triangle$CGSSCFA) to not interfere with the necessary nuclear localization in yeast. This should not interfere with their ability to interact with other proteins.

In yeast-two-hybrid experiments, the yeast strain used was auxotroph for leucine, tryptophan, histidine, and adenine. Introduced into a bait (pGBKT7) or prey (pGADT7) plasmids, the two proteins of interest are fused to one half of the GAL4 transcription factor, the DNA binding domain (BD) and the activation domain (AD), respectively. Additionally, the two plasmids express either the *TRP1* gene, which allows the synthesis of tryptophan, or the *LEU2* gene for leucine synthesis. This allows selection of transformed yeast cells on medium lacking leucine and tryptophan. Two interacting proteins of interest result in reconstitution of the GAL4 transcription factor, which leads to expression of GAL4. GAL4 then induces the expression of reporter genes *HIS3* and *ADE2* leading to synthesis of histidine and adenine. This allows selection of interaction on medium lacking histidine or adenine.

Co-expression of RIPa (Fig. 5A), RIPb (Fig. 5B), or RIPc (Fig. 5C) with CA RACB and wild-type RACB led to yeast growth on QDO plates (-Leu -Trp -Ade - His), indicating interaction between two proteins. The same was true for CA RAC1 and wild-type

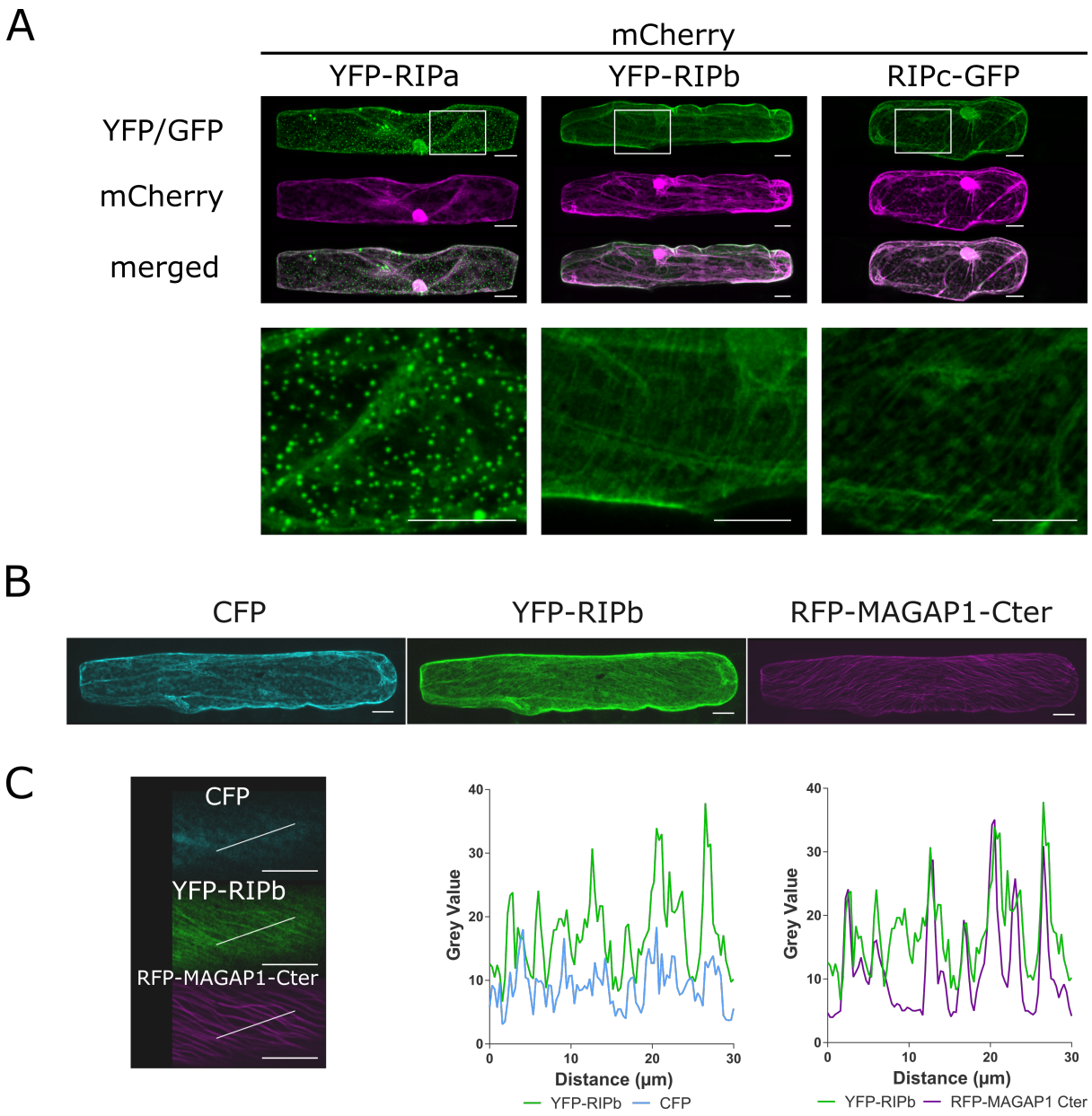

Figure 4: Subcellular localization of RIP proteins. YFP and GFP-tagged barley RIPs (YFP-RIPa, YFP-RIPb, RIPc-GFP), respectively (A). Plasmids coding for fluorophore tagged proteins were introduced into barley epidermal cells by biolistic transformation. Images were taken 24 hours after bombardment (hab). Cytosolic mCherry served as a transformation marker. Images show z-stacks of XY optical sections of the upper half of the cells. The bottom side images show magnifications of the section in the white box in the upper images. RIPb localizes to the microtubule cytoskeleton (B). YFP-RIPb was co-transformed with the microtubule marker RFP-MAGAP1-Cter and cytosolic CFP as transformation marker. The left hand side panel in C) shows a magnification of a single XY section of the image in B). The graphs on the right hand side in C) show the fluorescence profile of CFP compared to YFP, and YFP compared to RFP over the linear ROI (white line) in the panel on the left hand side. Scaling bars in the bottom right corner of each channel indicates 20µm.

RAC1. No yeast growth was obtained from co-expression with DN RACB and DN RAC1, which indicates that there should be no interaction. Also no growth was obtained when yeast was transformed with bait, or prey plasmids and the corresponding empty vectors (EV), showing that yeast growth was not due to auto-activation of reporter gene expression. This suggests that all RIPs of barley interacted with RAC1 as well as RACB in yeast. Since the wild-type ROPs can switch between active and inactive state, it is most likely that RIP proteins interact with activated ROPs. Immunoblotting results from a different yeast-two-hybrid assay, which gave the same results for the interaction between RIPs and RACB, show that all RACB variants and all RIPs are expressed in yeast (Supp. Fig. S3). This means the non-interaction with DN RACB is most likely not due to a lack of expressed protein. For this western blot, I used HA and Myc-tags encoded in the pGADT7 and pGBKT7 plasmids, respectively, in between the GAL4 domains and the protein of interest. Expressed proteins were extracted from yeast and separated by SDS-PAGE.

To confirm the interaction with RACB *in planta*, I also performed bimolecular fluorescence complementation (BiFC). Single epidermal cells were transformed with plasmids encoding split-YFP fusion proteins with the N-terminal part (nYFP), or the C-terminal part (cYFP) of YFP. nYFP-RIPa, nYFP-RIPb, or nYFP-RIPc were co-expressed with cYFP-CA RACB or cYFP-DN RACB. Excitation of the separated split YFP truncations should only lead to background fluorescence at most, whereas two proteins interacting should result in YFP fluorescence due to the two parts of YFP complementing. I took images of transiently transformed cells 24 to 48 hours after bombardment (hab) by CLSM. Confirming the results of the yeast-two-hybrid, YFP signal was restored for all co-expressions of RIPs with CA RACB. On the other hand, co-expression with DN RACB resulted in weak background fluorescence. Signal quantification and normalization showed that the restored YFP signal was significantly stronger on average when RIPs were co-expressed with CA RACB, than with DN RACB (Fig. 6A, B, C, right hand side).

The interaction between RIPa and CA RACB seems to occur exclusively at filamentous structures, most likely microtubules (Fig. 6A). This differs clearly from the intracellular localization of RIPa when expressed alone, which was mainly in the cytosol and in speckle-like agglomerates close to the cell periphery (Fig. 4A, left hand side panel). This is supported by recruitment experiments in which YFP-RIPa was expressed together with untagged CA RACB or DN RACB and the cells were imaged by CLSM (Supp. Fig. S4, experiments by Dr. Caroline Höfle). Co-expression with DN RACB resembled the localization pattern of YFP-RIPa alone, while co-expression with CA RACB resulted in a shift in localization to the cell periphery, presumably the plasma

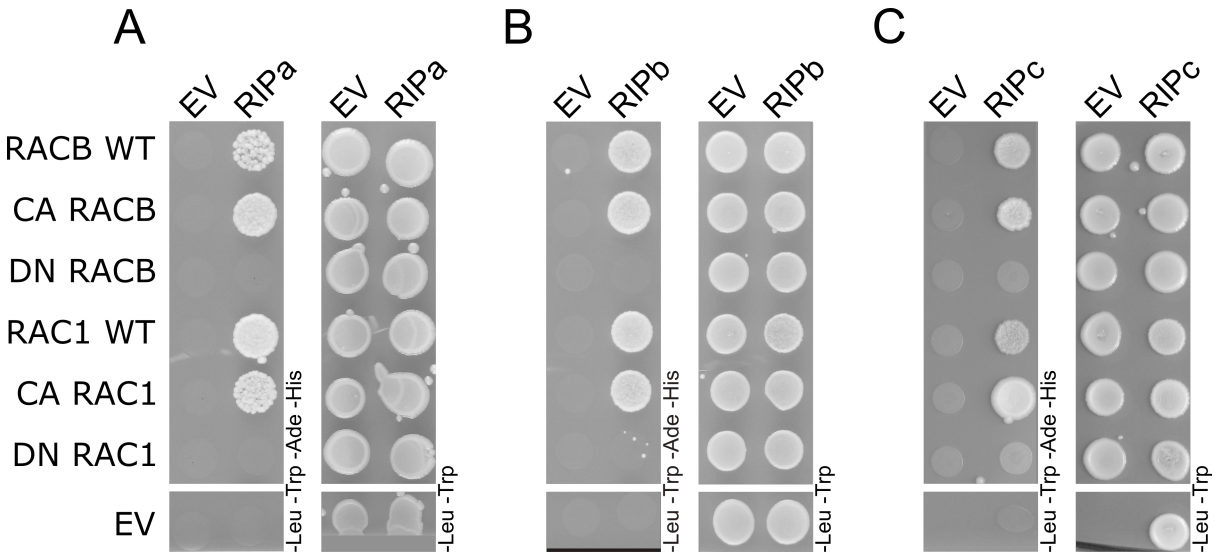

Figure 5: Barley RIP and ROP proteins can interact in yeast. RIPa (A), RIPb (B), and RIPc (C) were tested in a yeast-two-hybrid assay for their interaction with wild-type (WT), constitutively activated (CA), and dominant negative (DN) RAC1 and RACB. As control, all constructs were tested against the respective empty vector (EV). As transformation control, yeast was dropped on SD medium without leucine (-Leu) and tryptophan (-Trp). For the selection of positive interactions SD medium additionally lacking adenine (-Ade) and histidine (-His) was used.

membrane, and microtubules. Similar results were obtained by co-expression of CA RAC1 and DN RAC1 (Supp. Fig. S4, Experiments by Dr. Caroline Höfle). Hence, co-expression of a ROP G-protein changes the localization of RIPa, which, considering the results from Y2H and BiFC, strongly suggests that RIPa and the two G-proteins interact *in planta*. Additionally, I co-expressed YFP-RIPa with CFP-CA RACB and compared the localization pattern of both fusion proteins (Fig. 7B). Both proteins were found at what appears to be the microtubule cytoskeleton. In combination with BiFC experiments and Y2H these results suggest, that over-expressed RIPa localizes in agglomerates close to the cell periphery and the cytosol. Upon G-protein interaction with RACB, it appears to be recruited to the microtubule cytoskeleton where both proteins directly interact. A similar pattern seems to occur upon interaction with RAC1. Although I have less data for the latter interaction, Y2H and recruitment experiments indicate, that both proteins are able to interact. This is supported by BiFC experiments, in which RIPa interacted with RAC1 at microtubules as well (Hoefle et al., 2020).

Interaction of RIPb and CA RACB in BiFC was observed at the cell periphery and at microtubules. Here, the microtubule localization occurred in only about 50% of the investigated cells (Fig. 6B). In the rest of the cells, the interaction occurred only in the cell periphery. Recruitment experiments resulted in similar results. The localization

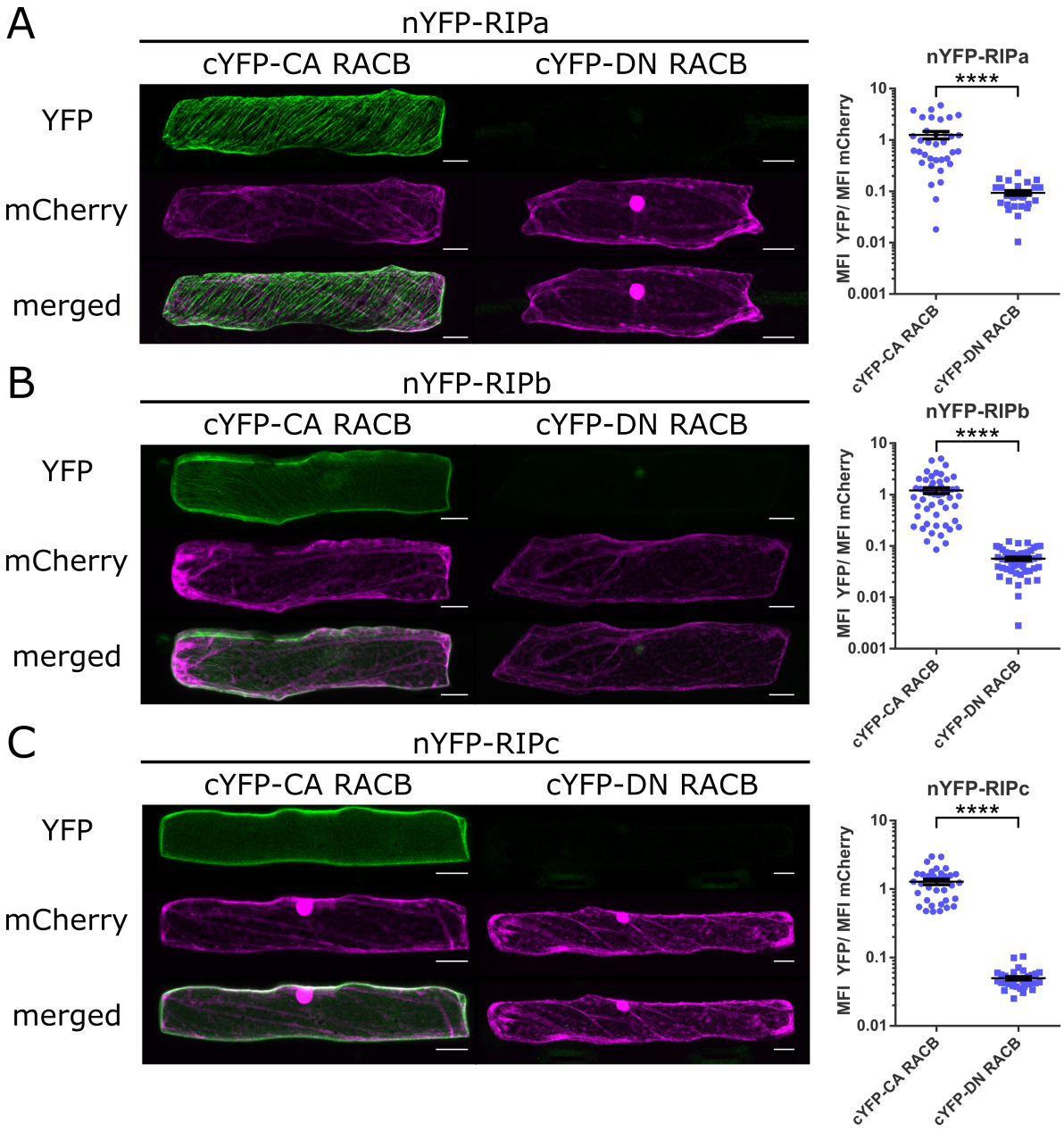

Figure 6: Interaction between RIP proteins and RACB *in planta*. Interaction of RIPa (A), RIPb (B), and RIPc (C) with RACB was tested in BiFC experiments by introducing a split-YFP-tagged (nYFP, SPYNE) RIP fusion protein as well as a split-YFP-tagged (cYFP, SYPCE) fusion protein of CA RACB and DN RACB, respectively, into single epidermal cells of barley leaves by biolistic transformation. Images were taken 24 hab and show z-stacks of XY optical sections of upper half of the cells. mCherry was co-transformed as a transformation marker and internal reference. Scaling bars represent 20µm. Mean Fluorescence Intensity (MFI) was measured over a linear ROI in the cell periphery of a single XY optical section in at least 35 cells. Graphs on the right hand side show the ratios between YFP and mCherry signal in every measured cell. Stars represent significance by to Student's t-test $p<0.0001$. Image brightness was increased for displaying purposes identically for CA RACB and DN RACB combinations. Measurements of intensities were made on the original data.

of RIPb shifted away from the cytosol towards the cell periphery, when co-expressed with CA RACB or CA RAC1 (Fig. 7A). Co-expression with DN RACB or DN RAC1 resulted in more cytosolic localization of YFP-RIPb, as it was observed when YFP-RIPb was expressed alone. As mentioned above, YFP-RIPb showed partial signal overlay with the plasma membrane marker pm-rk (Supp. Fig. S5A). Additional co-expression of CA RACB resulted in a more complete overlap of the YFP-RIPb signal and the mCherry signal of pm-rk (Supp. Fig. S5B), supporting the impression that the RIPb localization shifts to the plasma membrane. Although YFP-RIPb also localized to the microtubules alone, at this point it cannot be concluded, whether this localization is due to the intrinsic ability of RIPb to localize to microtubules, or if the interaction with endogenous G-proteins results in this localization. Interestingly, co-expression with wild-type RACB or RAC1 resulted in similar localization to co-expression with the CA variants (Fig. 7A). Co-expression of YFP-RIPb with CFP-CA RACB resulted in strong co-localization of both proteins at microtubules and the cell periphery (Fig. 7B), again mirroring the results from BiFC and recruitment experiments. The change of RIPb localization in combination with a G-protein is difficult to pinpoint. It seems that RIPb by itself localizes to microtubules and the plasma membrane. It might then either recruit the G-protein to microtubules, or gets recruited by the G-protein even stronger to the plasma membrane. However, further investigations need to be made before any conclusions can be drawn.

RIPc seems to interact with RACB exclusively at the cell periphery, presumably the plasma membrane, in BiFC experiments (Fig. 6C). However, it should be mentioned it is possible that the N-terminal tag of the BiFC construct masks a microtubule localization, which was observed when RIPc was expressed alone with a C-terminal GFP tag (Fig. 4A, right hand side panel). However, this localization completely coincides with the results from recruitment experiments where I observed a shift in localization to the cell periphery when YFP-RIPc is co-expressed with untagged CA or wild-type RACB and RAC1 (Fig. 7A). Co-expression with DN RACB or RAC1 resulted in cytosolic localization, again differing from the localization of RIPc-GFP (Fig. 4 , right hand side panel), which was additionally found at microtubules. Co-expression of YFP-RIPc with CFP-CA RACB lead to co-localization of both proteins in the cytosol and at the cell periphery (Fig. 7B). There is a clear shift in localization of RIPc to the cell periphery, presumably the plasma membrane, when G-proteins are co-expressed. It can, however, not be excluded that there is also an undetected microtubule localization of the RIPc – ROP complex, because of the N-terminal tags used in these experiments and their apparent effect on microtubule localization of RIPc.

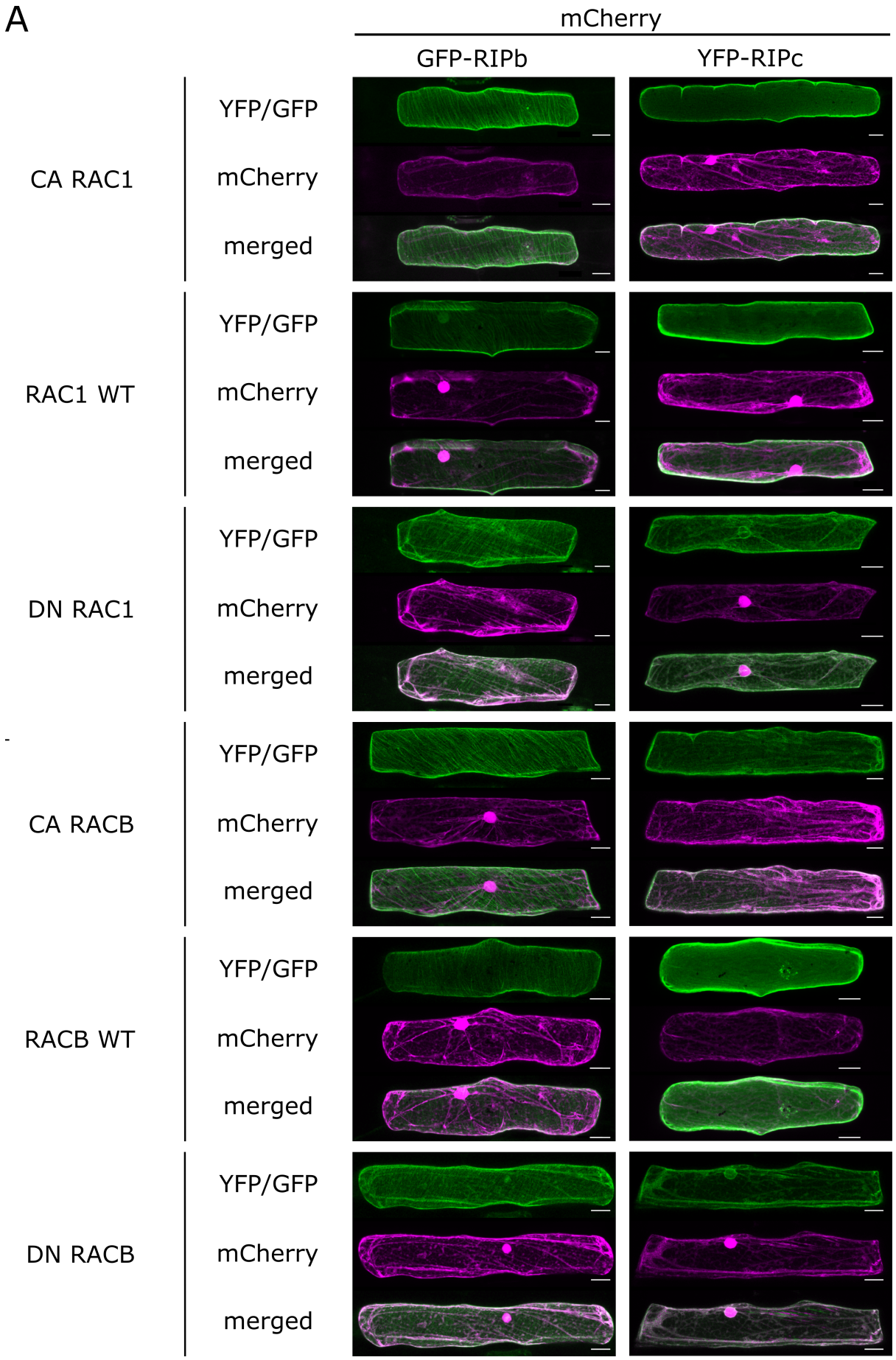
A
mCherry
GFP-RIPb
YFP-RIPc
CA RAC1
YFP/GFP
mCherry
merged
RAC1 WT
YFP/GFP
mCherry
merged
DN RAC1
YFP/GFP
mCherry
merged
CA RACB
YFP/GFP
mCherry
merged
RACB WT
YFP/GFP
mCherry
merged
DN RACB
YFP/GFP
mCherry
merged

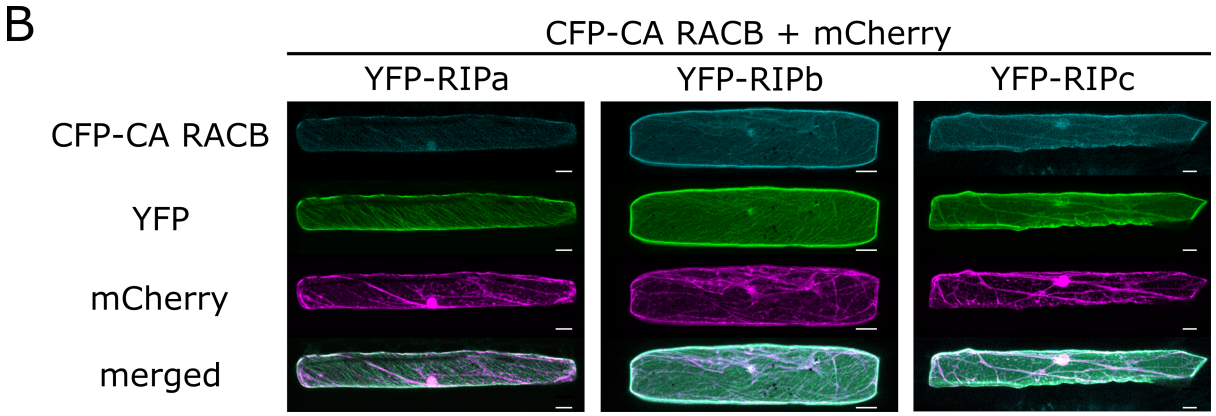

Figure 7: Intracellular recruitment of RIP proteins by ROPs of barley. Single epidermal cells of barley leaves were transiently transformed by biolostic transformation. GFP-RIPb and YFP-RIPc show different localization patterns (A) when co-expressed with either RAC1 or RACB in different states of activity (CA, WT, DN). Images were taken 24-48 hab and show z-stacks of XY optical sections of upper half of the cells. RIPs co-localize with CA RACB (B). YFP-tagged RIP fusion proteins were introduced into single epidermal cells by biolistic transformation together with CFP-CA RACB and mCherry as a transformation marker. Images were taken 24-48 hab and show z-stacks of XY optical sections of upper half of the cells. Scaling bars represent 20µm. Image brightness was increased for displaying purposes.

3.4 Influence of RIPs on penetration success of *Bgh*

Since all RIP proteins of barley seem to be able to interact with the susceptibility factor RACB *in planta*, I wondered whether RIPs might also influence the interaction of barley with *Bgh*. RACB was shown to influence penetration success of *Bgh* and establishment of the haustorium (Schultheiss et al., 2002). I therefore introduced either over-expression or RNAi silencing constructs into single epidermal cells of barley by particle bombardment. Afterwards, I inoculated the leafs with powdery mildew conidia and determined the penetration rate of *Bgh* into the transformed cells. At early time points, about 24 hours after inoculation, the interaction either ended in an established haustorium or in papilla formation beneath the appressorium. The penetration rate was calculated as the percentage of cells with established haustoria, among all attacked cells. As negative control the respective empty vector was introduced.

Individual silencing of *RIPa*, *RIPb*, and *RIPc* had a comparable effect on the penetration rate (Fig. 8A). All showed an average increase of about 20% compared to the control. Cells expressing a *RIPb* silencing construct, showed a tendency towards increased susceptibility, but did not create reproducible results. Silencing of *RIPa* and *RIPc* resulted in higher reproducibility, but due to the high variation between the ex-

periments, did not result in a statistically significant effect. In all experiments, silencing of *RIPa* resulted in an at least slightly higher susceptibility of barley to *Bgh*. The penetration rate into transformed cells was between 9% and 40% higher, compared to the empty vector control. Similar results were obtained for *RIPc*, were 5 out of 6 experiments resulted in a slight increase in penetration rate of 10% to 55%.

In order to properly evaluate the observed effects of gene silencing, it is important to measure silencing efficiencies of the introduced constructs. Since it is not possible to measure protein levels of endogenous RIPs in single transformed cells, I co-expressed the RNAi plasmids with GFP tagged over-expression constructs of the respective gene and measured GFP fluorescence in transformed cells. I compared these signals to control cells transformed with the empty RNAi plasmid (pIPKTA30N) and the GFP constructs. Silencing of RIP proteins should result in decreased GFP fluorescence relative to cytosolic mCherry, which I used as a reference in each cell. The silencing efficiency over all was relatively weak. Silencing of *RIPa* had an efficiency of about 38% (Supp. Fig. S7). Similar results were obtained for *RIPb*, which showed a 45% signal reduction. Silencing of *RIPc* seems to have been the most efficient with about 90% measured signal reduction. Since the silencing for *RIPa* and *RIPb* was not very efficient I can not exclude that there might be a hidden effect of silencing these two genes, which was not observed in the penetration assay. It is possible that more efficient silencing or even knock-out might influence the interaction more strongly. Silencing of *RIPc* was quite efficient and the results are relatively reproducible. However, if RIPc negatively influences susceptibility, or positively influences defense, the effect seems to be rather weak.

More reproducible results were obtained when RIP proteins were over-expressed with a CaMV35S promotor construct. Over-expression of RIPa and RIPc had no effect on the penetration rate of *Bgh* conidia into transformed cells (Fig. 8B). In both cases the average penetration rate in the over-expressing cells was at the same level as the empty vector control. However, over-expression of RIPb led to an average increase of about 23%. This increase was consistent throughout all experiments and showed significance as indicated by Student's t-test (α=0.05). This qualifies RIPb as a potential mediator of susceptibility signaling downstream of RACB.

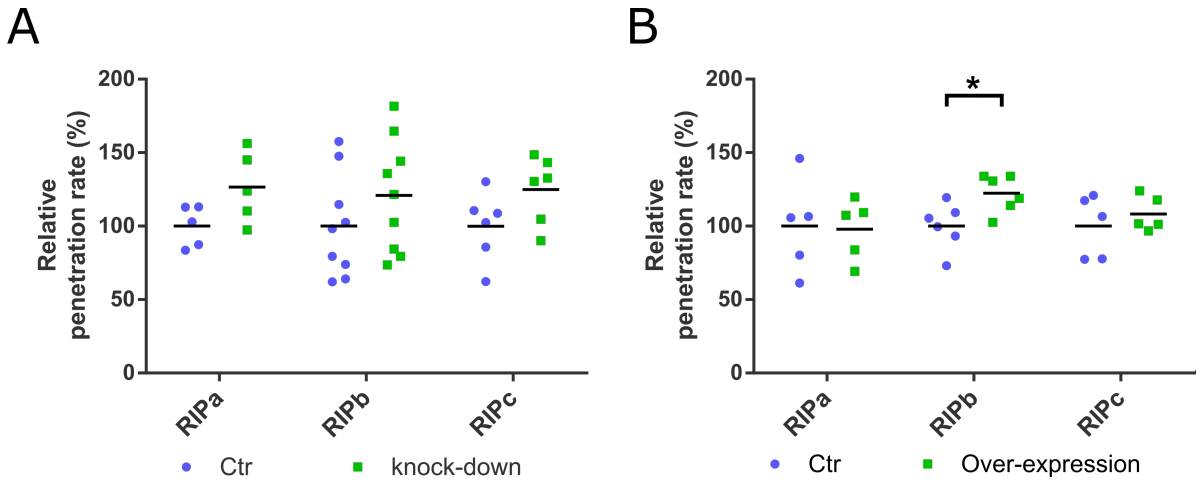

Figure 8: Effect of RIP proteins on susceptibility of barley to *Bgh*. RIPs were either knocked-down by RNAi silencing (A), or over-expressed with a CaMV35S promotor (B) in single epidermal cells after biolistic transformation. Dots represent individual experiments. Over-expression or silencing constructs were co-transformed with cytosolic GFP as transformation marker to identify transformed cells. Leaves were inoculated with *Bgh* 24 hab in case of over-expression and 48 hab in case of silencing. Cells transformed with the respective empty vector served as control (Ctr). Penetration rate was counted 24 hours after inoculation (hai) in at least 5 different experiments and at least 80 interactions were counted per construct. Penetration rate was calculated as the amount of penetrated cells among all attacked cells. For the relative penetration rate the mean of all experiments of the respective control was set as 100% and all individual values were calculated relative to that. Star indicates significance relative to the respective control calculated with Student's t-test $p<0.05$.

3.5 Structure-function analysis of RIPb

The SMART tool (Schultz et al., 1998) was used for protein structure analysis of RIP proteins and RIPb in particular. All investigated RIP proteins consisted of an predicted N-terminal coiled-coil (cc) domain containing the QD/EEL motif as well as a C-terminal cc domain containing the QWRKAA motif (Fig. 9A). The same general structure was also shown for Arabidopsis RIP3/MIDD1 (Mucha et al., 2010). Based on these predictions, I created truncations of RIPb to further investigate domain functions of the protein. The N-terminal cc domain was predicted to range from AA71-129 according to SMART (Schultz et al., 1998), hence the fist truncation, which was designated as CC1 domain, spans AA1-132. The C-terminal cc domain was predicted to range from AA423-550, which is why the C-terminal truncation spans AA 420-612 and was termed CC2 domain. In between the CC1 and CC2 domain lies the variable region Va, which strongly differs between RIPs, but in case of RIPb also has two predicted cc domains (AA195-230, AA274-293). The Va domain used in this work spans from AA129-423 and was used either alone or fused to CC1 (CC1Va) or CC2 (VaCC2).

The truncations were first tested for their localization by transiently expressing YFP tagged fusion proteins in barley epidermal cells. Cytosolic mCherry was used as a transformation marker (Fig. 9B). The CC1 domain, as well as the Va domain exclusively localized to the cytosol. Interestingly, the longer CC1Va truncation containing the CC1 and the Va domain localized to the microtubules and the cytosol. However, the VaCC2 truncation, containing the Va and the CC2 domain did not localize to the microtubules. This suggests that the CC1 domain with the QDEL motif and the Va domain are both necessary for microtubule localization, but not sufficient. I also introduced mutations into the QDEL motif to find out whether it is important for microtubule localization of RIPb. I choose an aspartate to asparagine exchange (D85N) and additionally a glutamate to glutamine exchange (E86Q) in order to preserve the structure, but change the polarity of the amino acids. These mutations however, did not result in a loss of microtubule localization (Supp. Fig. S8), which suggests that this motif might not be involved in microtubule localization of RIPb, or the mutations were not sufficient to disrupt the function of this motif. Nevertheless, further experiments where I investigated the localization of the CC1 domains of all barley RIPs fused to a C-terminal GFP-tag, show that the CC1 domain of RIPb was the only one not localized to microtubules in the majority of cells. RIPbCC1 showed weak microtubule localization only in 1 out of 10 cells, while in case of RIPaCC1 (AA1-136) it was 11 out of 15 cells, and for RIPcCC1 (AA1-109) 6 out of 10 cells (Supp. Fig. S9). This strongly indicates that in all RIPs the CC1 domain is important for microtubule localization, but in RIPb also the Va domain seems to be necessary. The VaCC2 and CC2 truncation of RIPb appear to localize to the cell periphery next to the cytosol, which was also observed for full length RIPb. The very C-terminus of RIPb contains a lysine-rich region (Fig 3A). This region was reported to be involved in membrane localization of other RIPs in Arabidopsis, which would explain this localization pattern (Li et al., 2008). Similar to full length RIPb, YFP-RIPbCC2 showed partial overlap with the plasma membrane marker pm-rk in co-localization experiments (Supp. Fig. S5C, experiments by Dr. Stefan Engelhardt), indicating that the CC2 domain of RIPb is sufficient for membrane localization of RIPb.

According to literature, the QWRKAA motif in the C-terminal cc domain (CC2) of RIPs is necessary for ROP interaction (Lavy et al., 2007). To see if this holds true for RIPb, I tested the truncations in yeast-two-hybrid experiments against CA RACB. As observed before, yeast growth on QDO plates was obtained for the combination of full length RIPb and CA RACB (Fig. 9C). Next to the full length protein, co-expression of CA RACB with the two truncations containing the CC2 domain (RIPbVaCC2, RIPbCC2) and hence the QWRKAA motif also led to yeast growth, indicating interaction.

No yeast growth was observed from co-expression of the corresponding empty vector, or the truncations lacking the CC2 domain (CC1, CC1Va, Va). Furthermore, in a different experiment double mutations of Q540L and W541G in the QWRKAA motif led to a complete abolishment of yeast growth in combination with wild-type RACB and CA RACB (Supp. Fig. S10), indicating a loss of interaction between RIPb-Q540L-W541G and RACB. Interaction between RIPbCC2 and CA RACB was also confirmed by ratiometric BiFC experiments. YFP signal was restored when RIPbCC2 was co-expressed with CA RACB, but not with DN RACB (Fig. 10A). Quantification of at least 30 cells per interaction showed strong differences in YFP signal between the two combinations (Fig. 10A, right hand side). The interaction between RIPbCC2 and CA RACB appears to exclusively take place at the plasma membrane (Fig. 10A, left hand side). This fits to the localization of YFP-RIPbCC2 (Fig. 9B) and previously published results, which showed activated RACB to be localized to the plasma membrane (Schultheiss et al., 2003). Recruitment experiments with the plasma membrane marker pm-rk showed again that the partial overlay of YFP-RIPbCC2 (Supp. Fig. S5C) shifts to a complete overlay in presence of CA RACB (Supp. Fig. S5D). This shows, in accordance with the results for YFP-RIPb, that the CC2 domain, just as full length RIPb, gets recruited to the plasma membrane by RACB.

Since the CC1Va truncation lacks the QWRKAA motif and is hence not able to interact with RACB in yeast, RACB interaction seems to be unnecessary for microtubule localization of RIPb. This is also confirmed by recruitment experiments (Fig. 9E). RIPbCC1Va did localize to microtubules and co-expression with CA RACB did not lead to a change in localization. In contrast to YFP-RIPb, which is recruited away from the cytosol to the plasma membrane, as was observed before (Fig. 7A, S5). Both fusion proteins were present at microtubules, though (Fig. 9E).

Next to the interaction with RACB, I was also questioning whether RIPb can interact with itself and therefore potentially be able to form dimers or oligomers. I first tested the interaction in yeast-two-hybrid, where co-expression of full length RIPb in the bait and the prey plasmid led to yeast growth on QDO plates, indicating auto-interaction (Fig. 9D). Interestingly, all truncations containing the Va region (CC1Va, Va, VaCC2) were also able to induce yeast growth in combination with full length RIPb, suggesting that amino acids in this region are necessary for auto-interaction. No yeast growth was observed from co-transformation of the corresponding empty vector, or by co-expression of RIPb with the CC1 domain and the CC2 domain, respectively. In consideration of the results from Fig. 9B, where only RIPbCC1Va was localized to microtubules, this indicates that dimerization or oligomerization of RIPb might contribute to microtubule localization. The CC1 domain was necessary but not sufficient for microtubule local-

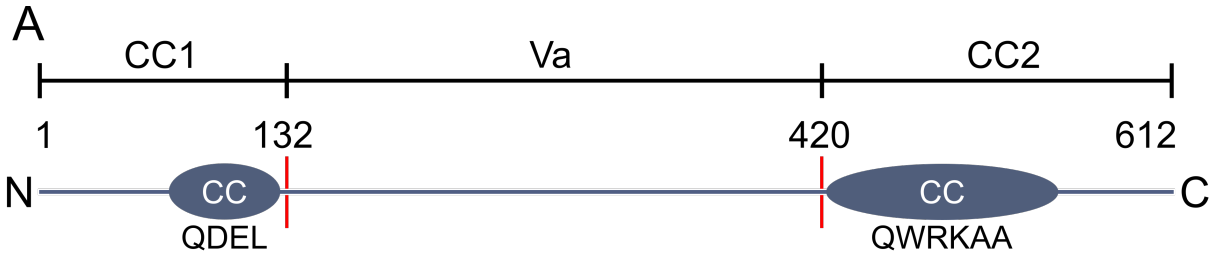
A
CC1
Va
CC2
1
132
420
612
N
CC
CC
C
QDEL
QWRKAA

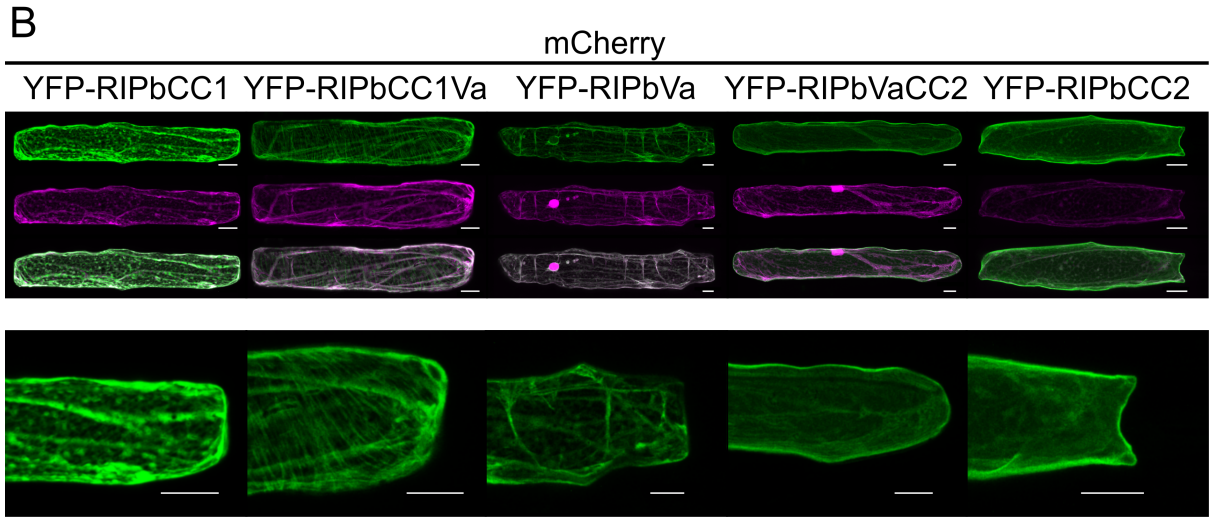
B
mCherry
YFP-RIPbCC1
YFP-RIPbCC1Va
YFP-RIPbVa
YFP-RIPbVaCC2
YFP-RIPbCC2

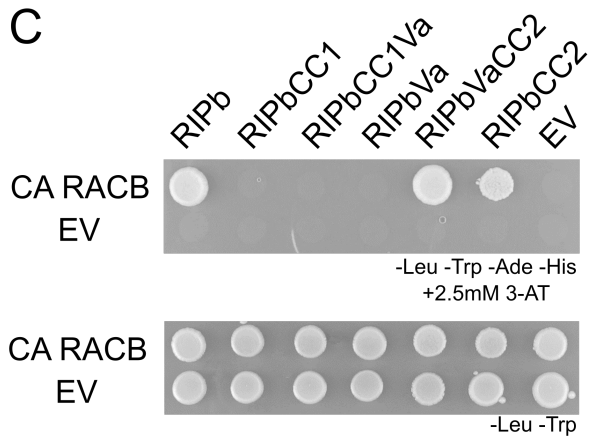
C
RIPb
RIPbCC1
RIPbCC1Va
RIPbVa
RIPbVaCC2
RIPbCC2
EV
CA RACB
EV
-Leu -Trp -Ade -His
+2.5mM 3-AT
CA RACB
EV
-Leu -Trp

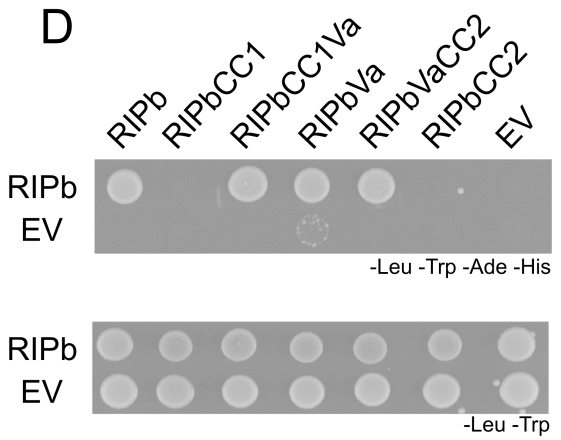
D
RIPb
RIPbCC1
RIPbCC1Va
RIPbVa
RIPbVaCC2
RIPbCC2
EV
RIPb
EV
-Leu -Trp -Ade -His
RIPb
EV
-Leu -Trp

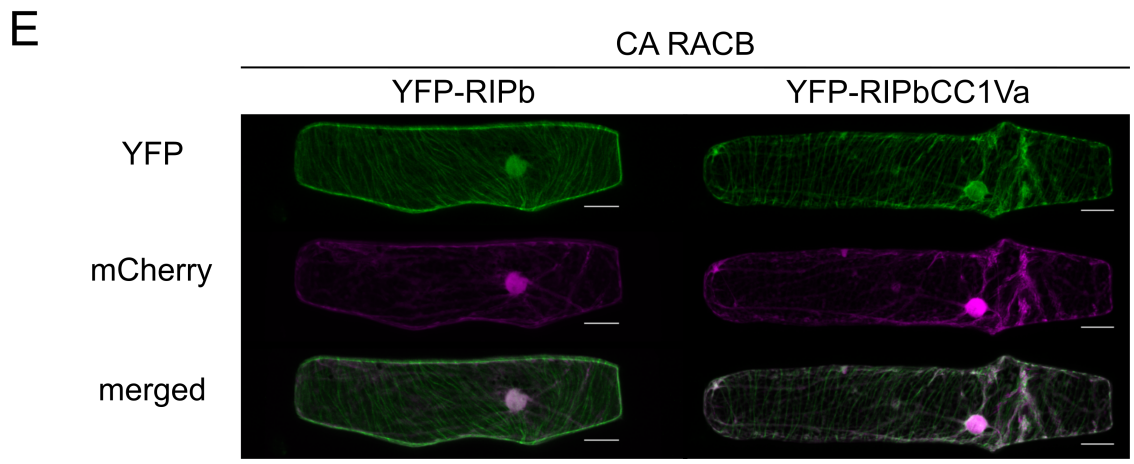
E
CA RACB
YFP-RIPb
YFP-RIPbCC1Va
YFP
mCherry
merged

Figure 9: Truncations of RIPb. RIPb was divided into three parts based on the predicted secondary structure (A). The CC1 domain contains the N-terminal coiled-coil domain with the QDEL motif. The CC2 domain contains the C-terminal coiled-coil domain with the QWRKAA motif. Both domains are connected by the variable domain (Va). Red lines symbolize cutting sites. Numbers represent the respective amino acid used as domain boundary. YFP fusions of five different truncations were expressed in single epidermal cells after biolistic transformation. RIPbCC1, RIPbVa, and RIPbCC2 contain only the respective domain. RIPbCC1Va and RIPbVaCC2 contain the N- and C-terminal domain together with the Va domain. mCherry was co-expressed as a transformation marker. The images on the bottom of B) show magnifications of the YFP channel in the respective upper images. Scaling bars represent 20µm. Images show z-stacks of XY optical sections of upper half of the cells. Truncations were tested in yeast-two-hybrid for their interaction with CA RACB (C) and RIPb (D). As a control, all constructs were tested against the empty vector (EV). For transformation control, yeast was dropped on SD medium without leucine (-Leu) and tryptophan (-Trp). For the selection of positive interactions, SD medium additionally lacking adenine (-Ade) and histidine (-His) was used. 2.5mM 3-AT were added to the medium if required to avoid unspecific interactions. YFP fusion proteins of full length RIPb and the RIPbCC1Va truncation were co-expressed with CA RACB and cytosolic mCherry as transformation marker (E). Scaling bars represent 20µm. Images show z-stacks of XY optical sections of upper half of the cells.

ization and only the CC1Va truncation was found at microtubules, which, according to the yeast-two-hybrid, should also be able to auto-interact. Auto-interaction of RIPb was also confirmed in BiFC. nYFP-RIPb co-expressed with cYFP-RIPb resulted in a strong restoration of YFP signal from transformed cells (Fig. 10B). The signal was almost exclusively found at the microtubule cytoskeleton, supporting the hypothesis that RIPb localizes to microtubules as an oligomer. As a negative control for the RIPb – RIPb interaction in BiFC, I co-expressed cYFP-RIPb with MAGAP1-nYFP, a described microtubule localized interactor of RACB, which is partially recruited to the plasma membrane by CA RACB (Hoefle et al., 2011). No YFP signal was restored when RIPb and MAGAP1 were co-expressed. However, when MAGAP1-nYFP was co-expressed with cYFP-CA RACB, YFP signal was again restored and signal quantification confirmed a much stronger signal from RIPb – RIPb and MAGAP1 – CA RACB interactions, compared to the MAGAP1 – RIPb interaction (Fig. 10B, C). To confirm that the structures observed in the RIPb – RIPb interaction were indeed microtubules, I again co-expressed the microtubule marker RFP-MAGAP1-Cter (Fig. 10E) with the two RIPb BiFC constructs. The intensity plot of the fluorescence profile over the linear ROI in Fig. 10F confirms that RIPb auto-interaction takes place at microtubules, since YFP

and RFP signal nicely overlap. Quantification of microtubule to cytosol signal ratio for RIPb, comparing YFP-RIPb and the BiFC signal, supports this as well. In different cells microtubule as well as cytosolic signal was measured and averaged. The microtubule to cytosol signal ratio was much higher for the BiFC complex, where the signal should only come from oligomeric RIPb, compared to YFP-RIPb, which should show signals derived from monomeric as well as oligomeric RIPb (Fig. 10D). This shows that relatively more signal was deriving from the microtubules than from the cytosol. Indeed the signal ratio was comparable to the one of the microtubule marker RFP-MAGAP1-Cter, suggesting that the RIPb oligomerization predominately takes place at microtubules.

3.6 Influence of RIPb truncations on susceptibility

To further analyze the functionality of the RIPb domains, I investigated the influence of the truncations on susceptibility of barley to penetration by *Bgh*. I therefore transiently over-expressed the truncations in single epidermal cells of barley leaves and evaluated the penetration rate of *Bgh* into these cells as it was done for full length RIPs (section 3.4). Over-expression of RIPbCC1 showed an increase in penetration rate of about 30% (Fig. 11A). This is a slightly stronger effect than the one for full length RIPb (Fig. 8B). Over-expression of RIPbCC2, which is able to interact with RACB, increased penetration rate even more by about 75%. This effect seems to be RIPbCC2 specific, since over-expression of the CC2 domain of RIPa (Fig. 11B) did not have such a strong effect. I chose RIPa for this experiment, since RIPa is phylogenetically closer to RIPb than RIPc (Fig. 3B). RIPa showed the same pattern as RIPb in yeast-two-hybrid against CA RACB, as only the truncations containing the CC2 domain showed yeast growth, indicating that RIPaCC2 can also interact with RACB (Supp. Fig. S11). Interestingly, the effect of RIPbCC1 and RIPbCC2 completely disappeared when the respective longer truncation, containing the Va region, was expressed. RIPbCC1Va and RIPbVaCC2 did not affect susceptibility of barley cells and the penetration rate was at the same level as in cells with the empty vector control. This suggests that the variable region, and therefore the auto-interaction of RIPb as seen in section 3.5, might have some regulatory influence on the susceptibility effect of RIPb.

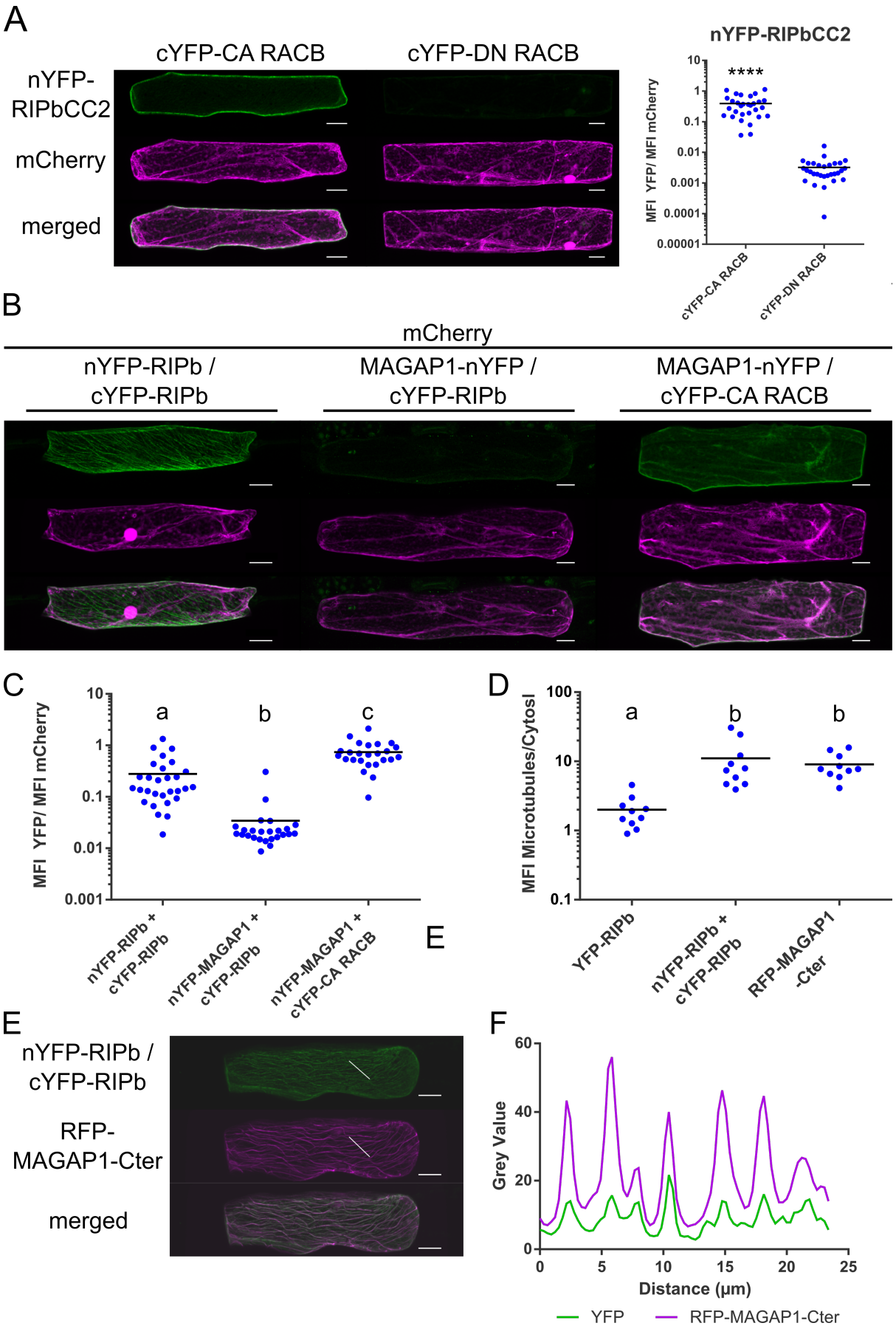
A
cYFP-CA RACB
cYFP-DN RACB
nYFP-RIPbCC2
mCherry
merged
nYFP-RIPbCC2
****
MFI YFP/ MFI mCherry
cYFP-CA RACB
cYFP-DN RACB
B
mCherry
nYFP-RIPb / cYFP-RIPb
MAGAP1-nYFP / cYFP-RIPb
MAGAP1-nYFP / cYFP-CA RACB
C
MFI YFP/ MFI mCherry
a
b
c
nYFP-RIPb + cYFP-RIPb
nYFP-MAGAP1 + cYFP-RIPb
nYFP-MAGAP1 + cYFP-CA RACB
D
MFI Microtubules/Cytosol
a
b
b
YFP-RIPb
nYFP-RIPb + cYFP-RIPb
RFP-MAGAP1 -Cter
E
nYFP-RIPb / cYFP-RIPb
RFP-MAGAP1-Cter
merged
F
Grey Value
Distance (µm)
YFP
RFP-MAGAP1-Cter

Figure 10: Interaction between RIPbCC2 and RACB, and auto-interaction of RIPb *in planta*. Interaction of RIPbCC2 and RACB was tested in BiFC experiments (A) by introducing a split-YFP tagged (nYFP, SPYNE) RIPbCC2 fusion protein as well as a split-YFP (cYFP, SPYCE) fusion protein of CA RACB or DN RACB into single epidermal cells of barley leaves by biolistic transformation. Images were taken 24 hab and show z-stacks of XY optical sections of upper half of the cells. mCherry was co-transformed as a transformation marker and internal reference. Scaling bars represent 20µm. MFI was measured over a linear ROI in the cell periphery of a single XY optical section in 30 cells. The graph on the right hand side shows the ratios between YFP and mCherry signal in every measured cell. Stars represent differences in significance indicated by Student's t-test ($p<0.0001$).
Auto-interaction of RIPb was tested in BiFC as well by co-expressing both split-YFP fusion proteins of RIPb in single epidermal cells (B). As negative control, cYFP-RIPb was co-expressed with MAGAP1 fused to nYFP. For the positive control of the negative control cYFP-CA RACB was co-expressed with MAGAP1. Images were taken 24 hab and show z-stacks of XY optical sections of upper half of the cells. mCherry was co-transformed as a transformation marker and internal reference. Scaling bars represent 20µm. MFI was measured over a linear ROI in the periphery of a single optical section in at least 25 cells. The graph in C) shows the ratios between YFP and mCherry signal in every measured cell. Letters in C) indicate statistically significant differences calculated by one-way ANOVA (Tukey's multiple comparison test). Ratio between microtubule signal and cytosolic signal (D) was measured for YFP-RIPb alone, BiFC signal for RIPb – RIPb interaction, and microtubule marker RFP-MAGAP1-Cter. Each signal was measured in 10 cells for each construct. Letters indicate significance calculated by one-way ANOVA (Tukey's multiple comparison test). E) shows co-expression of the BiFC constructs nYFP-RIPb and cYFP-RIPb with the microtubule marker RFP-MAGAP1-Cter. F) shows YFP and RFP fluorescence profiles as grey values of the signals over the ROI (white line) in D).

However, in order to fully evaluate the influence of these truncations, possible variations in protein levels of the RIPb truncations needed to be considered. IP experiments, where YFP fusion proteins of the truncations were expressed in barley protoplasts and precipitated with αGFP magnetic beads, showed that the protein levels of YFP-RIPbCC1 and YFP-RIPbCC2 were much higher than the protein levels of full length YFP-RIPb and YFP-RIPbVaCC2, resulting in much stronger bands on the western blot (Supp. Fig. S12A, experiments by Lukas Weiss). Assuming that the protein levels of untagged proteins were comparable, this indicates that there might be a correlation between protein levels and influence on susceptibility. Similar results were achieved from measuring signal intensities of the YFP fusion constructs in epidermal cells by confocal microscopy. Using constant settings for the measurements, the results show higher signal intensity on average for the shorter YFP-RIPbCC1 and YFP-

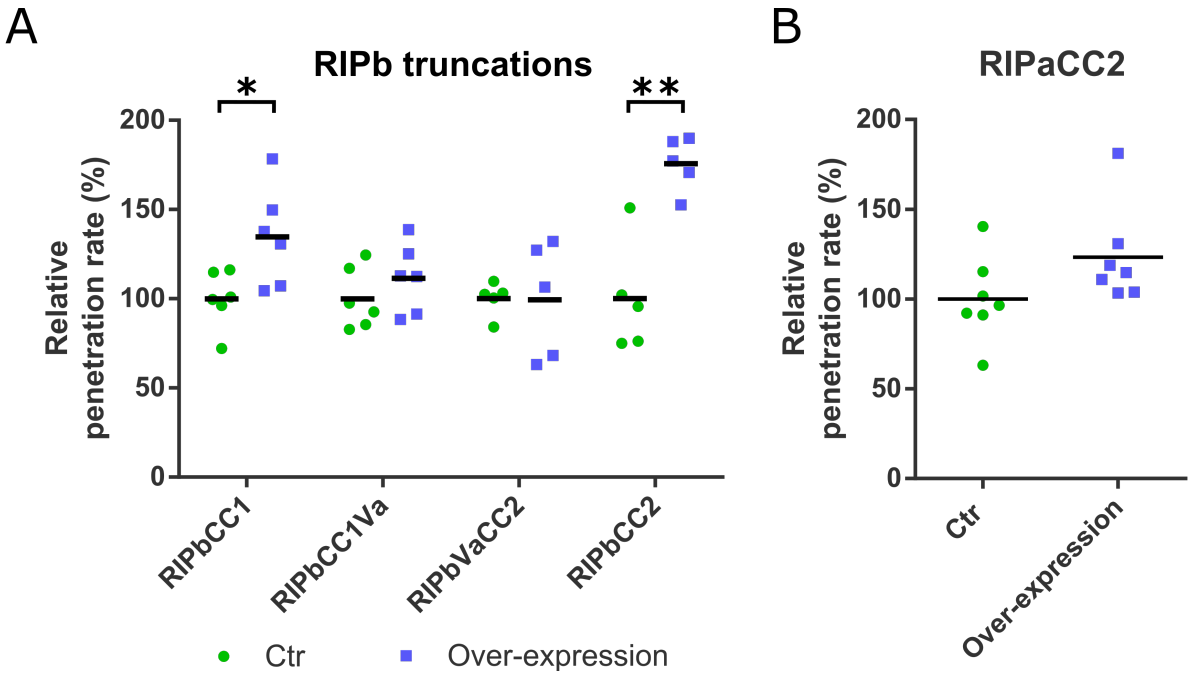

Figure 11: Effect of RIPb truncations on susceptibility of barley to *Bgh*. RIPb truncations were over-expressed with a CaMV35S promotor (A) in single epidermal cells after biolistic transformation. Additionally the CC2 domain of RIPa was over-expressed (B). Dots represent a value from an individual experiment. Over-expression or silencing constructs were co-transformed with cytosolic GFP as transformation marker to identify transformed cells. Leaves were inoculated with *Bgh* 24 hab. The empty vector served as control (Ctr). Penetration rate was counted in at least 5 different experiments in at least 80 cells per construct. Penetration rate was calculated as the amount of penetrated cells among all attacked cells. For the relative penetration rate the mean of all experiments of the respective control was set as 100% and all individual values were calculated relative to that. Stars indicate significance relative to the respective control by Student's t-test. (*, $p<0.05$; **, $p<0.01$)

RIPbCC2 truncations, while YFP-RIPb and YFP-RIPbCC2Va showed a comparably weaker signal (Supp. Fig. S12B, experiments by Lukas Weiss). These experiments suggest that the protein levels of the truncations might influence the penetration rate.

3.7 RIPb and RACB co-localize at the site of fungal attack

Since over-expression of RIPb and RIPbCC2 indicate that RIPb might act downstream of RACB in susceptibility, I wondered whether this was represented by the intracellular localization of RIPb during fungal attack. Therefore, I inoculated barley leaves, containing transformed cells, 24 hab and imaged the intracellular localization of YFP-RIPb in attacked epidermal cells at early stages of the interaction at about 24 hours after inoculation (hai). Additionally, I co-expressed RACB since both proteins might

act together in susceptibility signaling. The images show that YFP-RIPb organizes in a ring-like orientation around the penetration site, together with wild-type CFP-RACB (Fig. 12A). Although this is similar for free mCherry, which comes from cytosolic accumulation around the haustorial neck, the ring is more defined for RACB and RIPb. Very similar results were observed when RIPb was co-expressed with CFP-CA RACB (Fig. 12B). Interestingly, the accumulation was not restricted to haustorial necks in penetrated cells, but at papilla as well when the fungal attack was repelled. However, while the accumulation ended in a defined ring-like structure when a haustorium was established, in cases were the penetration attempt ended in a papilla the accumulation of RACB and RIPb was more fringed, possibly due to membrane protrusions by the papilla as observed by An et al. (2006b).

When YFP-RIPbCC2 was co-expressed with CFP-CA RACB (Fig. 12C), it led to strong signal accumulations at all sites of attack 24 hai. There was no obvious difference in localization compared to full length RIPb, although the signal intensity at the site of attack seemed to be stronger. As mentioned before (see section 3.6), YFP-RIPbCC2 accumulates higher protein levels than full length RIPb, which would explain the stronger signal accumulation during the attack. This might correlate with the increased susceptibility of cells expressing RIPbCC2, though it was not possible to measure this.

The localization of YFP-RIPbCC2 was not restricted to the plasma membrane but also to ring-like structures around the haustorial neck, and possibly the extrahaustorial membrane. To better elucidate this, I also looked at the interaction at 48 hai hoping a stronger signal accumulation would improve the explanatory power of the results (Fig. 12D). In order to highlight differences between YFP-RIPbCC2 and cytosolic mCherry, I analyzed signal intensities over a linear ROI of a single XY optical section of the z-stack. The signals proved to be clearly distinct and suggest localization of YFP-RIPbCC2 at membrane of the extrahaustorial neck (Fig. 12E).

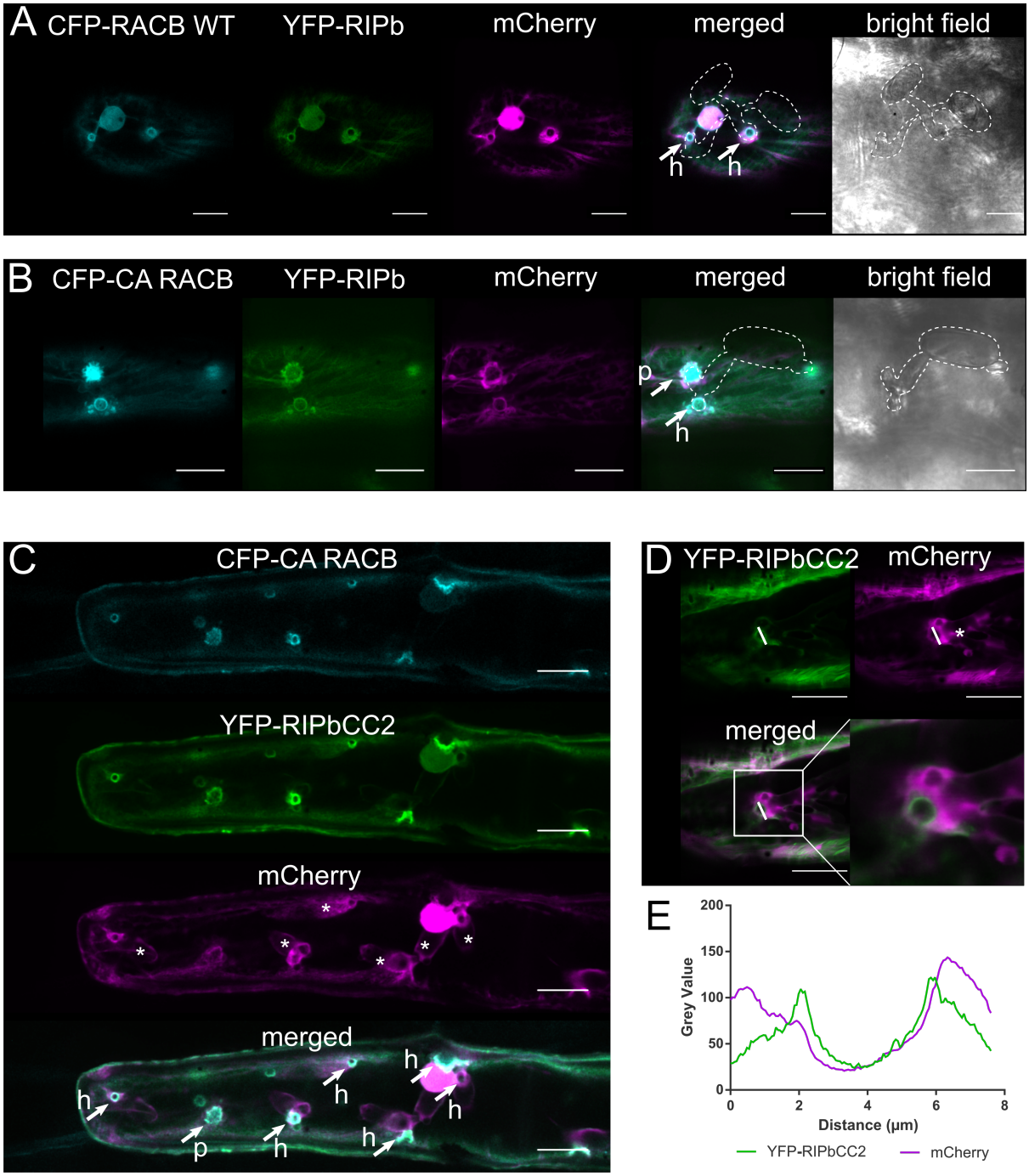

Figure 12: Co-localization of RIPb and RACB at the site of fungal attack. Single epidermal cells of barley leaves were transiently transformed by biolistic transformation. YFP-RIPb (A, B) or YFP-RIPbCC2 (C, D) was introduced into leaves together with CFP-RACB WT (A) or CFP-CA RACB (B, C). Cytosolic mCherry was used as a transformation marker. Transformed leaves were inoculated with *Bgh* 24 hab. Images were taken 24 hai (A, B, C) and 48 hai (D). Dashed lines in A) and B) highlight the position of fungal spores with the appressorium on top of the cells. Arrows indicates site of fungal attack resulting in either a haustorium (h) or a papilla (p). Scaling bars represent 20µm. The graph in E) shows the signal profile as grey values across a linear ROI (white line) in (D). Asterisks in C) and D) mark the position of the established haustorium.

3.8 Identification of downstream interactors

Xylem cell differentiation in plants is associated with secondary cell wall formation by the CELLULOSE SYNTHASE, which moves along the microtubule cytoskeleton during this task (Zhong and Ye, 2015). In Arabidopsis, it was reported that a complex of RIP3/MIDD1, ROP11, and KINESIN13A is involved in local microtubule depletion and hence the formation of cell wall pits, leading to the sieve like structure of xylem cells (Mucha et al., 2010; Oda et al., 2010; Oda and Fukuda, 2012, 2013). Since local microtubule depletion might also be important for haustoria establishment in the interaction of barley and the powdery mildew fungus and several connections between RACB and the microtubule cytoskeleton exist (Hoefle et al., 2011; Nottensteiner et al., 2018), I wondered whether a similar mechanism might be deployed via the RACB – RIPb signaling pathway. I therefore tried to identify KIN13A in barley. Blast searches resulted in two possible candidates as orthologs of the Arabidopsis KIN13A in barley. I named them *KIN13A1* (HORVU3Hr1G042330.2) and *KIN13A2* (HORVU3Hr1G055940.1) with a 63% and 53% amino acid similarity to the Arabidopsis Kin13A (At3g16630), respectively.

I tested both of them for their interaction with RIPb in Y2H. Next to the full length kinesins, I also tested the C-termini of both proteins, since they are reported to contain the RIP binding domain and the C-terminus of HvKin13A1 (AA522-AA792) shows strong homology to the C-terminus of AtKin13A (Mucha et al., 2010). I also tested the possible interaction with RIPa and RIPc. No yeast growth was observed for Kin13A1 or Kin13A1-Cter (Supp. Fig. S13). For KIN13A2 and KIN13A2-Cter (AA486-AA702) yeast growth was observed with all combinations of RIP proteins. Unfortunately, control samples with the empty vector also showed yeast growth, indicating auto-activation of the promotor, which does not allow to draw conclusions from the results. However, in all following conducted experiments I never observed any recruitment of Kin13A1 and Kin13A2 by RIPs, or any influence on the microtubule organization (data not shown). Considering that I also never observed a negative effect of RIPs on microtubule stability, I concluded, that microtubule depletion by a RACB, RIPb and KIN13A complex is probably not a mechanism in barley, though it can not be excluded with absolute certainty. However, for a possible mode of barley RIPa, RAC1, and MAGAP1 in microtubule organization see Hoefle et al. (2020).

3.8.1 Untargeted Yeast Screening for downstream interactors

Since the targeted approach did not yield conclusive results, I tried a yeast screening as a next step. *RIPb* was introduced into the bait plasmid for yeast-two-hybrid and

Table 3: List of identified potential interactors of RIPb from yeast screening

Locus	Annotation	Description
HORVU1Hr1G062650.1	Coatomer subunit delta (δCOP)	Retrograde vesicle transport
HORVU4Hr1G004780.2	Costars	Actin organization
HORVU5Hr1G084010.1	Synaptotagmin-7	Vesicle-Membrane fusion
HORVU5Hr1G052030.1	C2 domain ABA-related (CAR1)	Calcium dependent lipid binding (CaLB domain)

tested against a cDNA library of barley introduced into prey plasmids. If the cDNA codes for a protein that interacts with RIPb, colony growth should be observed for this combination. After the transformation, plasmid was extracted from the growing yeast colony and sequenced. The DNA sequence was then compared to databases (NCBI BLAST, IPK Barley Blast server).

Among the obtained putative interaction partners, I identified four genes of particular interest, because they could act in ROP-related processes (see Table 3). Coatomer subunit δ (δCOP) is part of the coat protein complex I (COPI) and involved in retrograde vesicle transport from Golgi to the ER, a process that is regulated by Arf G-proteins. Previously, the gamma subunit COP1γ was shown to be necessary for full penetration resistance of barley against *Bgh* (Ostertag et al., 2013). The crystal structure of the mouse COPI complex revealed that δCOP interacts with Arf1 (Yu et al., 2012). Arf G-proteins are also known targets for pathogen effectors, for instance the *P. syringae* effector HopM1 targets the ArfGEF MIN7 of Arabidopsis for degradation, leading to the suppression of PTI (Nomura et al., 2006). Costars was named based on its homology to the C-terminus of STARS (Straited Muscle Activator of Rho Signaling). In mammalian muscles, STARS links RHO signaling, actin regulation, and cellular reprogramming, while Costars was reported in *Dictyostelium discoidium* to be involved in actin depolymerization in pseudopods and hence influence motility (Pang et al., 2010). Synaptotagmin-7 (Syt7) is part of the Synaptotagmin family, which is involved in vesicle fusion by connecting t-SNARE and v-SNARE complexes. Synaptotagmins contain two C2 domains, which mediate membrane localization upon Ca^{2+} signal perception. Calcium-dependent ABA related 1 (CAR1) belongs to a family of plant specific small proteins containing a single C2 domain. Some of the 11 members of the protein family in Arabidopsis were shown to recruit ABA-receptors to the plasma membrane in response to calcium signaling and induce membrane curvature (Rodriguez et al., 2014; Diaz et al., 2016).

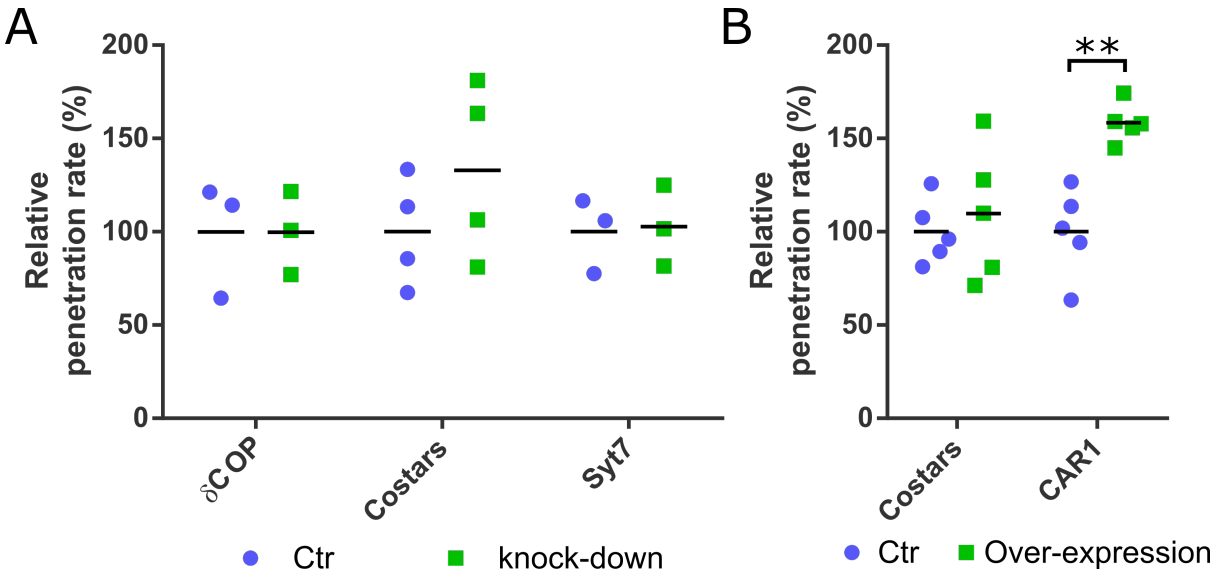

Figure 13: Influence of potential downstream interactors of RIPb on susceptibility. RNAi silencing constructs of δCOP, Costars and Synaptotagmin-7 (Syt7) (A), or over-expression constructs of Costars and CAR1 (B) were introduced into single epidermal cells of barley leaves by biolistic transformation. The respective empty vector served as control (Ctr). Cytosolic GFP was co-expressed as a transformation marker. Leaves were inoculated with *Bgh* 48 hab for silencing constructs and 24 hab for over-expression constructs. Penetration rate for was counted 24 hai. At least 3 experiments were conducted for each gene of interest and in each experiment at least 80 cells were counted per construct. Blue and green dots represent results from individual experiments. Stars indicate significance relative to respective control by Student's t-test. $p<0.01$

In a first step, I tried to confirm the interactions with RIPb by targeted yeast-two-hybrid. Since the extracted plasmid containing δCOP got lost in the process and Costars showed sequence irregularities, I cloned new constructs of both genes into prey plasmids, but used the original plasmids extracted from the yeast screening for Syt7 and CAR1. Next to RIPb, interaction with RIPa and RIPc was tested as well for possible interaction specificity. No yeast growth could be observed for the newly cloned constructs δCOP and Costars in combination with either of the RIPs (Supp. Fig. S14). Yeast grew for Syt7 only in combination with the empty plasmid, indicating auto-activation of the promotor. This was also true for CAR1, but here colonies grew also in combination with RIPa and RIPb, but not with RIPc. These results alone did not allow for confirmation of the interactions, hence different methods needed to be used.

To streamline work load, I first tested the four genes for their influence on susceptibility of barley to *Bgh*. Only genes influencing penetration rate of *Bgh*, should be further investigated. Therefore, I created RNAi silencing constructs of δCOP, Costars, and

Syt7. Unfortunately, it was not possible to obtain RNAi constructs for CAR1. Silencing of δCOP and Syt7 had no effect on susceptibility (Fig. 13A). Penetration rate over three experiments was comparable to the empty vector control. Silencing of Costars on the other hand led to a slight increase in susceptibility, though the variation between the experiments was high. With regards to these results, I also over-expressed Costars as well as CAR1. Over-expression of Costars had no significant effect on susceptibility over five experiments (Fig. 13B). Over-expression of CAR1 on the other hand led to a strong increase of about 60%. This is comparable to the effect of over-expression of the RIPbCC2 domain, which averaged at 75% (Fig. 11A).

These results made further investigation into CAR1 interesting. Semiquantitative PCR showed transcript of CAR1 in the whole leaf, as well as in the epidermis of barley leaves (Fig. 14A). No obvious changes in transcript levels were observed in the epidermis upon infection with the powdery mildew fungus. Transcript levels of CAR1 appeared to increase in the whole leaf after inoculation, although this was inconsistently observed in several experiments. Further analyses need to be made, to verify this. These results showed however, that CAR1 is expressed in the epidermis, similar to RIPb (Fig. 3C). Within the cell CAR1 seems to be present in the cytosol, since YFP-CAR1 co-localized with free mCherry when transiently expressed in barley epidermal cells (Fig. 14B). This indicates no spatial separation between RIPb and CAR1 under natural conditions.

I then performed additional experiments to confirm the interaction between RIPb and CAR1. I first tried BiFC experiments where cYFP-RIPb was tested against nYFP-CAR1 (Fig. 14C). As a negative control cYFP-RIPb was tested against MAGAP1-nYFP, a different RACB interactor (Hoefle et al., 2011). YFP fluorescence restoration was obtained with co-expressed RIPb and CAR1, but not with RIPb and MAGAP1 (Fig. 14C). Quantification of at least 25 cells showed a strong difference between cells where RIPb was co-expressed with CAR1, and cells where RIPb was co-expressed with MAGAP1 (Fig. 14C, right hand side). The signal occurred mainly in the cell periphery and at microtubules, which resembles the signal locations observed for RIPb and for RIPb – RACB interactions (Fig. 4, Fig. 6). However, YFP-CAR1, when expressed alone, was found only in the cytosol (Fig. 14B), suggesting it was recruited to microtubules and cell periphery by RIPb.

As an additional way to confirm the interaction, I performed Fluorescence Lifetime Imaging (FLIM). Here, I used meGFP-RIPb as donor and mCherry-CAR1 as acceptor. As a negative control I tested meGFP-RIPb against mCherry-MAGAP1 and also the donor only. In FLIM, donor (in this case GFP) fluorescence lifetime is measured on a single photon detector after excitation with a pulsed laser. Spatial proximity of donor

and acceptor due to the interaction of two proteins results in Förster resonance energy transfer (FRET) between donor and acceptor. This results in fluorescence lifetime reduction of the donor fluorophore, which can be measured.

FLIM was measured in the cell periphery, since this was the expected location of the interaction, according to BiFC experiments (Fig. 14C). Excitation of the donor only without any acceptor present resulted in a GFP fluorescence lifetime of about 2.7ns on average (Fig. 14D). A slight, but statistically significant reduction to about 2.6ns was measured in the negative control between RIPb and MAGAP1. This means that the presence of the acceptor in the cell, already has an influence on GFP fluorescence lifetime, since both proteins do not interact according to the BiFC experiments (Fig. 10B). This is probably due to the high amount of protein in the cell from expression under control of the CaMV35S promotor and both proteins being partially enriched at microtubules. However, co-expression of meGFP-RIPb and mCherry-CAR1 led to a strong reduction of GFP fluorescence lifetime, to approximately 2.3ns. This supports the hypothesis that the two proteins can interact with each other *in planta*.

Taken together, these results suggest CAR1 as a downstream interactor of RIPb and therefore possibly RACB. Since over-expression of CAR1 also led to a strong increase in susceptibility, as we described for RIPb and especially RIPbCC2, it seems to be possible that CAR1 acts in a signaling pathway between RACB, RIPb, and CAR1 to support fungal accommodation.

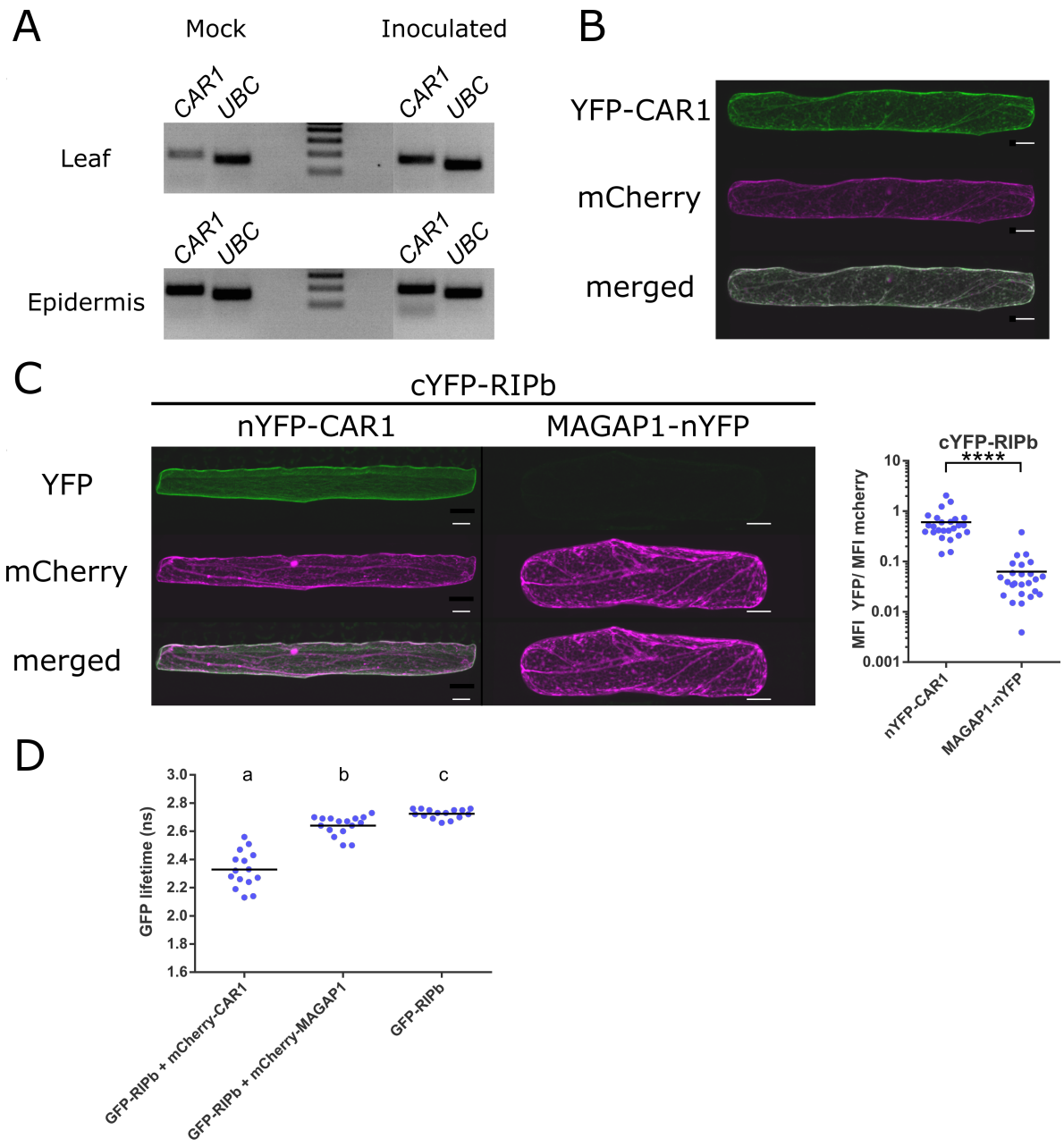
A
Mock
Inoculated
CAR1
UBC
CAR1
UBC
Leaf
CAR1
UBC
CAR1
UBC
Epidermis
B
YFP-CAR1
mCherry
merged
C
cYFP-RIPb
nYFP-CAR1
MAGAP1-nYFP
YFP
mCherry
merged
cYFP-RIPb
****
MFI YFP/ MFI mcherry
10
1
0.1
0.01
0.001
nYFP-CAR1
MAGAP1-nYFP
D
a
b
c
GFP lifetime (ns)
3.0
2.8
2.6
2.4
2.2
2.0
1.8
1.6
GFP-RIPb + mCherry-CAR1
GFP-RIPb + mCherry-MAGAP1
GFP-RIPb

Figure 14: RIPb interaction with CAR1. Semiquantitative PCR shows transcription levels of CAR1 in whole leaves and the epidermis of barley leaves in plants inoculated with *Bgh* or uninoculated plants (A). As control, the constitutively expressed housekeeping gene *HvUBC* was used. Same amounts of cDNA were used for sqPCR reactions and an identical amount of PCR product was used for electrophoretic separation. Expected amplicon sizes are 186bp for *CAR1* and 156bp for *UBC*. CAR1 fusion proteins with an N-termial YFP-tag were transiently expressed in barley epidermal cells by biolistic transformation (B). Free mCherry was co-expressed as a transformation marker. Localization of CAR1 was analyzed with a confocal fluorescence microscope 24 hab. CAR1 was tested in BiFC experiments for its interaction with RIPb (C). Therefore CAR1 was fused to nYFP truncation (nYFP-CAR1) and tested for its interaction with cYFP-RIPb. As a negative control cYFP-RIPb was tested against MAGAP1-nYFP. Cytosolic mCherry was co-expressed as a transformation marker and internal reference. Constructs were introduced into barley epidermal cells by biolistic transformation. Micrographs in C) show representative images 24 hab. Scaling bars represents 20µm. For quantification (C, right hand graph) MFI was measured for YFP and mCherry in at least 25 cells on a linear ROI in the cell periphery. The ratio between YFP and mCherry signal was calculated for each cell. Interaction was also quantified by FLIM-FRET with a pulsed laser on a single photon detector (D). GFP-RIPb was used as donor while mCherry-CAR1 was used as acceptor. As negative control mCherry-MAGAP1 and GFP-RIPb (donor only) were used. Letters in D) indicate different significance categories by one-way ANOVA (Tukey‘s Test).

4 Discussion

4.1 Cell polarity in plant - pathogen interactions

Cellular polarization is a key mechanism during plant development. It is essential to generate for example tip growth in pollen tubes or root hairs. Attack by haustoria establishing pathogens generates a single focal point at the site of the penetration attempt. Here it is important for both pathogen and host that the host cell polarizes to the site of attack. Either to generate a concentrated defense or to facilitate the successful penetration and establishment of the haustorium as the main feeding cell of the pathogen. Experiments by Hardham et al. (2008) show that a mechanical stimulus, as it is generated by the pathogen during the penetration attempt, is enough to induce polarization reactions in the host cell, in this case *A. thaliana*. Actin, the ER, and peroxisomes all accumulate underneath the artificial pressure point they generated with a microneedle, while microtubules are depleted. Similar results were observed before, in different pathosystems. In early experiments in parsley with the oomycete pathogen *P. infestans* cytoplasmic aggregation was observed, as well as translocation of the nucleus to the site of attack, while microtubules were also depleted (Gross et al., 1993). In interactions of *E. pisi* with the non-host barley, both microtubules and actin focused to the site of attack in a radial manner (Kobayashi et al., 1997). The same was reported for microtubules and actin in interacions of barley with *Bgh* where the cell successfully repelled the fungus, but not in interactions when a haustorium was established (Opalski et al., 2005; Hoefle et al., 2011). Here, polarization seems to be more associated with defense reactions. However, in Arabidopsis challenged with adapted and non-adapted oomycete species, no noticeable difference was detected in polarization between compatible and incompatible interactions. The authors found focusing of actin and accumulation of ER and Golgi vesicles at the site of attack independent of the outcome (Takemoto et al., 2003). In compatible interactions of Arabidopsis with the powdery mildew fungus *E. cichoracearum* cytoplasm, peroxisomes, mitochondria, and Golgi bodies accumulated at the site of attack (Koh et al., 2005).

One visible outcome of defense polarization in plant cells is papilla formation. Papilla are cell wall fortifications, containing the β-1,3-glucan callose, that prevent pathogens from penetrating the host cell (Aist, 1976). One of the earliest observed steps in papilla formation is the recruitment of the callose synthase PMR4 in Arabidopsis to the site of attack (Ellinger et al., 2013). The authors speculate that PMR4 might be transported in multivesicular boodies (MVB), which are also reported to be present close to the site of attack in barley (An et al., 2006b). The Arf GTPase ARFA1b/c was

found at these MVBs and experiments with the dominant negative ARFA1b/1c-T31N mutant showed its importance for callose deposition (Bohlenius et al., 2010). Effective papillae may require H_2O_2 and phenolic compounds to be integrated into callose depositions (Thordal-Christensen et al., 1997; Hückelhoven et al., 1999; McLusky et al., 1999), indicating that papilla formation requires polarized transport to the site of attack. Actin was shown in Arabidopsis to be essential for papilla formation (Shimada et al., 2006) and chemical disruption of the actin cytoskeleton was shown in different interactions to negatively effect early defense reactions (Kobayashi et al., 1997; Kobayashi and Hakuno, 2003). Arabidopsis PEN1 and its barley equivalent ROR2 are syntaxins involved in basal defense against powdery mildews (Freialdenhoven et al., 1996; Collins et al., 2003). ROR2 was originally discovered in a screen for mutations, braking *mlo*-mediated resistance in barley. Both proteins are required for timely callose deposition and provide a link between exocytosis and defense (Assaad et al., 2004). Interestingly, the susceptibility factor MLO also localizes to the site of fungal attack like ROR2/PEN1 (Bhat et al., 2005), indicating that MLO might get recruited there by the pathogen to regulate exocytosis and hence papilla formation via ROR2/PEN1. In another pathosystem between the liverwort *Marchantia polymorpha* and the oomycete *Phytophthora palmivora* the host syntaxin SYP13B, but not the related SYP13A is recruited to distinct hyphal domains, indicating that the pathogen recruits specific components of the exocytosis machinery to reprogram transport for its needs (Carella et al., 2018).

Haustoria of filamentous pathogens are surrounded by the extrahaustorial membrane (EHM), which originates as an invagination from the host plasma membrane. However, the EHM is mechanistically and compositionally distinct from the host plasma membrane. In experiments with Arabidopsis and the powdery mildews *Golovinomyces orontii* and *E. cichoracearum* both plasma membrane marker and arabinogalactan protein epitopes were present in the plasma membrane, but excluded from the EHM (Koh et al., 2005; Micali et al., 2011). Generation of the EHM of *Bgh* seems to originate mainly from the plant. The EHM is spatially closely associated with the host ER and shares multiple features with it (Micali et al., 2011; Kwaaitaal et al., 2017). This suggests there is a secretory pathway from the ER to the EHM. However, inhibition of ER to Golgi transport did not influence establishment of the haustorium, suggesting an alternative secretory pathway (Kwaaitaal et al., 2017). Another route for membrane secretion derives from the aforementioned MVBs, which were found to not only accumulate at papillae, but also accumulate in cells containing a haustorium (An et al., 2006a). RPW8.1/2 is an Arabidopsis R-protein that confers broad resistance to powdery mildew fungi of the Golovinomyces genus and so far the only known protein that

exclusively localizes to the EHM. RPW8 was also found in vesicles in the plant cell suggesting a dedicated vesicle stream to the haustorium (Wang et al., 2009).

These studies strongly suggest that there is polarized transport from the plant to the haustorium. The data as of today indicate that both pathogen and host have an interest in establishing host cell polarity. It could be that pathogens like *Bgh* manipulate plant polarization processes and direct them for their own purposes. In this case it would be possible that a lot of components of the polarization machinery would act in susceptibility as well as in resistance.

4.2 The susceptibility factor RACB

Cellular polarization requires a positional cue, which focuses the polarization towards an organizational center. Although it is difficult to determine what the earliest signal is, during development of all eukaryotic organisms RHO are often at the forefront of polarization. In fission yeast *Schizosaccharomyces pombe*, optogenetic recruitment of activated Cdc42, a Rho family G-protein, to the plasma membrane, leads to a positive feedback where the GEF Scd1 gets recruited to Cdc42 hubs, which in turn leads to more recruitment of Cdc42 (Lamas et al., 2020). This positive feedback loop was dependent on the scaffold protein Scd2 and the connection it provides between Scd1 and the kinase PAK1. This shows that recruitment of G-proteins might be sufficient to establish polarization. In Arabidopsis, ROP2 accumulates at the apical membrane in root hairs and is necessary for root hair initiation and outgrowth (Jones et al., 2002). It appears to be responsible for maintenance of microtubule dynamics via the kinesin ARK1/MRH2 (Yang et al., 2007; Eng and Wasteneys, 2014). ROP1 regulates actin dynamics in pollen tubes by interacting with RIC4 to promote actin polymerization and with RIC3 to promote actin depolymerization (Gu et al., 2005). ROPs are central to polarization in plants, which makes it very likely for these G-proteins to be involved in polarization processes during plant pathogen interactions as well.

One aim of this work was to identify downstream interactors for the ROP family G-protein RACB, a susceptibility factor in the interaction of barley with the barley powdery mildew fungus *Blumeria graminis* f.sp. *hordei* (Schultheiss et al., 2002). The mode of action for RACB-dependent susceptibility signaling is still not clear, but RACB has no influence on early defense responses like the production of ROS and MAP kinase signaling upon elicitor treatment (Scheler et al., 2016). RACB however, does influence polarization processes. While RACB RNAi plants develop no root hairs, plants overexpressing CA RACB show a typical bulb-like root hair phenotype likely resulting from a lack of containment of the polarization zone (Pathuri et al., 2008; Hoefle et al., 2011;

Scheler et al., 2016). This can also be observed by slower nucleus migration to the site of fungal attack in RNAi plants (Scheler et al., 2016). Nuclear migration seems to be dependent on the actin cytoskeleton. Inhibition of actin polymerization with cytochalasin E in cowpea challenged with the rust fungus *Uromyces vignae*, prevented nuclear movement (Skalamera and Heath, 1998). RACB RNAi plants also show a defect in subsidiary cell development of leaf stomata (Scheler et al., 2016). Subsidiary cells originate from asymmetric cell division of the subsidiary mother cell (SMC). This requires polarization of the SMC with nuclear movement to the site of the neighboring guard mother cell and formation of an actin patch at this site. Stomatal development defects were also observed in ROP2 and ROP9 double mutants in maize through impairment of nuclear migration and actin patch formation (Humphries et al., 2011). The involvement of RACB in different developmental processes might provide various ways for *Bgh* to manipulate RACB signaling. The *Bgh* genome codes for about 500 predicted candidates for secreted effector proteins (CSEP) (Pedersen et al., 2012). For comparison, the hemi-biotrophic bacterium *P. syringiae* has an estimated 50 effector proteins (Schechter et al., 2006). For such a plethora of effectors it would not be surprising if RACB and the RACB signaling pathway was target to more than one effector protein. One effector that was shown to target RACB is ROPIP1, which was identified in a yeast screening for RACB interactors (Nottensteiner et al., 2018). ROPIP1 is a small peptide, encoded on the retrotransposable element Eg-R1. Eg-R1 likely has thousands of insertions in the *Bgh* genome, which might result in many complemented open reading frames linking ROPIP1 to signal peptides or other N-terminal sequences. Expression of ROPIP1 increased susceptibility of barley epidermal cells to *Bgh* and the interaction with RACB takes place at microtubules and the plasma membrane. ROPIP1 also negatively influences microtubule stability, which was also detected after silencing of the RACB regulator RBK1 (Huesmann et al., 2012; Reiner et al., 2015). The microtubules might therefore be a target for pathogen interference via RACB.

4.3 RIP proteins in barley

In this work, three ROP INTERACTIVE PARTNER (RIP) proteins were identified in barley. RIP proteins were identified by their conserved N-terminal QDEL motif and the C-terminal QWRKAA motif. I also identified three RIP proteins in the monocots *Brachipodium distachyon* and rice (*Oryza sativa* ssp. *japonica*). The results for rice differ from results obtained by Li et al. (2008), who identified four RIPs in rice. However, in my searches I was only able to recover three of these from the Rice Genome Annotation Project database (Kawahara et al., 2013). This dataset was not yet available

when the study by Li and colleagues was published. The QDEL motif in all investigated monocots, with the two negatively charged amino acids aspartate and glutamate differs from the QEEL motif in Arabidopsis, which has two glutamate instead (Supp. Fig. S1). Due to the similar chemical properties of the two amino acids however, a change in functionality can not be expected. The phylogenetic tree groups one RIP of each investigated monocot together, resulting in one branch for each monocot RIP (Fig. 3B). The five RIPs from the only investigated dicot *Arabidopsis thaliana* did not group pairwise with the monocot RIPs. Since all investigated monocots are relatively closely related, it would be interesting to see whether all monocots have three RIPs and if so, how functionality developed when monocot and dicot RIPs are compared.

Semiquantitative PCR reveals that in barley *RIPb* and *RIPc* are well expressed in first leaves of barley plants as well as the epidermis of these leaves (Fig. 3C). Only very little expression was observed for *RIPa*, if any. *RIPa* transcript was, however, present in root tissue (Supp. Fig. S2).

This work shows that all three RIP proteins from barley were able to interact with RACB as well as RAC1 in yeast and *in planta* (Fig. 5, 6). RIPs interacted with wild-type and CA, but not DN variants of ROPs, supporting the notion that RIPs are downstream interactors of ROPs after activation. It was shown before for Arabidopsis RIPs that there seems to be no or only little interaction specificity between RIPs and ROPs. AtRIP1/ICR1 was reported to interact with ROPs 1, 2, 6, 9, 10, and 11 (Lavy et al., 2007; Bloch et al., 2008; Li et al., 2008; Hazak et al., 2010). AtRIP3/MIDD1 was shown to interact with ROPs 1, 2, and 11 (Mucha et al., 2010; Oda and Fukuda, 2012). How interactions between RIPs and ROPs are regulated remains elusive. For barley, it appears all ROPs are expressed in the leaf (Schultheiss et al., 2003) and at least two out of three RIPs (RIPb, RIPc) are expressed there as well (Fig. 3C). This means there seems to be no spatial separation between the potential interaction partners, at least not on tissue level. My results suggest that ROPs and RIPs will interact independent of a stimulus. Both wild-type RACB and RAC1 interacted with RIPs in yeast (Fig. 5) and, considering the recruitment experiments (Fig. 7), also *in planta*, without any additional stimulus, which would activate G-protein signaling. Li et al. (2008) also noted a possible positive effect of AtRIP1 on ROP signaling and speculated about a regulatory function of AtRIP1. However, in contrast to barley RIPs, in their experiments AtRIP1 also interacted with DN ROP1 *in vitro*.

It was reported before that downstream scaffold proteins in G-protein signaling interact with specific guanosine nucleotide exchange factors (GEF). For example, in animals the RacGEF Tiam1 interacts with the scaffold proteins IB2 and spinophilin. Interaction with IB2 triggers the activation of the p38 kinase cascade, while interaction

with spinophilin promotes the ability of Tiam1 to activate p70 S6 kinase, which also binds spinophilin and its activity is RAC dependent. At the same time, binding to spinophilin suppresses the ability of Tiam1 to activate Pak1 kinase, which is another Rac downstream interactor (Buchsbaum et al., 2002, 2003). A direct link between GEFs and a G-protein downstream interactor was described for the RhoGEF, GEF-H1 in humans. GEF-H1 directly binds to Sec5 of the exocyst complex. This interaction promotes RhoA activation in order to regulate exocytosis (Pathak et al., 2012). It was reported in yeast that the scaffold protein Bem1p interacts with the Cdc42 GEF, Cdc24, and the kinase PAK to regulate cell polarity during yeast budding (*S. cerevisiae*) (Butty et al., 2002; Kozubowski et al., 2008). In this context it is reasonable to speculate that RIPs might interact with GEFs *in planta*. This way, co-expression with RACB might lead to interaction and activation, which would explain the similar localization pattern for fluorophore tagged RIPs when co-expressed with CA ROPs compared to WT ROPs (Fig. 7A, S4).

As described for Arabidopsis before, all RIP proteins share a similar secondary structure, with a minimum of two predicted coiled-coil (cc) domains, one at the N-terminus and one at the C-terminus (Fig. 9A). The N-terminal cc domain contains a QDEL motif, which is of unknown function. This work shows that the N-terminus itself is important for microtubule localization of RIPs. However, full structural integrity of the QDEL motif is not required for the localization to microtubules since mutations in this domain had no effect on microtubule localization of RIPb (Supp. Fig. S8). The C-terminal cc domain contains the QWRKAA motif, which was reported to be responsible for ROP interaction (Lavy et al., 2007). Double mutations Q540L and W541G in the QWRKAA motif rendered RIPb unable to interact with RACB in yeast as well (Supp. Fig. S10). Experiments also show that only RIPb truncations containing the CC2 domain, which consists of the C-terminal cc domain and the QWRKAA motif, interacted with RACB in yeast (Fig. 9). Interaction between RIPbCC2 and RACB was also confirmed by BiFC experiments (Fig. 10A). These results confirm the literature in the importance of the QWRKAA motif for ROP interaction. In between the two cc domains all RIPs contain a variable region (Va). This region strongly differs between RIPs and no conserved motifs or domains could be detected. The Va region of RIPb contains two additional predicted cc domains, for RIPa it contains one cc domain, and no cc domain was predicted in the Va region of RIPc. The Va region of RIPb is necessary for auto-interaction (Fig. 9, 10), but since this region is relatively large (290AA), it was not possible to pinpoint this to a specific motif during this thesis. RIPa was also able to interact with itself in yeast, but no tests have been made to investigate, whether the Va region is responsible for that (Hoefle et al., 2020).

All three RIPs show distinct localization patterns when transiently expressed in barley epidermal cells. RIPa localizes to the cytosol and speckles, which were located in the cell periphery. These speckles were mostly stationary and did not coincide with any vesicle markers we tested (Experiments by Dr. Caroline Höfle, Data not shown). RIPa was able to interact with itself in yeast (Hoefle et al., 2020), suggesting these speckles might be some kind of aggregation due to auto-interaction. RIPb can be found in the cytosol, at microtubules, and at the plasma membrane (Fig. 4, S5). I was able to show that the N-terminal CC1 domain of RIPb is necessary for microtubule localization, but it might be dependent on RIPb oligomerization, since only the truncation containing both the CC1 domain and the Va region for auto-interaction is able to localize to microtubules (Fig. 9B). BiFC signal from RIPb auto-interaction was also restored almost exclusively from microtubules (Fig. 6). RIPc localizes to microtubules and the cytosol when fused to an C-terminal tag. The microtubule localization was disrupted by an N-terminal fluorophore tag.

As in yeast, BiFC (Fig. 6) and recruitment experiments (Fig. 7, Supp. Fig. S4) show that RIPs were able to interact with RACB and RAC1 *in planta*. When RIPs are co-expressed with barley ROPs a shift in localization can be observed, most strongly for RIPa. In interaction with CA RACB the speckle localization of RIPa gets lost completely. The BiFC experiments show a strong microtubule localization of the interaction partners, while recruitment experiments show microtubule and cell periphery localization. This needs to be studied in future experiments. Co-expression with CFP-CA RACB shows that both proteins localize to microtubules (Fig. 7). CA RACB was previously shown to localize to the plasma membrane, but not to microtubules (Schultheiss et al., 2003), suggesting that microtubule localization of RIPa and RACB is a result of their interaction. CA RAC1 recruits RIPa to the cell periphery and microtubules, though the localization at the cell periphery seems to be more pronounced. This is also supported by BiFC data (Hoefle et al., 2020). These results clearly demonstrate that RIPa can interact with both RACB and RAC1 *in planta*. RAC1 is apparently involved in the organization of membrane domains together with RIPa. Co-expression with RAC1 and MAGAP1 resulted in the establishment of RIPa in patches enclosed by microtubules (Hoefle et al., 2020). Very similar patterns were observed for AtRIP3/MIDD1 by Oda and Fukuda (2012), which is involved in xylem cell development. RIPa might hold a similar function as AtRIP3/MIDD1.

The localization of RIPb also changes during the interaction with RACB or RAC1. RIPb itself can be found in the cytosol, at microtubules and at the plasma membrane (Fig. 4, S5A). Co-expression with a ROP G-protein shifts the localization stronger to the plasma membrane, while the cytosolic signal almost disappears and the mi-

crotubule signal remains (Fig. 7). This is very similar between RACB and RAC1. Co-localization experiments with the plasma membrane marker pm-rk showed nicely a partial overlay of YFP-RIPb and pm-rk signal, arising from the shared cytosolic and membrane localization of RIPb (Supp. Fig. S5A). Introduction of CA RACB shifts the localization further to the plasma membrane, which results in a complete overlay of YFP-RIPb and pm-rk signals (Supp. Fig. S5B). Unsurprisingly, the same can be observed for YFP-RIPbCC2, since this domain is the RACB interacting domain (Supp. Fig. S5C,D; Fig. 9C). Co-expression with CFP-CA RACB (Fig. 7B) showed a similar result as co-expression with untagged CA RACB (Fig. 7A). RIPb was mainly localized at the microtubules and strongly at the plasma membrane, while CFP-CA RACB showed a similar pattern (Fig. 7B). In BiFC experiments, the interaction between RIPb and RACB occurred mostly at the plasma membrane and in around 50% of cases also at the microtubules, indicating that another factor might play a role in this (Fig. 6B). Though RIPb was also found at the plasma membrane by itself, these results suggest that on the one hand RIPb is recruited by RACB to the plasma membrane, while on the other hand RACB is recruited to the microtubules by RIPb. This work shows that auto-interaction of RIPb might be necessary for its microtubule localization. It is tempting to speculate that RACB interacts with monomeric RIPb at the cell periphery, while interacting with oligomeric RIPb at microtubules. However, at this point I can not exclude beyond all doubt that monomeric RIPb is also able to localize to microtubules. Nevertheless, the data strongly support that RIPb can directly interact with RACB and this interaction takes place at the microtubule cytoskeleton and the plasma membrane.

RIPc localizes mainly to the cytosol when expressed alone but was also found at the microtubules when expressed with a C-terminal tag (Fig. 4A). In recruitment experiments RIPc interacted stronger to RAC1 than RACB, since co-expression with wild-type and CA RAC1 resulted in strong signal at the cell periphery. No additional cytosolic signal could be detected, indicating a complete recruitment to the cell periphery, presumably the plasma membrane (Fig. 7A). Co-expression with RACB also resulted in a shift of signal to the cell periphery but cytosolic signal was still prevalent. Co-expression with CFP-CA RACB had a similar outcome in that both signals were found in the cell periphery but also in the cytosol (Fig. 7B). BiFC experiments however, show that the interaction between RIPc and RACB occurs only in the cell periphery (Fig. 6C). I cannot exclude that RIPc and ROP G-proteins also interact at microtubules, since all co-expression experiments were performed with N-terminal tags on RIPc, which might interfere with its microtubule localization. The interaction with RAC1 appears mainly at the cell periphery. This work also shows that RIPc and RACB are able to interact *in planta*.

4.4 RIPs and Microtubules

Both Rho/ROP G-proteins and microtubules are involved in cellular polarization processes in various organisms and are known to influence each other. However, only a few direct connections between microtubules and Rho/ROP G-proteins have been described. One example comes from fission yeast *Schizosaccharomyces pombe*. Although microtubules are not needed for polarized growth directly, they are known to determine the site of polarization (Sawin and Snaith, 2004). In a well described process, microtubules orientate with their plus-ends to the site of future polarization and subsequently transport the formin For3 and the phoshphatase PP1. While For3 is involved in actin polymerization, PP1 helps keeping GEF1 in an active, dephosphorylated state. GEF1 activates the Rho protein Cdc42, which establishes polarization (Martin et al., 2005; Kokkoris et al., 2014; Das et al., 2015). Microtubules also restrict the localization of Rga4, a GAP that is free in the cytosol and can inactivate Cdc42 thereby restricting the zone of polarization (Tay et al., 2018). In the moss *Physcomitrella patens*, as in other organisms, polarization in tip growing cells was found to be ROP dependent (Burkart et al., 2015). Similar to the process in *S. pombe*, microtubules determine the site of cell growth by orienting their plus-ends towards the growth zone and transport a formin (For2a) to the site of polarization (Wu and Bezanilla, 2018). Root hairs in general develop by outgrowth from a single trichoblasts cells in the root epidermis. ROPs and microtubules were shown to be of great importance for this process. However, although the topic is well researched, the connection between microtubules and ROPs is still not clear. It was discovered early in lettuce that a flexible microtubule network is important for root hair initiation and similar results have been observed in Arabidopsis (Takahashi et al., 2003; Van Bruaene et al., 2004). The reason for this remains unknown, but root hair initiation itself is also dependent on ROP2 in Arabidopsis (Jones et al., 2002). Microtubules are also important for directionality of root hair elongation. Although disruption of microtubule dynamics with stabilizing and destabilizing drugs did not change the speed of tip growth, it resulted in a waving growth phenotype and in higher drug concentrations, branching of root hairs from multiple growth zones (Bibikova et al., 1999). A very similar effect was observed in Arabidopsis plants over-expressing ROP2, where branching of root hairs appeared as well (Jones et al., 2002). Kang et al. (2017) found the microtubule associated protein MAP18 to bind inactive ROP2, competing with ROP-GDI1, and thereby influencing its localization at the plasma membrane. Additionally, the Kinesin ARK1/MRH2 was shown to be involved in inducing microtubule catastrophe events in root hairs downstream of ROP2, which is also necessary for normal tip growth (Yang et al., 2007; Eng and Wasteneys, 2014). ROP2 was also found to influence microtubule organization during

salt stress by interacting with the CRIB-domain containing protein RIC1, which has a negative effect on microtubule recovery (Li et al., 2017). This mechanism however, has not yet been identified in root hairs. RIC1 is also involved in microtubule ordering in epidermal cells of Arabidopsis by interacting with ROP6 and the katanin KTN1 (Fu et al., 2009; Lin et al., 2013). All this provides a clear link between microtubules and G-proteins and shows that a downstream interactor, in this case RIC1 can have different effects on microtubules. Another connection between ROPs and microtubules has been described in xylem cell development in Arabidopsis. The microtubule localized RIP3/MIDD1 interacts with microtubule depolymerizing kinesin KIN13A and ROP11 to locally depolymerize microtubules in progenitor xylem cells, leading to microtubule depleted zones where no secondary cell wall is established (Mucha et al., 2010; Oda et al., 2010; Oda and Fukuda, 2012, 2013).

The results of this work suggest RIP proteins act as a general connector between ROPs and microtubules in barley and possibly monocots in general. RIPb and RIPc were able to localize to microtubules by themselves. At least for RIPb, participation of a ROP can almost be excluded, since the CC1Va truncation, which is not able to interact with ROPs due to the missing QWRKAA motif at the C-terminus, localized to microtubules (Fig. 4, 9). RIPa appears to localize to microtubules only in interaction with a ROP G-protein (Fig. 6A, S4). Both RIPa and RIPb were also able to recruit ROPs to microtubules (Fig. 7, S4). The CC1 domain of RIPs plays a crucial part in microtubule localization. The CC1 domain of both RIPa and RIPc localizes to microtubules and although the CC1 domain of RIPb did not, it still was required in order for RIPb to localize to microtubules (Fig. 9, S9). The role of RIPs remains elusive, but, as mentioned above, there are plenty of developmental processes were ROPs and microtubules act together. RIPa is involved in membrane pattern formation together with RAC1. Co-expression of barley RIPa, RAC1 and MAGAP1 leads to symmetry breaking and RIPa-enriched membrane patches restricted by microtubules (Hoefle et al., 2020). Most likely RIPa is involved in establishing zones of ROP activity, similar to what was observed for RIP3/MIDD1 in Arabidopsis (Oda and Fukuda, 2012). To further unravel RIP function in barley, stable transgenic knock-out plants will be necessary to fully understand which processes are affected in which tissues.

4.5 RIP proteins in susceptibility

The barley ROP protein RACB is a susceptibility factor in the interaction of barley with the barley powdery mildew fungus, *Bgh* (Schultheiss et al., 2002, 2003). The main goal of this work was to find downstream interactors of RACB in order to get closer to a po-

tential mechanism in which RACB would act during susceptibility signaling. In plants, most described signaling pathways of ROPs involve RIC or RIP proteins, which are expected to act as scaffolds connecting the G-protein to downstream interactors. Hence, this thesis focused on RIP proteins. Of the three barley RIPs, RIPb had the highest transcription levels in leaves and the epidermis (Fig. 3C). While RIPc was expressed in leaves as well, RIPa was only detected in trace amounts. No observable changes in transcript levels were detected after challenging plants with powdery mildew. However, the expression levels of RIPb appeared to be relatively high in comparison to the control, which was the housekeeping gene *UBC* in this case. The amount of protein present under normal circumstances might be sufficient for facilitating susceptibility (Fig. 3C). This is similar to RACB, which also undergoes only minor changes in expression during infection with *Bgh* (Schultheiss et al., 2002). This work shows that all RIPs were able to interact with RACB in yeast and *in planta* (Fig. 5, 6), which is why I analyzed their influence on the barley – *Bgh* interaction. Over-expression of RIPa and RIPc in single epidermal cells resulted in no significant differences in penetration rate of *Bgh*. Over-expression of RIPb however, consistently and significantly increased susceptibility in my experiments by about 25% (Fig. 8B), indicating that RIPb could be a downstream component in RACB signaling. Silencing of RIPs on the other hand had no significant effect on the penetration rate of *Bgh*. Expression of all RNAi constructs results in a tendency for increased susceptibility. ROP signaling pathways are considered to be very finely balanced, hence disruption of the pathway could render plants slightly more susceptible because of pleiotropic effects. However, measurement of silencing efficiency of the RNAi constructs showed with the exception of RIPc (90%), silencing efficiencies for RIPs were not very high (around 50%) (Fig. S7). Maybe with better silencing constructs or a complete knock-out more significant results could be attained. RACB was also shown to interact with RIC171 in susceptibility (Schultheiss et al., 2008) and might also interact with other downstream interactors in susceptibility signaling. Silencing of only one susceptibility pathways might not necessarily result in a significant change in the interaction outcome, whereas up-regulation might do so.

Analysis of RIPb truncations revealed that over-expression of the N-terminal CC1 domain had a similar effect on penetration rate of *Bgh* as over-expression of full length RIPb. An even stronger effect was observed for over-expression of the C-terminal CC2 domain (Fig. 11A). Here the penetration rate increased by about 75% relative to the control. Interestingly, both longer constructs containing the Va domain of RIPb did not affect susceptibility. As discussed before, the Va domain of RIPb is necessary for auto-interaction of RIPb and this auto-interaction likely takes place at microtubules (Fig. 9D, 10). These results suggest that auto-interaction at microtubules might cause

some kind of inhibitory state of RIPb and that RIPb needs to dissociate from the microtubules in order to get activated, or at least to fulfill its function in susceptibility signaling. Another example for a similar mechanism is the aforementioned human GEF-H1, which localizes to microtubules in an inactive state. Upon microtubule depolymerization, GEF-H1 is freed and activates RhoA (Krendel et al., 2002). Another indicator that both RIPbCC1 and RIPbCC2 are less regulated than longer truncations or full length RIPb are the protein levels of YFP-tagged fusion proteins in transformed cells. Both measurement of fluorescence signal and IP from transformed protoplasts show that RIPbCC1 and RIPbCC2 are much more abundant than longer versions (Supp. Fig. S12). Since the expression of all constructs is driven by a CaMV35S promotor, differences in protein levels are likely due to posttranscriptional regulation. It could be that motifs necessary for this regulation are also present in the Va domain. In this case the auto-interaction at microtubules could be independent from its signaling function in susceptibility since differences in expression levels would explain the results. However, the different expression levels are unlikely the sole reason for differences in penetration rate, since both RIPbVaCC2 and full length RIPb showed very similar protein levels, but had significantly different effects on susceptibility. Both CC1 and CC2 domain might be able to interact with downstream interactors, which would explain why they were able to influence susceptibility. Studies with the Arabidopsis RIP3/MIDD1 protein show that the CC1 domain is necessary for the interaction with KIN13A (Mucha et al., 2010) while the CC2 domain of RIP1 can interact with Sec3a and CMI1 (Lavy et al., 2007; Hazak et al., 2019). It it possible that both CC1 and CC2 of RIPb are able to fulfill signaling function in susceptibility, though in the case of CC1 this function would have to be ROP independent. By contrast, RIPbCC2 could interact with RACB and simultaneously with a downstream interactor, facilitating RACB signaling. The amino acid AtRIP1-W338 is necessary for the interaction between AtRIP1 and AtCMI1 (Hazak et al., 2019). This amino acid corresponds to RIPb-W607 and is conserved in most RIP proteins (Supp. Fig. S1). Considering RIPbCC2 might also be less regulated than full length RIPb, due to the lack of microtubule localization and indicated by higher protein levels, this would explain the strong effect on the penetration rate of *Bgh*.

4.6 A possible mode of action for RIPb in susceptibiliy

Previous studies highlighted several connections between RACB and the microtubule cytoskeleton. MAGAP1 is a microtubule associated GAP that counters the RACB effect on the barley – *Bgh* interaction (Hoefle et al., 2011). The kinase RBK1 interacts

with RACB and influences microtubule stability likely by controlling RACB abundance via SKP1-like, which is part of the SCF-E3 ubiquitin ligase complex (Huesmann et al., 2012; Reiner et al., 2015). The *Bgh* effector ROPIP1 targets RACB. Both proteins interact at microtubules and ROPIP1 negatively influences microtubule stability when transiently expressed in barley epidermal cells (Nottensteiner et al., 2018). Although RIPb also localizes to microtubules (Fig. 4) and thereby provides another link between RACB and the microtubule cytoskeleton, no influence on microtubule stability could be observed by over-expression of RIPb. I also could not detect any interaction with barley KIN13As (Supp Fig. S13) or a negative influence on microtubule stability of both proteins as described for Arabidopsis (Mucha et al., 2010; Oda and Fukuda, 2013). However, the microtubule depolymerizing effect of ROPIP1 could be a mechanism to free RIPb from microtubules. As discussed above, the function of RIPb in susceptibility seems to take place at the plasma membrane, while microtubule-localized truncations of RIPb did not induce susceptibility. The fungus hence could secrete ROPIP1 into the plant cell to remove RIPb from microtubules. In recruiting RACB to microtubules, ROPIP1 might also bring RACB in proximity to RIPb.

In order to identify a possible mode of action for RACB – RIPb signaling, I performed a yeast-two-hybrid screening against a cDNA library of barley and identified CAR1 as a downstream interactor of RIPb (Fig. 14). BiFC and FLIM-FRET experiments support CAR1 as an interaction partner. As RACB and RIPb (Fig. 3C), CAR1 shows a constitutive expression level in leaves and epidermal cell layers of barley, but its expression is not influenced by *Bgh* infection (Fig. 14A). CAR1 localizes to the cytosol when transiently expressed in barley epidermal cells (Fig. 14B), but the interaction with RIPb seems to take place at microtubules and the cell periphery according to BiFC experiments (Fig. 14C). Measurements for FLIM were also made in the cell periphery. That matches the localization of the interaction between RIPb and RACB, making it possible for all three proteins to interact there (Fig. 6). Although it was not possible in the timeframe of this project to create silencing constructs for CAR1, overexpression increased the penetration rate of *Bgh* into transformed barley cells by about 60% and hence to a similar level as RIPbCC2. CAR1 is a short protein of 171 amino acids and contains a C2 domain. C2 domains, not to be confused with the CC domains of RIPs, bind phospholipids in response to calcium binding and were first described for the Protein Kinase C (Xu et al., 1997). The positive charge of the Ca^{2+} ion is used to bind negatively charged phospholipids. CAR proteins were originally discovered in Arabidopsis where they are reported to interact with PYR/PYL ABA receptors in a Ca^{2+}-dependent manner. Binding of CAR proteins to the membrane then creates positive membrane curvature (Rodriguez et al., 2014; Diaz et al., 2016). Ca^{2+} and phos-

pholipids have been described as major contributors to polarization processes. Both in pollen tubes and root hairs, phosphatidylinositol-4,5-bisphosphate (PtdIns(4,5)P_2) accumulates at the apices of both structures (Kost et al., 1999; Helling et al., 2006; Kusano et al., 2008). Phosphoinositides have a well-established connection to ROP G-protein signaling. Arabidopsis RAC2/ROP5 associates with PtdIns(4,5)P_2 at the tip of pollen tubes and the accumulation of PtdIns(4,5)P_2 itself is ROP-dependet (Kost et al., 1999; Helling et al., 2006). In Arabidopsis root hairs ROP10 interacts with FAB1 at the shank of root hairs. FAB1 is involved in the generation of phosphoinositol-3,5-bisphosphate, which also accumulates at the shank. In contrast, ROP2 interacts with PIP5 Kinase 3, which generates PtdIns(4,5)P_2 at the root hair tip (Hirano et al., 2018). Interestingly, a recent study shows the accumulation of PtdIns(4,5)P_2 in the extrahaustorial membrane during the interaction of Arabidopsis with the powdery mildew fungus *E. cichoracearum* (Qin et al., 2020). This indicates that similar mechanisms could be important during polarization in development and susceptibility signaling. An attack by the fungus could trigger accumulation of phospholipids at the penetration site induced by an unknown stimulus. This could lead to polarized growth, in this case ingrowth, of the attacked cell. A role for RACB in ”inverted tip growth” during fungal attack, was also suggested by Schultheiss et al. (2003) and further elaborated by Opalski et al. (2005) after discovering the influence of RACB on actin organization.

Plant root hairs as well as pollen tubes have also been reported to establish a calcium gradient with the highest concentration at the respective tip (Rathore et al., 1991; Wymer et al., 1997). Although, there seems to be no Ca^{2+} gradient involved in root hair initiation, induction of a new artificial Ca^{2+} gradient in root hairs led to new outgrowth at the site with the highest calcium concentration (Wymer et al., 1997; Bibikova et al., 1999). In pollen tubes it was shown that establishment of a Ca^{2+} gradient is dependent on ROPs (Li et al., 1999). In root hairs the Ca^{2+} gradient was disturbed by over-expression of ROP4 and ROP6, and recently it was shown that the RLK CAP1 interacts with RopGEF1 to control the Ca^{2+} gradient, probably via ROP2 (Molendijk et al., 2001; Jones et al., 2002; Bai et al., 2014; Huang et al., 2019). The calcium channel CNGC14 localizes to the tip of root hairs in the same pattern that was reported for ROP G-proteins, which would at least allow an indirect interaction (Zhang et al., 2017). Although, calcium is usually associated with early defense responses during PTI (Seybold et al., 2014), there are also connections between calcium signaling and susceptibility in the barley – *Bgh* interaction. Binding of the transmembrane protein MLO to calmodulin for example is necessary for full MLO mediated susceptibility (Kim et al., 2002) making it likely for Ca^{2+} to have an influence on MLO-mediated susceptibility. Additionally, an increase of apoplastic pCa, indicating a decrease in

apoplastic Ca^{2+} and likely corresponding to an increase in cytosolic Ca^{2+} concentration, has been observed in barley during attack by *Bgh*. These changes in pCa were not just present in early time points, probably due to PTI, but also at intermediate time points (Felle et al., 2004). Since this was observed in susceptible barley plants, the authors suggested that these changes could stem from susceptibility signaling, rather than defense signaling.

Plants affected in RACB signaling by over-expression of CA RACB or knock-down of RACB show a typical root hair phenotype. This indicates that RACB is involved in polarization processes during development and might also be involved in similar processes during *Bgh* attack (Pathuri et al., 2008; Hoefle and Hückelhoven, 2014; Scheler et al., 2016). Like all RIP proteins, RIPb has a lysine-rich C-terminus (WKKGPK). A similar motif (WRKKGQK) is responsible for membrane localization of AtRIP1/ICR1 in pollen tubes, specifically the PtdIns(4,5)P_2-rich region at the pollen tube tip (Kost et al., 1999; Li et al., 2008). Considering this, it is likely for the C-terminus of RIPb to be involved in phospholipid binding as well. Like RIPb, RACB also has a polybasic stretch at the C-terminus, which was shown in other ROPs to be involved in anionic lipid interaction (Schultheiss et al., 2003; Platre et al., 2019). A conserved cystein residue (C158) was shown in AtROP6 to be S-acylated upon activation (Sorek et al., 2017). This provides a potential mode of action where RACB, RIPb, and CAR1 meet in phospholipid-rich zones at the plasma membrane to promote polarization. CAR1 could thereby provide a link between RACB signaling and Ca^{2+}. This work shows that RACB and RIPb both localize to the site of fungal attack, supporting this hypothesis (Fig. 12). In successfully penetrated cells, YFP-RIPb and both wild-type and CA CFP-RACB localize in a ring-like structure around the haustorial neck region, which was clearly visible 24 hours after inoculation. In my experiments this accumulation was much more defined than the signal of free mCherry, which was also present at the site of attack due to cytosolic accumulation. However, I did not only find signal accumulation in successfully penetrated cells around the haustorial neck, but also in repelled interactions ending in papilla formation. The signal at the papilla was less defined and more fringy in what could be membrane protrusions around the papilla extensions. This suggests that accumulation of these two proteins alone is not sufficient to make plant cells fully susceptible. RIPbCC2 had a much stronger influence on susceptibility than full length RIPb (Fig. 11), but also higher expression levels (Fig. S12). YFP-RIPbCC2 therefore accumulated stronger at the site of attack. Measurements at later time points (48 hours after inoculation) show clear YFP-RIPbCC2 signal at the membrane of the haustorial neck (Fig. 12D, E). As mentioned above, the extrahaustorial membrane was found to contain PtdIns(4,5)P_2, supporting the idea that RIPb can

localize to phospholipid rich domains.

With the current knowledge it is difficult to draw conclusions on the mode of action for RIPb and RACB. It might be that both proteins get recruited by *Bgh*, either directly or indirectly, and influence polarization at the site of attack. Whether this is novel polarization, or repurposing of existing polarization can not yet be answered. It seems like both proteins would interact with phospholipid-rich areas at the site of attack and the EHM and the involvement of CAR1 would provide an additional interesting link to Ca^{2+}. CAR1 could either interact downstream of the RACB-RIPb complex and further connect it to signaling components, or it might be involved in positional regulation of the RACB-RIPb complex in response to Ca^{2+} signaling. However, in order to evaluate this option more questions need to be answered. Though there are hints, it is not proven that an intracellular Ca^{2+} gradient is present in susceptibility and also that CAR1 would actually react to it. Additionally, the interaction of RIPb and RACB with phospholipids at the site of attack and the EHM is, although very likely, not proven yet. Nevertheless, RIPb provides a convincing link between polarization and RACB signaling in susceptibility and opens a door to many questions about the nature of polarization in interactions with *Bgh* specifically, and haustoria establishing pathogens in general. Maybe influencing and artificially fine-tuning polarization could be a novel way for crop protection.

5 Summary

Barley is one of the most important crops and the barley powdery mildew disease caused by *Blumeria graminis* f.sp. *hordei* (*Bgh*) is a wide spread disease causing considerable economic losses. The barley protein RACB (Ras-related C3 botulinum toxin substrate B) is a small monomeric ROP G-protein of the Rho of Plants (ROP) class and a susceptibility factor in the interaction of barley and *Bgh*. RACB is involved in penetration resistance against *Bgh*, but seems to have no influence on classical defense reactions themselves. In this work, I investigated ROP INTERACTIVE PARTNER (RIP) proteins with focus on their interaction with the susceptibility factor RACB in order to unravel the RACB signaling pathway in susceptibility. RIPs are suggested to act as scaffold proteins connecting ROP G-proteins with downstream executors. Three RIP proteins were found in barley, RIPa, RIPb, and RIPc, with respective homologs in rice and Brachypodium. All RIPs show distinct localization patterns within epidermal leaf cells and all RIPs have the possibility to localize to microtubules, making them connectors between G-proteins and microtubules. While RIPa and RIPc seem to have no significant influence on the interaction of barley with *Bgh*, over-expression of RIPb rendered barley leaves consistently more susceptible to *Bgh*. Especially the ROP interacting C-terminal CC2 domain of RIPb seems to play a role in the interaction. This domain alone has an even stronger effect on susceptibility than full length RIPb and might also be able to interact with downstream interactors. RIPb, like all RIPs was able to interact with RACB in yeast and *in planta*. The interaction with RACB takes place at the plasma membrane and microtubules. Both RACB and RIPb accumulated at the site of attack, creating a ring-like aggregation around the entry site of the fungus. RIPb also interacted with the C2 domain containing protein Calcium-dependent ABA related 1 (CAR1), providing a connection to Ca^{2+} and phospholipid binding. However, whether this interaction is downstream of RACB – RIPb, or CAR1 regulates the localization of the RACB-RIPb complex needs to be further investigated.

This work also provided more insight into the nature of RIP proteins, which are only little researched to date. All RIP proteins were able to interact with microtubules, either by themselves or in interaction with a ROP G-proteins. The N-terminal CC1 domain seems to be responsible for this interaction. In case of RIPb its variable Va region seems to be necessary for RIPb – RIPb interaction and microtubule localization. The results of this work indicate that RIPs might provide a general link between microtubules and G-proteins in grasses.

6 Zusammenfassung

Gerste ist eines der wichtigsten Getreide. *Blumeria graminis* f.sp. *hordei* (*Bgh*) ist Auslöser der Mehltau-Krankheit auf Gerste und verursacht jährlich beträchtliche ökonomische Schäden. Das Gerstenprotein RACB (Ras-related C3 botulinum toxin substrate B) gehört zu den kleinen monomeren G-Proteinen der Rho of Plants (ROP)-Klasse und ist ein Anfälligkeitsfaktor in der Interaktion von Gerste und *Bgh*. RACB ist an der Penetrationsresistenz gegen *Bgh* beteiligt, hat aber keinen direkten Einfluss auf klassische pflanzliche Abwehrreaktionen. In dieser Arbeit untersuchte ich ROP INTERACTIVE PARTNER (RIP) Proteine der Gerste mit speziellem Fokus auf deren Interaktion mit dem Anfälligkeitsfaktor RACB, um dazu beizutragen den RACB-Signalweg während der Gerste – *Bgh* Interaktion aufzuklären. Man geht davon aus, dass es sich bei RIPs um Gerüstproteine handelt, die ROP G-Proteine mit nachgelagerten Interaktoren verbinden. Es wurden die drei RIP Proteine RIPa, RIPb und RIPc in der Gerste identifiziert mit jeweiligen Homologen in Reis und Brachypodium. Alle RIPs zeigten spezifische Lokalisierungsmuster in Epidermiszellen und können potentiell an das Mikrotubulicytoskelett lokalisieren, was sie zu einer molekularen Brücke zwischen ROP G-Proteinen und Mikrotubuli machen würde. Während RIPa und RIPc keinen signifikanten Einfluss auf die Anfälligkeit der Gerste gegenüber *Bgh* zeigten, führte die Überexpression von RIPb zu einer reproduzierbar erhöhten Penetrationsrate. Besonders die C-terminale CC2 Domäne von RIPb, welche auch mit ROPs interagieren kann, scheint eine Rolle in der Interaktion zu spielen. Diese Domäne allein hatte einen noch stärkeren Effekt auf die Anfälligkeit als Volllängen-RIPb und könnte außerdem in der Lage sein mit Interaktoren die an der Signalweiterleitung beteiligt sind zu interagieren. RIPa, RIPb und RIPc waren in der Lage mit RACB in Hefe und *in planta* zu interagieren. Die Interaktion zwischen RIPb und RACB fand an der Plasmamembran und an den Mikrotubuli statt. Sowohl RACB als auch RIPb akkumulierten in einer Ring-ähnlichen Ansammlung an der Penetrationsstelle zwischen Gerste und *Bgh*. RIPb interagierte außerdem mit dem Protein Calcium-dependent ABA related 1 (CAR1). Dieses besitzt eine C2 Domäne was auf eine mögliche Verbindung zur Ca^{2+}-gesteuerten Signalübertragung und Phospholipidbindung hindeutet. Um aufzuklären ob es sich hierbei um eine nachgeschaltete Signalkomponente handelt, oder ob CAR1 vielleicht die Lokalisierung des RACB-RIPb Proteinkomplexes reguliert, müssen allerdings weiterführende Experimente gemacht werden.

Diese Arbeit bietet zudem weiteren Einblick in die Funktionalität von RIP Proteinen, die bisher verhältnismäßig wenig erforscht wurden. Alle RIP Proteine waren in der Lage, entweder selbst, oder durch die Interaktion mit ROP G-Proteinen, mit

dem Mikrotubulicytoskelett zu interagieren. Die N-terminale CC1 Domäne ist hierfür notwendig. Im Falle von RIPb scheint die mittlere Va Domäne für die Autointeraktion von RIPb und für die Mikrotubulilokalisierung notwendig zu sein. Die Ergebnisse dieser Arbeit zeigen, dass RIPs eine generelle Verbindung zwischen ROP G-Proteinen und Mikrotubuli in Gräsern darstellen könnten.

7 References

Afzal, A. J., da Cunha, L., and Mackey, D. (2011). Separable fragments and membrane tethering of arabidopsis RIN4 regulate its suppression of PAMP-triggered immunity. *Plant Cell*, 23(10):3798–3811.

Aist, J. R. (1976). Papillae and other related wound plugs of plant cells. *Annual Review of Phytopathology*, 14:145–163.

Akamatsu, A., Fujiwara, M., Hamada, S., Wakabayashi, M., Yao, A., Wang, Q., Kosami, K., Dang, T. T., Kaneko-Kawano, T., Shimamoto, K., and Kawano, Y. (2020). The Small GTPase OsRac1 forms two distinct immune receptor complexes containing the PRR OsCERK1 and the NLR Pit. *BioRxiv*.

Akamatsu, A., Wong, H. L., Fujiwara, M., Okuda, J., Nishide, K., Uno, K., Imai, K., Umemura, K., Kawasaki, T., Kawano, Y., and Shimamoto, K. (2013). An OsCEBiP/OsCERK1-OsRacGEF1-OsRac1 module is an essential early component of chitin-induced rice immunity. *Cell Host Microbe*, 13(4):465–476.

Aktories, K. (2015). Rho-modifying bacterial protein toxins. *Pathog Dis*, 73(9):ftv091.

Aktories, K., Braun, U., Rosener, S., Just, I., and Hall, A. (1989). The rho gene product expressed in *E. coli* is a substrate of botulinum ADP-ribosyltransferase C3. *Biochem Biophys Res Commun*, 158(1):209–213.

An, Q., Ehlers, K., Kogel, K. H., van Bel, A. J., and Hückelhoven, R. (2006a). Multivesicular compartments proliferate in susceptible and resistant MLA12-barley leaves in response to infection by the biotrophic powdery mildew fungus. *New Phytol*, 172(3):563–576.

An, Q., Hückelhoven, R., Kogel, K. H., and van Bel, A. J. (2006b). Multivesicular bodies participate in a cell wall-associated defence response in barley leaves attacked by the pathogenic powdery mildew fungus. *Cell Microbiol*, 8(6):1009–1019.

Asai, T., Tena, G., Plotnikova, J., Willmann, M. R., Chiu, W.-L., Gomez-Gomez, L., Boller, T., Ausubel, F. M., and Sheen, J. (2002). MAP kinase signalling cascade in Arabidopsis innate immunity. *Nature*, 415(6875):977–983.

Assaad, F. F., Qiu, J. L., Youngs, H., Ehrhardt, D., Zimmerli, L., Kalde, M., Wanner, G., Peck, S. C., Edwards, H., Ramonell, K., Somerville, C. R., and Thordal-Christensen, H. (2004). The PEN1 syntaxin defines a novel cellular compartment upon fungal

attack and is required for the timely assembly of papillae. *Mol Biol Cell*, 15(11):5118–5129.

Axtell, M. J. and Staskawicz, B. J. (2003). Initiation of RPS2-specified disease resistance in arabidopsis is coupled to the AvrRpt2-directed elimination of RIN4. *Cell*, 112(3):369–377.

Badr, A., Muller, K., Schafer-Pregl, R., El Rabey, H., Effgen, S., Ibrahim, H. H., Pozzi, C., Rohde, W., and Salamini, F. (2000). On the origin and domestication history of Barley (*Hordeum vulgare*). *Mol Biol Evol*, 17(4):499–510.

Bai, L., Ma, X., Zhang, G., Song, S., Zhou, Y., Gao, L., Miao, Y., and Song, C. P. (2014). A Receptor-Like Kinase Mediates Ammonium Homeostasis and Is Important for the Polar Growth of Root Hairs in Arabidopsis. *Plant Cell*, 26(4):1497–1511.

Barth, H., Olenik, C., Sehr, P., Schmidt, G., Aktories, K., and Meyer, D. K. (1999). Neosynthesis and activation of Rho by *Escherichia coli* cytotoxic necrotizing factor (CNF1) reverse cytopathic effects of ADP-ribosylated Rho. *J Biol Chem*, 274(39):27407–27414.

Basu, D., Le, J., Zakharova, T., Mallery, E. L., and Szymanski, D. B. (2008). A SPIKE1 signaling complex controls actin-dependent cell morphogenesis through the heteromeric WAVE and ARP2/3 complexes. *Proceedings of the National Academy of Sciences*, 105(10):4044–4049.

Berken, A., Thomas, C., and Wittinghofer, A. (2005). A new family of RhoGEFs activates the Rop molecular switch in plants. *Nature*, 436(7054):1176–1180.

Bhat, R. A., Miklis, M., Schmelzer, E., Schulze-Lefert, P., and Panstruga, R. (2005). Recruitment and interaction dynamics of plant penetration resistance components in a plasma membrane microdomain. *Proc Natl Acad Sci U S A*, 102(8):3135–3140.

Bibikova, T. N., Blancaflor, E. B., and Gilroy, S. (1999). Microtubules regulate tip growth and orientation in root hairs of arabidopsis thaliana. *Plant J*, 17(6):657–665.

Bigeard, J., Colcombet, J., and Hirt, H. (2015). Signaling mechanisms in pattern-triggered immunity (PTI). *Mol Plant*, 8(4):521–39.

Birnboim, H. C. and Doly, J. (1979). A rapid alkaline extraction procedure for screening recombinant plasmid DNA. *Nucleic Acids Res*, 7(6):1513–1523.

Bloch, D., Hazak, O., , M., and Yalovsky, S. (2008). A novel ROP/RAC GTPase effector integrates plant cell form and pattern formation. *Plant Signal Behav*, 3(1):41–43.

Bohlenius, H., Morch, S. M., Godfrey, D., Nielsen, M. E., and Thordal-Christensen, H. (2010). The multivesicular body-localized GTPase ARFA1b/1c is important for callose deposition and ROR2 syntaxin-dependent preinvasive basal defense in barley. *Plant Cell*, 22(11):3831–3844.

Buchsbaum, R. J., Connolly, B. A., and Feig, L. A. (2002). Interaction of Rac exchange factors Tiam1 and Ras-GRF1 with a scaffold for the p38 mitogen-activated protein kinase cascade. *Mol Cell Biol*, 22(12):4073–4085.

Buchsbaum, R. J., Connolly, B. A., and Feig, L. A. (2003). Regulation of p70 S6 kinase by complex formation between the Rac guanine nucleotide exchange factor (Rac-GEF) Tiam1 and the scaffold spinophilin. *J Biol Chem*, 278(21):18833–18841.

Burkart, G. M., Baskin, T. I., and Bezanilla, M. (2015). A family of ROP proteins that suppresses actin dynamics, and is essential for polarized growth and cell adhesion. *J Cell Sci*, 128(14):2553–2564.

Buschges, R., Hollricher, K., Panstruga, R., Simons, G., Wolter, M., Frijters, A., van Daelen, R., van der Lee, T., Diergaarde, P., Groenendijk, J., Topsch, S., Vos, P., Salamini, F., and Schulze-Lefert, P. (1997). The barley *Mlo* gene: a novel control element of plant pathogen resistance. *Cell*, 88(5):695–705.

Butty, A. C., Perrinjaquet, N., Petit, A., Jaquenoud, M., Segall, J. E., Hofmann, K., Zwahlen, C., and Peter, M. (2002). A positive feedback loop stabilizes the guanine-nucleotide exchange factor Cdc24 at sites of polarization. *EMBO J*, 21(7):1565–1576.

Cameron, C. and Geitmann, A. (2018). Cell mechanics of pollen tube growth. *Curr Opin Genet Dev*, 51:11–17.

Cao, Y., Liang, Y., Tanaka, K., Nguyen, C. T., Jedrzejczak, R. P., Joachimiak, A., and Stacey, G. (2014). The kinase LYK5 is a major chitin receptor in Arabidopsis and forms a chitin-induced complex with related kinase CERK1. *Elife*, 3.

Carella, P., Gogleva, A., Tomaselli, M., Alfs, C., and Schornack, S. (2018). *Phytophthora palmivora* establishes tissue-specific intracellular infection structures in the earliest divergent land plant lineage. *Proc Natl Acad Sci U S A*, 115(16):E3846–E3855.

Carver, T., Kunoh, H., Thomas, B., and Nicholson, R. (1999). Release and visualization of the extracellular matrix of conidia of *Blumeria graminis*. *Mycological Research*, 103(5):547 – 560.

Catanzariti, A. M., Dodds, P. N., and Ellis, J. G. (2007). Avirulence proteins from haustoria-forming pathogens. *FEMS Microbiol Lett*, 269(2):181–188.

Cavazza, T. and Vernos, I. (2016). The RanGTP Pathway: From Nucleo-Cytoplasmic Transport to Spindle Assembly and Beyond. *Front Cell Dev Biol*, 3:82.

Chang, F., Gu, Y., Ma, H., and Yang, Z. (2013). AtPRK2 promotes ROP1 activation via RopGEFs in the control of polarized pollen tube growth. *Mol Plant*, 6(4):1187–1201.

Chardin, P., Boquet, P., Madaule, P., Popoff, M. R., Rubin, E. J., and Gill, D. M. (1989). The mammalian G protein rhoC is ADP-ribosylated by *Clostridium botulinum* exoenzyme C3 and affects actin microfilaments in Vero cells. *EMBO J*, 8(4):1087–1092.

Chen, C. Y., Cheung, A. Y., and Wu, H. M. (2003). Actin-depolymerizing factor mediates Rac/Rop GTPase-regulated pollen tube growth. *Plant Cell*, 15(1):237–249.

Chinchilla, D., Zipfel, C., Robatzek, S., Kemmerling, B., Nürnberger, T., Jones, J. D. G., Felix, G., and Boller, T. (2007). A flagellin-induced complex of the receptor FLS2 and BAK1 initiates plant defence. *Nature*, 448(7152):497–500.

Chiou, J. G., Balasubramanian, M. K., and Lew, D. J. (2017). Cell Polarity in Yeast. *Annu Rev Cell Dev Biol*, 33:77–101.

Christensen, T. M., Vejlupkova, Z., Sharma, Y. K., Arthur, K. M., Spatafora, J. W., Albright, C. A., Meeley, R. B., Duvick, J. P., Quatrano, R. S., and Fowler, J. E. (2003). Conserved subgroups and developmental regulation in the monocot *rop* gene family. *Plant Physiol*, 133(4):1791–1808.

Christiansen, K. M., Gu, Y., Rodibaugh, N., and Innes, R. W. (2011). Negative regulation of defence signalling pathways by the EDR1 protein kinase. *Mol Plant Pathol*, 12(8):746–758.

Collins, N. C., Thordal-Christensen, H., Lipka, V., Bau, S., Kombrink, E., Qiu, J. L., Hückelhoven, R., Stein, M., Freialdenhoven, A., Somerville, S. C., and Schulze-Lefert, P. (2003). SNARE-protein-mediated disease resistance at the plant cell wall. *Nature*, 425(6961):973–977.

Consonni, C., Humphry, M. E., Hartmann, H. A., Livaja, M., Durner, J., Westphal, L., Vogel, J., Lipka, V., Kemmerling, B., Schulze-Lefert, P., Somerville, S. C., and Panstruga, R. (2006). Conserved requirement for a plant host cell protein in powdery mildew pathogenesis. *Nat Genet*, 38(6):716–720.

Costamilan, L. M. (2005). Variability of the wheat powdery mildew pathogen *Blumeria graminis* f.sp. *tritici* in the 2003 crop season. *Fitopatol. bras.*, 30(4):420–422.

Cox, A. D. and Der, C. J. (2010). Ras history: The saga continues. *Small GTPases*, 1(1):2–27.

Das, M., Nunez, I., Rodriguez, M., Wiley, D. J., Rodriguez, J., Sarkeshik, A., Yates, J. R., r., Buchwald, P., and Verde, F. (2015). Phosphorylation-dependent inhibition of Cdc42 GEF Gef1 by 14-3-3 protein Rad24 spatially regulates Cdc42 GTPase activity and oscillatory dynamics during cell morphogenesis. *Mol Biol Cell*, 26(19):3520–3534.

Deslandes, L., Olivier, J., Peeters, N., Feng, D. X., Khounlotham, M., Boucher, C., Somssich, I., Genin, S., and Marco, Y. (2003). Physical interaction between RRS1-R, a protein conferring resistance to bacterial wilt, and PopP2, a type III effector targeted to the plant nucleus. *Proc Natl Acad Sci U S A*, 100(13):8024–8029.

Diaz, M., Sanchez-Barrena, M. J., Gonzalez-Rubio, J. M., Rodriguez, L., Fernandez, D., Antoni, R., Yunta, C., Belda-Palazon, B., Gonzalez-Guzman, M., Peirats-Llobet, M., Menendez, M., Boskovic, J., Marquez, J. A., Rodriguez, P. L., and Albert, A. (2016). Calcium-dependent oligomerization of CAR proteins at cell membrane modulates ABA signaling. *Proc Natl Acad Sci U S A*, 113(3):E396–405.

Dodds, P. N. and Rathjen, J. P. (2010). Plant immunity: towards an integrated view of plant-pathogen interactions. *Nat Rev Genet*, 11(8):539–548.

Douchkov, D., Nowara, D., Zierold, U., and Schweizer, P. (2005). A high-throughput gene-silencing system for the functional assessment of defense-related genes in barley epidermal cells. *Molecular Plant-Microbe Interactions*, 18(8):755–761.

Dransart, E., Olofsson, B., and Cherfils, J. (2005). RhoGDIs revisited: novel roles in Rho regulation. *Traffic*, 6(11):957–966.

Draz, I. S., Esmail, S. M., Abou-Zeid, M. A. E.-H., and Essa, T. A. E.-M. (2019). Powdery mildew susceptibility of spring wheat cultivars as a major constraint on grain yield. *Annals of Agricultural Sciences*, 64(1):39 – 45.

Duan, Q., Kita, D., Li, C., Cheung, A. Y., and Wu, H. M. (2010). FERONIA receptor-like kinase regulates RHO GTPase signaling of root hair development. *Proc Natl Acad Sci U S A*, 107(41):17821–17826.

Edwards, H. H. (2002). Development of primary germ tubes by conidia of *Blumeria graminis* f.sp. *hordei* on leaf epidermal cells of *Hordeum vulgare*. *Canadian Journal of Botany*, 80(10):1121–1125.

Ellinger, D., Naumann, M., Falter, C., Zwikowics, C., Jamrow, T., Manisseri, C., Somerville, S. C., and Voigt, C. A. (2013). Elevated early callose deposition results in complete penetration resistance to powdery mildew in arabidopsis. *Plant Physiol*, 161(3):1433–1444.

Eng, R. C. and Wasteneys, G. O. (2014). The Microtubule Plus-End Tracking Protein ARMADILLO-REPEAT KINESIN1 Promotes Microtubule Catastrophe in Arabidopsis. *Plant Cell*, 26(8):3372–3386.

Engelhardt, S., Kopischke, M., Hofer, J., Probst, K., McCollum, C., and Hückelhoven, R. (2019). Barley RIC157 is involved in RACB-mediated susceptibility to powdery mildew. *BioRxiv*.

Engelhardt, S., Trutzenberg, A., and Hückelhoven, R. (2020). Regulation and Functions of ROP GTPases in Plant-Microbe Interactions. *Cells*, 9(9).

Feiguelman, G., Fu, Y., and Yalovsky, S. (2018). ROP GTPases Structure-Function and Signaling Pathways. *Plant Physiol*, 176(1):57–79.

Felix, G., Duran, J. D., Volko, S., and Boller, T. (1999). Plants have a sensitive perception system for the most conserved domain of bacterial flagellin. *Plant J*, 18(3):265–276.

Felle, H. H., Herrmann, A., Hanstein, S., Hückelhoven, R., and Kogel, K. H. (2004). Apoplastic pH signaling in barley leaves attacked by the powdery mildew fungus *Blumeria graminis* f. sp. *hordei*. *Mol Plant Microbe Interact*, 17(1):118–123.

Feng, F., Yang, F., Rong, W., Wu, X., Zhang, J., Chen, S., He, C., and Zhou, J. M. (2012). A Xanthomonas uridine 5'-monophosphate transferase inhibits plant immune kinases. *Nature*, 485(7396):114–118.

Feng, J., Wang, F., Liu, G., Greenshields, D., Shen, W., Kaminskyj, S., Hughes, G. R., Peng, Y., Selvaraj, G., Zou, J., and Wei, Y. (2009). Analysis of a *Blumeria graminis*-secreted lipase reveals the importance of host epicuticular wax components for fungal adhesion and development. *Mol Plant Microbe Interact*, 22(12):1601–1610.

Fortune Business Insights, Agriculture Market Research Report (2020). Crop Protection Chemicals Market Size, Share & COVID-19 Impact Analysis, By Type (Herbicides, Isecticides, Fungicides, and Others), Source (Synthetic Chemicals and Biologicals), Mode of Application (Foliar Spray, Soil Treatment, Seed Treatment, and Others), Crop Type, and Regional Forecast, 2020-2027.

Freialdenhoven, A., Peterhansel, C., Kurth, J., Kreuzaler, F., and Schulze-Lefert, P. (1996). Identification of Genes Required for the Function of Non-Race-Specific *mlo* Resistance to Powdery Mildew in Barley. *Plant Cell*, 8(1):5–14.

Friebel, A., Ilchmann, H., Aepfelbacher, M., Ehrbar, K., Machleidt, W., and Hardt, W. D. (2001). Sope and sope2 from salmonella typhimurium activate different sets of RhoGTPases of the host cell. *J Biol Chem*, 276(36):34035–34040.

Frye, C. A. and Innes, R. W. (1998). An Arabidopsis mutant with enhanced resistance to powdery mildew. *Plant Cell*, 10(6):947–956.

Frye, C. A., Tang, D., and Innes, R. W. (2001). Negative regulation of defense responses in plants by a conserved MAPKK kinase. *Proc Natl Acad Sci U S A*, 98(1):373–378.

Fu, Y. and Galan, J. E. (1999). A Salmonella protein antagonizes Rac-1 and Cdc42 to mediate host-cell recovery after bacterial invasion. *Nature*, 401(6750):293–297.

Fu, Y., Gu, Y., Zheng, Z., Wasteneys, G., and Yang, Z. (2005). Arabidopsis interdigitating cell growth requires two antagonistic pathways with opposing action on cell morphogenesis. *Cell*, 120(5):687–700.

Fu, Y., Wu, G., and Yang, Z. (2001). Rop gtpase-dependent dynamics of tip-localized f-actin controls tip growth in pollen tubes. *J Cell Biol*, 152(5):1019–1032.

Fu, Y., Xu, T., Zhu, L., Wen, M., and Yang, Z. (2009). A ROP GTPase signaling pathway controls cortical microtubule ordering and cell expansion in Arabidopsis. *Curr Biol*, 19(21):1827–1832.

Fukuda, H. (1996). Xylogenesis: Initiation, Progression, and Cell Death. *Annu Rev Plant Physiol Plant Mol Biol*, 47:299–325.

Gao, C., Sun, P., Wang, W., and Tang, D. (2020). Arabidopsis E3 ligase KEG associates with and ubiquitinates MKK4 and MKK5 to regulate plant immunity. *J Integr Plant Biol*.

Gassmann, W., Hinsch, M. E., and Staskawicz, B. J. (1999). The Arabidopsis RPS4 bacterial-resistance gene is a member of the TIR-NBS-LRR family of disease-resistance genes. *Plant J*, 20(3):265–277.

Genth, H., Gerhard, R., Maeda, A., Amano, M., Kaibuchi, K., Aktories, K., and Just, I. (2003). Entrapment of Rho ADP-ribosylated by Clostridium botulinum C3 exoenzyme in the Rho-guanine nucleotide dissociation inhibitor-1 complex. *J Biol Chem*, 278(31):28523–28527.

Gómez-Gómez, L. and Boller, T. (2000). FLS2: An LRR Receptor–like Kinase Involved in the Perception of the Bacterial Elicitor Flagellin in Arabidopsis. *Molecular Cell*, 5(6):1003 – 1011.

Gouy, M., Guindon, S., and Gascuel, O. (2009). SeaView Version 4: A Multiplatform Graphical User Interface for Sequence Alignment and Phylogenetic Tree Building. *Molecular Biology and Evolution*, 27(2):221–224.

Griffis, A. H., Groves, N. R., Zhou, X., and Meier, I. (2014). Nuclei in motion: movement and positioning of plant nuclei in development, signaling, symbiosis, and disease. *Front Plant Sci*, 5:129.

Gross, P., Julius, C., Schmelzer, E., and Hahlbrock, K. (1993). Translocation of cytoplasm and nucleus to fungal penetration sites is associated with depolymerization of microtubules and defence gene activation in infected, cultured parsley cells. *EMBO J*, 12(5):1735–1744.

Gu, Y., Fu, Y., Dowd, P., Li, S., Vernoud, V., Gilroy, S., and Yang, Z. (2005). A Rho family GTPase controls actin dynamics and tip growth via two counteracting downstream pathways in pollen tubes. *J Cell Biol*, 169(1):127–138.

Gu, Y., Li, S., Lord, E. M., and Yang, Z. (2006). Members of a novel class of Arabidopsis Rho guanine nucleotide exchange factors control Rho GTPase-dependent polar growth. *Plant Cell*, 18(2):366–381.

Guindon, S., Dufayard, J.-F., Lefort, V., Anisimova, M., Hordijk, W., and Gascuel, O. (2010). New Algorithms and Methods to Estimate Maximum-Likelihood Phylogenies: Assessing the Performance of PhyML 3.0. *Systematic Biology*, 59(3):307–321.

Guo, H., Ahn, H. K., Sklenar, J., Huang, J., Ma, Y., Ding, P., Menke, F. L. H., and Jones, J. D. G. (2020). Phosphorylation-Regulated activation of the Arabidopsis RRS1-R/RPS4 Immune Receptor Complex Reveals Two Distinct Effector Recognition Mechanisms. *Cell Host Microbe*, 27(5):769–781 e6.

Hansjakob, A., Bischof, S., Bringmann, G., Riederer, M., and Hildebrandt, U. (2010). Very-long-chain aldehydes promote in vitro prepenetration processes of *Blumeria graminis* in a dose- and chain length-dependent manner. *New Phytol*, 188(4):1039–1054.

Hardham, A. R., Takemoto, D., and White, R. G. (2008). Rapid and dynamic subcellular reorganization following mechanical stimulation of Arabidopsis epidermal cells mimics responses to fungal and oomycete attack. *BMC Plant Biol*, 8:63.

Hardt, W. D., Chen, L. M., Schuebel, K. E., Bustelo, X. R., and Galan, J. E. (1998). *S. typhimurium* encodes an activator of Rho GTPases that induces membrane ruffling and nuclear responses in host cells. *Cell*, 93(5):815–826.

Haverkort, A. J., Boonekamp, P. M., Hutten, R., Jacobsen, E., Lotz, L. A. P., Kessel, G. J. T., Visser, R. G. F., and van der Vossen, E. A. G. (2008). Societal Costs of Late Blight in Potato and Prospects of Durable Resistance Through Cisgenic Modification. *Potato Research*, 51(1):47–57.

Hazak, O., Bloch, D., Poraty, L., Sternberg, H., Zhang, J., Friml, J., and Yalovsky, S. (2010). A Rho Scaffold Integrates the Secretory System with Feedback Mechanisms in Regulation of Auxin Distribution. *Plos Biology*, 8(1).

Hazak, O., Mamon, E., Lavy, M., Sternberg, H., Behera, S., Schmitz-Thom, I., Bloch, D., Dementiev, O., Gutman, I., Danziger, T., Schwarz, N., Abuzeineh, A., Mockaitis, K., Estelle, M., Hirsch, J. A., Kudla, J., and Yalovsky, S. (2019). A novel Ca^{2+}-binding protein that can rapidly transduce auxin responses during root growth. *PLoS Biol*, 17(7):e3000085.

Helling, D., Possart, A., Cottier, S., Klahre, U., and Kost, B. (2006). Pollen tube tip growth depends on plasma membrane polarization mediated by tobacco PLC3 activity and endocytic membrane recycling. *Plant Cell*, 18(12):3519–3534.

Hiei, Y., Ishida, Y., and Komari, T. (2014). Progress of cereal transformation technology mediated by Agrobacterium tumefaciens. *Frontiers in Plant Science*, 5:1–11.

Hirano, T., Konno, H., Takeda, S., Dolan, L., Kato, M., Aoyama, T., Higaki, T., Takigawa-Imamura, H., and Sato, M. H. (2018). PtdIns(3,5)P2 mediates root hair shank hardening in arabidopsis. *Nat Plants*, 4(11):888–897.

Hoefle, C. and Hückelhoven, R. (2014). A barley Engulfment and Motility domain containing protein modulates Rho GTPase activating protein HvMAGAP1 function in the barley powdery mildew interaction. *Plant Mol Biol*, 84(4-5):469–78.

Hoefle, C., Huesmann, C., Schultheiss, H., Bornke, F., Hensel, G., Kumlehn, J., and Hückelhoven, R. (2011). A barley ROP GTPase ACTIVATING PROTEIN associates with microtubules and regulates entry of the barley powdery mildew fungus into leaf epidermal cells. *Plant Cell*, 23(6):2422–2439.

Hoefle, C., McCollum, C., and Hückelhoven, R. (2020). Barley ROP-Interactive Partner-a organizes into RAC1- and MICROTUBULE-ASSOCIATED ROP-GTPASE ACTIVATING PROTEIN 1-dependent membrane domains. *BMC Plant Biol*, 20(1):94.

Hong, D., Jeon, B. W., Kim, S. Y., Hwang, J. U., and Lee, Y. (2015). The ROP2-RIC7 pathway negatively regulates light-induced stomatal opening by inhibiting exocyst subunit Exo70B1 in Arabidopsis. *New Phytol*, 209(2):634 – 635.

Huang, C., Jiao, X., Yang, L., Zhang, M., Dai, M., Wang, L., Wang, K., Bai, L., and Song, C. (2019). ROP-GEF signal transduction is involved in AtCAP1-regulated root hair growth. *Plant Growth Regulation*, 87(1):1–8.

Huang, J. B., Liu, H., Chen, M., Li, X., Wang, M., Yang, Y., Wang, C., Huang, J., Liu, G., Liu, Y., Xu, J., Cheung, A. Y., and Tao, L. Z. (2014). ROP3 GTPase Contributes to Polar Auxin Transport and Auxin Responses and Is Important for Embryogenesis and Seedling Growth in Arabidopsis. *Plant Cell*, 26(9):3501–3518.

Hückelhoven, R., Fodor, J., Preis, C., and Kogel, K. H. (1999). Hypersensitive cell death and papilla formation in barley attacked by the powdery mildew fungus are associated with hydrogen peroxide but not with salicylic acid accumulation. *Plant Physiol*, 119(4):1251–1260.

Hückelhoven, R., Fodor, J., Trujillo, M., and Kogel, K. H. (2000). Barley Mla and Rar mutants compromised in the hypersensitive cell death response against *Blumeria graminis* f.sp. *hordei* are modified in their ability to accumulate reactive oxygen intermediates at sites of fungal invasion. *Planta*, 212(1):16–24.

Huesmann, C., Reiner, T., Hoefle, C., Preuss, J., Jurca, M. E., Domoki, M., Feher, A., and Hückelhoven, R. (2012). Barley ROP binding kinase1 is involved in microtubule organization and in basal penetration resistance to the barley powdery mildew fungus. *Plant Physiol*, 159(1):311–320.

Hume, P. J., Singh, V., Davidson, A. C., and Koronakis, V. (2017). Swiss Army Pathogen: The Salmonella Entry Toolkit. *Front Cell Infect Microbiol*, 7:348.

Humphries, J. A., Vejlupkova, Z., Luo, A., Meeley, R. B., Sylvester, A. W., Fowler, J. E., and Smith, L. G. (2011). ROP GTPases act with the receptor-like protein PAN1 to polarize asymmetric cell division in maize. *Plant Cell*, 23(6):2273–2284.

International Barley Genome Sequencing, C. (2012). A physical, genetic and functional sequence assembly of the barley genome. *Nature*, 491(7426):711–716.

Ito, Y., Kaku, H., and Shibuya, N. (1997). Identification of a high-affinity binding protein for N-acetylchitooligosaccharide elicitor in the plasma membrane of suspension-cultured rice cells by affinity labeling. *Plant J*, 12(2):347–356.

Jackson, C. L. and Bouvet, S. (2014). Arfs at a glance. *J Cell Sci*, 127(Pt 19):4103–4109.

Jaffe, A. B. and Hall, A. (2005). Rho GTPases: Biochemistry and biology. *Annual Review of Cell and Developmental Biology*, 21:247–269.

Jones, M. A., Raymond, M. J., Yang, Z., and Smirnoff, N. (2007). Nadph oxidase-dependent reactive oxygen species formation required for root hair growth depends on rop gtpase. *J Exp Bot*, 58(6):1261–1270.

Jones, M. A., Shen, J. J., Fu, Y., Li, H., Yang, Z., and Grierson, C. S. (2002). The Arabidopsis Rop2 GTPase is a positive regulator of both root hair initiation and tip growth. *Plant Cell*, 14(4):763–776.

Jørgensen, J. H. (1992). Discovery, characterization and exploitation of mlo powdery mildew resistance in barley. *Euphytica*, 63:141–152.

Jørgensen, J. H. and Mortensen, K. (1977). Primary Infection by *Erysiphe graminis* f.sp. *hordei* of Barley Mutants with Resistance Genes in the ml-o Locus. *Phytopathology*, 67:678–685.

Kaku, H., Nishizawa, Y., Ishii-Minami, N., Akimoto-Tomiyama, C., Dohmae, N., Takio, K., Minami, E., and Shibuya, N. (2006). Plant cells recognize chitin fragments for defense signaling through a plasma membrane receptor. *Proc Natl Acad Sci U S A*, 103(29):11086–11091.

Kang, E., Zheng, M., Zhang, Y., Yuan, M., Yalovsky, S., Zhu, L., and Fu, Y. (2017). The Microtubule-Associated Protein MAP18 affects ROP2 GTPase Activity during Root Hair Growth. *Plant Physiol*, 174(1):202–222.

Kaothien, P., Ok, S. H., Shuai, B., Wengier, D., Cotter, R., Kelley, D., Kiriakopolos, S., Muschietti, J., and McCormick, S. (2005). Kinase partner protein interacts with the LePRK1 and LePRK2 receptor kinases and plays a role in polarized pollen tube growth. *Plant J*, 42(4):492–503.

Katagiri, F., Thilmony, R., and He, S. Y. (2002). The *Arabidopsis thaliana-Pseudomonas syringae* interaction. *Arabidopsis Book*, 1:e0039.

Kawahara, Y., de la Bastide, M., Hamilton, J. P., Kanamori, H., McCombie, W. R., Ouyang, S., Schwartz, D. C., Tanaka, T., Wu, J., Zhou, S., Childs, K. L., Davidson, R. M., Lin, H., Quesada-Ocampo, L., Vaillancourt, B., Sakai, H., Lee, S. S., Kim, J., Numa, H., Itoh, T., Buell, C. R., and Matsumoto, T. (2013). Improvement of the *Oryza sativa* Nipponbare reference genome using next generation sequence and optical map data. *Rice (N Y)*, 6(1):4.

Kawano, Y., Akamatsu, A., Hayashi, K., Housen, Y., Okuda, J., Yao, A., Nakashima, A., Takahashi, H., Yoshida, H., Wong, H. L., Kawasaki, T., and Shimamoto, K. (2010). Activation of a Rac GTPase by the NLR family disease resistance protein Pit plays a critical role in rice innate immunity. *Cell Host Microbe*, 7(5):362–375.

Ke, D., Fang, Q., Chen, C., Zhu, H., Chen, T., Chang, X., Yuan, S., Kang, H., Ma, L., Hong, Z., and Zhang, Z. (2012). The small gtpase rop6 interacts with nfr5 and is involved in nodule formation in lotus japonicus. *Plant Physiol*, 159(1):131–143.

Kim, H., White, C. D., Li, Z., and Sacks, D. B. (2011). *Salmonella enterica* serotype Typhimurium usurps the scaffold protein IQGAP1 to manipulate Rac1 and MAPK signalling. *Biochem J*, 440(3):309–318.

Kim, H. S., Desveaux, D., Singer, A. U., Patel, P., Sondek, J., and Dangl, J. L. (2005a). The *Pseudomonas syringae* effector AvrRpt2 cleaves its C-terminally acylated target, RIN4, from Arabidopsis membranes to block RPM1 activation. *Proc Natl Acad Sci U S A*, 102(18):6496–6501.

Kim, M. C., Panstruga, R., Elliott, C., Muller, J., Devoto, A., Yoon, H. W., Park, H. C., Cho, M. J., and Schulze-Lefert, P. (2002). Calmodulin interacts with MLO protein to regulate defence against mildew in barley. *Nature*, 416(6879):447–451.

Kim, M. G., da Cunha, L., McFall, A. J., Belkhadir, Y., DebRoy, S., Dangl, J. L., and Mackey, D. (2005b). Two *Pseudomonas syringae* type III effectors inhibit RIN4-regulated basal defense in Arabidopsis. *Cell*, 121(5):749–759.

Klessig, D. F., Choi, H. W., and Dempsey, D. A. (2018). Systemic Acquired Resistance and Salicylic Acid: Past, Present, and Future. *Mol Plant Microbe Interact*, 31(9):871–888.

Kobayashi, I. and Hakuno, H. (2003). Actin-related defense mechanism to reject penetration attempt by a non-pathogen is maintained in tobacco BY-2 cells. *Planta*, 217(2):340–345.

Kobayashi, Y., Kobayashi, I., Funaki, Y., Fujimoto, S., Takemoto, T., and Kunoh, H. (1997). Dynamic reorganization of microfilaments and microtubules is necessary for the expression of non-host resistance in barley coleoptile cells. *Plant Journal*, 11(3):525–537.

Koh, S., Andre, A., Edwards, H., Ehrhardt, D., and Somerville, S. (2005). *Arabidopsis thaliana* subcellular responses to compatible *Erysiphe cichoracearum* infections. *Plant J*, 44(3):516–529.

Kokkoris, K., Gallo Castro, D., and Martin, S. G. (2014). The Tea4-PP1 landmark promotes local growth by dual Cdc42 GEF recruitment and GAP exclusion. *J Cell Sci*, 127(Pt 9):2005–2016.

Kost, B., Lemichez, E., Spielhofer, P., Hong, Y., Tolias, K., Carpenter, C., and Chua, N. H. (1999). Rac homologues and compartmentalized phosphatidylinositol 4, 5-bisphosphate act in a common pathway to regulate polar pollen tube growth. *J Cell Biol*, 145(2):317–330.

Kozubowski, L., Saito, K., Johnson, J. M., Howell, A. S., Zyla, T. R., and Lew, D. J. (2008). Symmetry-breaking polarization driven by a Cdc42p GEF-PAK complex. *Curr Biol*, 18(22):1719–1726.

Krendel, M., Zenke, F. T., and Bokoch, G. M. (2002). Nucleotide exchange factor GEF-H1 mediates cross-talk between microtubules and the actin cytoskeleton. *Nat Cell Biol*, 4(4):294–301.

Kunkel, B. N., Bent, A. F., Dahlbeck, D., Innes, R. W., and Staskawicz, B. J. (1993). RPS2, an Arabidopsis disease resistance locus specifying recognition of *Pseudomonas syringae* strains expressing the avirulence gene avrRpt2. *Plant Cell*, 5(8):865–875.

Kunze, G., Zipfel, C., Robatzek, S., Niehaus, K., Boller, T., and Felix, G. (2004). The N-Terminus of Bacterial Elongation Factor Tu Elicits Innate Immunity in Arabidopsis Plants. *The Plant Cell*, 16(12):3496–3507.

Kusano, H., Testerink, C., Vermeer, J. E., Tsuge, T., Shimada, H., Oka, A., Munnik, T., and Aoyama, T. (2008). The Arabidopsis Phosphatidylinositol Phosphate 5-Kinase PIP5K3 is a key regulator of root hair tip growth. *Plant Cell*, 20(2):367–380.

Kushnirov, V. V. (2000). Rapid and reliable protein extraction from yeast. *Yeast*, 16(9):857–860.

Kutschera, A., Dawid, C., Gisch, N., Schmid, C., Raasch, L., Gerster, T., Schaffer, M., Smakowska-Luzan, E., Belkhadir, Y., Vlot, A. C., Chandler, C. E., Schellenberger, R., Schwudke, D., Ernst, R. K., Dorey, S., Hückelhoven, R., Hofmann, T., and Ranf, S. (2019). Bacterial medium-chain 3-hydroxy fatty acid metabolites trigger immunity in Arabidopsis plants. *Science*, 364(6436):178–181.

Kwaaitaal, M., Nielsen, M. E., Bohlenius, H., and Thordal-Christensen, H. (2017). The plant membrane surrounding powdery mildew haustoria shares properties with the endoplasmic reticulum membrane. *J Exp Bot*, 68(21 - 22):5731 – 5743.

Laemmli, U. K. (1970). Cleavage of structural proteins during the assembly of the head of bacteriophage T4. *Nature*, 227(5259):680–685.

Lamas, I., Merlini, L., Vjestica, A., Vincenzetti, V., and Martin, S. G. (2020). Optogenetics reveals Cdc42 local activation by scaffold-mediated positive feedback and Ras GTPase. *PLoS Biol*, 18(1):e3000600.

Lavy, M., Bloch, D., Hazak, O., Gutman, I., Poraty, L., Sorek, N., Sternberg, H., and Yalovsky, S. (2007). A Novel ROP/RAC effector links cell polarity, root-meristem maintenance, and vesicle trafficking. *Curr Biol*, 17(11):947–952.

Lavy, M., Bracha-Drori, K., Sternberg, H., and Yalovsky, S. (2002). A cell-specific, prenylation-independent mechanism regulates targeting of type II RACs. *Plant Cell*, 14(10):2431–2450.

Lee, A. H., Hurley, B., Felsensteiner, C., Yea, C., Ckurshumova, W., Bartetzko, V., Wang, P. W., Quach, V., Lewis, J. D., Liu, Y. C., Bornke, F., Angers, S., Wilde, A., Guttman, D. S., and Desveaux, D. (2012). A bacterial acetyltransferase destroys plant microtubule networks and blocks secretion. *PLoS Pathog*, 8(2):e1002523.

Lee, H. A., Lee, H. Y., Seo, E., Lee, J., Kim, S. B., Oh, S., Choi, E., Choi, E., Lee, S. E., and Choi, D. (2017). Current Understandings of Plant Nonhost Resistance. *Mol Plant Microbe Interact*, 30(1):5–15.

Lee, Y. J., Szumlanski, A., Nielsen, E., and Yang, Z. (2008). Rho-GTPase-dependent filamentous actin dynamics coordinate vesicle targeting and exocytosis during tip growth. *J Cell Biol*, 181(7):1155–1168.

Lei, M. J., Wang, Q., Li, X., Chen, A., Luo, L., Xie, Y., Li, G., Luo, D., Mysore, K. S., Wen, J., Xie, Z. P., Staehelin, C., and Wang, Y. Z. (2015). The small GTPase ROP10 of *Medicago truncatula* is required for both tip growth of root hairs and nod factor-induced root hair deformation. *Plant Cell*, 27(3):806–822.

Lewis, J. D., Lee, A. H., Hassan, J. A., Wan, J., Hurley, B., Jhingree, J. R., Wang, P. W., Lo, T., Youn, J. Y., Guttman, D. S., and Desveaux, D. (2013). The Arabidopsis ZED1 pseudokinase is required for ZAR1-mediated immunity induced by the *Pseudomonas syringae* type III effector HopZ1a. *Proc Natl Acad Sci U S A*, 110(46):18722–18727.

Lewis, J. D., Wu, R., Guttman, D. S., and Desveaux, D. (2010). Allele-specific virulence attenuation of the *Pseudomonas syringae* HopZ1a type III effector via the Arabidopsis ZAR1 resistance protein. *PLoS Genet*, 6(4):e1000894.

Li, C., Lu, H., Li, W., Yuan, M., and Fu, Y. (2017). A ROP2-RIC1 pathway fine-tunes microtubule reorganization for salt tolerance in Arabidopsis. *Plant Cell Environ*, 40(7):1127–1142.

Li, E., Cui, Y., Ge, F.-R., Chai, S., Zhang, W.-T., Feng, Q.-N., Jiang, L., Li, S., and Zhang, Y. (2018). AGC1.5 Kinase Phosphorylates RopGEFs to Control Pollen Tube Growth. *Molecular Plant*, 11(9):1198 – 1209.

Li, H., Lin, Y., Heath, R. M., Zhu, M. X., and Yang, Z. (1999). Control of pollen tube tip growth by a Rop GTPase-dependent pathway that leads to tip-localized calcium influx. *Plant Cell*, 11(9):1731–1742.

Li, S., Gu, Y., Yan, A., Lord, E., and Yang, Z. B. (2008). RIP1 (ROP Interactive Partner 1)/ICR1 marks pollen germination sites and may act in the ROP1 pathway in the control of polarized pollen growth. *Mol Plant*, 1(6):1021–1035.

Lin, D., Cao, L., Zhou, Z., Zhu, L., Ehrhardt, D., Yang, Z., and Fu, Y. (2013). Rho GTPase signaling activates microtubule severing to promote microtubule ordering in Arabidopsis. *Curr Biol*, 23(4):290–297.

Lin, D., Nagawa, S., Chen, J., Cao, L., Chen, X., Xu, T., Li, H., Dhonukshe, P., Yamamuro, C., Friml, J., Scheres, B., Fu, Y., and Yang, Z. (2012). A ROP GTPase-

dependent auxin signaling pathway regulates the subcellular distribution of PIN2 in Arabidopsis roots. *Curr Biol*, 22(14):1319–1325.

Liu, J., Elmore, J. M., Fuglsang, A. T., Palmgren, M. G., Staskawicz, B. J., and Coaker, G. (2009). RIN4 functions with plasma membrane H^+-ATPases to regulate stomatal apertures during pathogen attack. *PLoS Biol*, 7(6):e1000139.

Liu, J., Elmore, J. M., Lin, Z. J., and Coaker, G. (2011). A receptor-like cytoplasmic kinase phosphorylates the host target RIN4, leading to the activation of a plant innate immune receptor. *Cell Host Microbe*, 9(2):137–146.

Liu, J., Liu, M., Qiu, L., and Xie, F. (2020). SPIKE1 Activates the GTPase ROP6 to Guide the Polarized Growth of Infection Threads in *Lotus japonicus*. *Plant Cell*.

Liu, T., Liu, Z., Song, C., Hu, Y., Han, Z., She, J., Fan, F., Wang, J., Jin, C., Chang, J., Zhou, J. M., and Chai, J. (2012). Chitin-induced dimerization activates a plant immune receptor. *Science*, 336(6085):1160–1164.

Lu, D., Wu, S., Gao, X., Zhang, Y., Shan, L., and He, P. (2010). A receptor-like cytoplasmic kinase, BIK1, associates with a flagellin receptor complex to initiate plant innate immunity. *Proceedings of the National Academy of Sciences*, 107(1):496–501.

Mackey, D., Belkhadir, Y., Alonso, J. M., Ecker, J. R., and Dangl, J. L. (2003). Arabidopsis RIN4 is a target of the type III virulence effector AvrRpt2 and modulates RPS2-mediated resistance. *Cell*, 112(3):379–389.

Mackey, D., Holt, B. F., r., Wiig, A., and Dangl, J. L. (2002). RIN4 interacts with *Pseudomonas syringae* type III effector molecules and is required for RPM1-mediated resistance in Arabidopsis. *Cell*, 108(6):743–754.

Martin, S. G., McDonald, W. H., Yates, J. R., r., and Chang, F. (2005). Tea4p links microtubule plus ends with the formin For3p in the establishment of cell polarity. *Dev Cell*, 8(4):479–491.

Mascher, M., Gundlach, H., Himmelbach, A., Beier, S., Twardziok, S. O., Wicker, T., Radchuk, V., Dockter, C., Hedley, P. E., Russell, J., Bayer, M., Ramsay, L., Liu, H., Haberer, G., Zhang, X. Q., Zhang, Q., Barrero, R. A., Li, L., Taudien, S., Groth, M., Felder, M., Hastie, A., Simkova, H., Stankova, H., Vrana, J., Chan, S., Munoz-Amatriain, M., Ounit, R., Wanamaker, S., Bolser, D., Colmsee, C., Schmutzer, T., Aliyeva-Schnorr, L., Grasso, S., Tanskanen, J., Chailyan, A., Sampath, D., Heavens, D., Clissold, L., Cao, S., Chapman, B., Dai, F., Han, Y., Li, H., Li, X., Lin, C., McCooke, J. K., Tan, C., Wang, P., Wang, S., Yin, S., Zhou, G., Poland, J. A., Bellgard,

M. I., Borisjuk, L., Houben, A., Dolezel, J., Ayling, S., Lonardi, S., Kersey, P., Langridge, P., Muehlbauer, G. J., Clark, M. D., Caccamo, M., Schulman, A. H., Mayer, K. F. X., Platzer, M., Close, T. J., Scholz, U., Hansson, M., Zhang, G., Braumann, I., Spannagl, M., Li, C., Waugh, R., and Stein, N. (2017). A chromosome conformation capture ordered sequence of the barley genome. *Nature*, 544(7651):427–433.

McLusky, S. R., Bennett, M. H., Beale, M. H., Lewis, M. J., Gaskin, P., and Mansfield, J. W. (1999). Cell wall alterations and localized accumulation of feruloyl-3 '-methoxytyramine in onion epidermis at sites of attempted penetration by *Botrytis allii* are associated with actin polarisation, peroxidase activity and suppression of flavonoid biosynthesis. *The Plant Journal*, 17(5):523–534.

Mendgen, K. and Hahn, M. (2002). Plant infection and the establishment of fungal biotrophy. *Trends Plant Sci*, 7(8):352–356.

Mendrinna, A. and Persson, S. (2015). Root hair growth: it's a one way street. *F1000Prime Rep*, 7:23.

Micali, C. O., Neumann, U., Grunewald, D., Panstruga, R., and O'Connell, R. (2011). Biogenesis of a specialized plant-fungal interface during host cell internalization of *Golovinomyces orontii* haustoria. *Cell Microbiol*, 13(2):210–226.

Mithen, R. (2001). Glucosinolates – biochemistry, genetics and biological activity. *Plant Growth Regulation*, 31(1):91–103.

Miya, A., Albert, P., Shinya, T., Desaki, Y., Ichimura, K., Shirasu, K., Narusaka, Y., Kawakami, N., Kaku, H., and Shibuya, N. (2007). CERK1, a LysM receptor kinase, is essential for chitin elicitor signaling in Arabidopsis. *Proc Natl Acad Sci U S A*, 104(49):19613–19618.

Molendijk, A. J., Bischoff, F., Rajendrakumar, C. S., Friml, J., Braun, M., Gilroy, S., and Palme, K. (2001). *Arabidopsis thaliana* Rop GTPases are localized to tips of root hairs and control polar growth. *EMBO J*, 20(11):2779–2788.

Mosquera, G., Giraldo, M. C., Khang, C. H., Coughlan, S., and Valent, B. (2009). Interaction transcriptome analysis identifies *Magnaporthe oryzae* BAS1-4 as Biotrophy-associated secreted proteins in rice blast disease. *Plant Cell*, 21(4):1273–1290.

Mucha, E., Hoefle, C., Hückelhoven, R., and Berken, A. (2010). RIP3 and AtKinesin-13A-A novel interaction linking Rho proteins of plants to microtubules. *European Journal of Cell Biology*, 89(12):906–916.

Muller, A. J., Hoffmann, C., Galle, M., Van Den Broeke, A., Heikenwalder, M., Falter, L., Misselwitz, B., Kremer, M., Beyaert, R., and Hardt, W. D. (2009). The *S. typhimurium* Effector SopE Induces Caspase-1 Activation in Stromal Cells to Initiate Gut Inflammation. *Cell Host Microbe*, 6(2):125–136.

Muschietti, J., Eyal, Y., and McCormick, S. (1998). Pollen tube localization implies a role in pollen-pistil interactions for the tomato receptor-like protein kinases LePRK1 and LePRK2. *Plant Cell*, 10(3):319–330.

Nelson, B. K., Cai, X., and Nebenfuhr, A. (2007). A multicolored set of *in vivo* organelle markers for co-localization studies in Arabidopsis and other plants. *Plant J*, 51(6):1126–1136.

Nibau, C., Wu, H. M., and Cheung, A. Y. (2006). RAC/ROP GTPases: 'hubs' for signal integration and diversification in plants. *Trends Plant Sci*, 11(6):309–315.

Nomura, K., Debroy, S., Lee, Y. H., Pumplin, N., Jones, J., and He, S. Y. (2006). A bacterial virulence protein suppresses host innate immunity to cause plant disease. *Science*, 313(5784):220–223.

Nomura, K., Melotto, M., and He, S. Y. (2005). Suppression of host defense in compatible plant-*Pseudomonas syringae* interactions. *Curr Opin Plant Biol*, 8(4):361–368.

Nottensteiner, M., Zechmann, B., McCollum, C., and Hückelhoven, R. (2018). A barley powdery mildew fungus non-autonomous retrotransposon encodes a peptide that supports penetration success on barley. *J Exp Bot*, 69(15):3745–3758.

O'Connell, R. J. and Panstruga, R. (2006). Tête á tête inside a plant cell: establishing compatibility between plants and biotrophic fungi and oomycetes. *New Phytol*, 171(4):699–718.

Oda, Y. and Fukuda, H. (2012). Initiation of Cell Wall Pattern by a Rho- and Microtubule-Driven Symmetry Breaking. *Science*, 337(6100):1333–1336.

Oda, Y. and Fukuda, H. (2013). Rho of plant GTPase signaling regulates the behavior of arabidopsis kinesin-13A to establish secondary cell wall patterns. *Plant Cell*, 25(11):4439–4450.

Oda, Y., Iida, Y., Kondo, Y., and Fukuda, H. (2010). Wood Cell-Wall Structure Requires Local 2D-Microtubule Disassembly by a Novel Plasma Membrane-Anchored Protein. *Current Biology*, 20(13):1197–1202.

Okuda, S., Tsutsui, H., Shiina, K., Sprunck, S., Takeuchi, H., Yui, R., Kasahara, R. D., Hamamura, Y., Mizukami, A., Susaki, D., Kawano, N., Sakakibara, T., Namiki, S., Itoh, K., Otsuka, K., Matsuzaki, M., Nozaki, H., Kuroiwa, T., Nakano, A., Kanaoka, M. M., Dresselhaus, T., Sasaki, N., and Higashiyama, T. (2009). Defensin-like polypeptide LUREs are pollen tube attractants secreted from synergid cells. *Nature*, 458(7236):357–361.

Oliver, R. P. and Ipcho, S. V. (2004). Arabidopsis pathology breathes new life into the necrotrophs-vs.-biotrophs classification of fungal pathogens. *Mol Plant Pathol*, 5(4):347–352.

Ono, E., Wong, H. L., Kawasaki, T., Hasegawa, M., Kodama, O., and Shimamoto, K. (2001). Essential role of the small GTPase Rac in disease resistance of rice. *Proc Natl Acad Sci U S A*, 98(2):759–764.

Opalski, K. S., Schultheiss, H., Kogel, K. H., and Hückelhoven, R. (2005). The receptor-like MLO protein and the RAC/ROP family G-protein RACB modulate actin reorganization in barley attacked by the biotrophic powdery mildew fungus blumeria graminis f.sp. hordei. *Plant J*, 41(2):291–303.

Ostertag, M., Stammler, J., Douchkov, D., Eichmann, R., and Hückelhoven, R. (2013). The conserved oligomeric golgi complex is involved in penetration resistance of barley to the barley powdery mildew fungus. *Molecular Plant Pathology*, 14(3):230–240.

Pang, T. L., Chen, F. C., Weng, Y. L., Liao, H. C., Yi, Y. H., Ho, C. L., Lin, C. H., and Chen, M. Y. (2010). Costars, a Dictyostelium protein similar to the C-terminal domain of STARS, regulates the actin cytoskeleton and motility. *J Cell Sci*, 123(Pt 21):3745–3755.

Pathak, R., Delorme-Walker, V. D., Howell, M. C., Anselmo, A. N., White, M. A., Bokoch, G. M., and Dermardirossian, C. (2012). The microtubule-associated Rho activating factor GEF-H1 interacts with exocyst complex to regulate vesicle traffic. *Dev Cell*, 23(2):397–411.

Pathuri, I. P., Zellerhoff, N., Schaffrath, U., Hensel, G., Kumlehn, J., Kogel, K. H., Eichmann, R., and Hückelhoven, R. (2008). Constitutively activated barley ROPs modulate epidermal cell size, defense reactions and interactions with fungal leaf pathogens. *Plant Cell Reports*, 27(12):1877–1887.

Pedersen, C., Ver Loren van Themaat, E., McGuffin, L. J., Abbott, J. C., Burgis, T. A., Barton, G., Bindschedler, L. V., Lu, X., Maekawa, T., Wessling, R., Cramer, R.,

Thordal-Christensen, H., Panstruga, R., and Spanu, P. D. (2012). Structure and evolution of barley powdery mildew effector candidates. *BMC Genomics*, 13:694.

Petutschnig, E. K., Jones, A. M., Serazetdinova, L., Lipka, U., and Lipka, V. (2010). The lysin motif receptor-like kinase (LysM-RLK) CERK1 is a major chitin-binding protein in *Arabidopsis thaliana* and subject to chitin-induced phosphorylation. *J Biol Chem*, 285(37):28902–28911.

Piffanelli, P., Zhou, F., Casais, C., Orme, J., Jarosch, B., Schaffrath, U., Collins, N. C., Panstruga, R., and Schulze-Lefert, P. (2002). The Barley MLO Modulator of Defense and Cell Death is Responsive to Biotic and Abiotic Stress Stimuli. *Plant Physiol*, 129(3):1076–1085.

Pirone, D. M., Carter, D. E., and Burbelo, P. D. (2001). Evolutionary expansion of CRIB-containing Cdc42 effector proteins. *Trends Genet*, 17(7):370–373.

Platre, M. P., Bayle, V., Armengot, L., Bareille, J., Marques-Bueno, M. D. M., Creff, A., Maneta-Peyret, L., Fiche, J. B., Nollmann, M., Miege, C., Moreau, P., Martiniere, A., and Jaillais, Y. (2019). Developmental control of plant Rho GTPase nano-organization by the lipid phosphatidylserine. *Science*, 364(6435):57–62.

Popoff, M. R. (2014). Bacterial factors exploit eukaryotic Rho GTPase signaling cascades to promote invasion and proliferation within their host. *Small GTPases*, 5.

Poraty-Gavra, L., Zimmermann, P., Haigis, S., Bednarek, P., , O., Stelmakh, O. R., Sadot, E., Schulze-Lefert, P., Gruissem, W., and Yalovsky, S. (2013). The Arabidopsis Rho of Plants GTPase AtROP6 Functions in Developmental and Pathogen Response Pathways. *Plant Physiol*, 161(3):1172–1188.

Qin, L., Zhou, Z., Li, Q., Zhai, C., Liu, L., Quilichini, T. D., Gao, P., Kessler, S. A., Jaillais, Y., Datla, R., Peng, G., Xiang, D., and Wei, Y. (2020). Specific Recruitment of Phosphoinositide Species to the Plant-Pathogen Interfacial Membrane Underlies Arabidopsis Susceptibility to Fungal Infection. *Plant Cell*.

Qiu, J.-L., Fiil, B. K., Petersen, K., Nielsen, H. B., Botanga, C. J., Thorgrimsen, S., Palma, K., Suarez-Rodriguez, M. C., Sandbech-Clausen, S., Lichota, J., Brodersen, P., Grasser, K. D., Mattsson, O., Glazebrook, J., Mundy, J., and Petersen, M. (2008). Arabidopsis MAP kinase 4 regulates gene expression through transcription factor release in the nucleus. *The EMBO Journal*, 27(16):2214–2221.

Rathore, K. S., Cork, R. J., and Robinson, K. R. (1991). A Cytoplasmic Gradient of Ca^{2+} is Correlated with the Growth of Lily Pollen Tubes. *Dev Biol*, 148(2):612–619.

Reiner, T., Hoefle, C., and Hückelhoven, R. (2015). A barley SKP1-like protein controls abundance of the susceptibility factor RACB and influences the interaction of barley with the barley powdery mildew fungus. *Mol Plant Pathol*, 17(2):184 – 195.

Rodriguez, L., Gonzalez-Guzman, M., Diaz, M., Rodrigues, A., Izquierdo-Garcia, A. C., Peirats-Llobet, M., Fernandez, M. A., Antoni, R., Fernandez, D., Marquez, J. A., Mulet, J. M., Albert, A., and Rodriguez, P. L. (2014). C2-Domain Abscisic Acid-Related Proteins Mediate the Interaction of PYR/PYL/RCAR Abscisic Acid Receptors with the Plasma Membrane and Regulate Abscisic Acid Sensitivity in Arabidopsis. *Plant Cell*, 26(12):4802–4820.

Sarris, P. F., Duxbury, Z., Huh, S. U., Ma, Y., Segonzac, C., Sklenar, J., Derbyshire, P., Cevik, V., Rallapalli, G., Saucet, S. B., Wirthmueller, L., Menke, F. L. H., Sohn, K. H., and Jones, J. D. G. (2015). A Plant Immune Receptor Detects Pathogen Effectors that Target WRKY Transcription Factors. *Cell*, 161(5):1089–1100.

Savary, S., Willocquet, L., Pethybridge, S. J., Esker, P., McRoberts, N., and Nelson, A. (2019). The global burden of pathogens and pests on major food crops. *Nature Ecology & Evolution*, 3(3):430–439.

Sawin, K. E. and Snaith, H. A. (2004). Role of microtubules and tea1p in establishment and maintenance of fission yeast cell polarity. *J Cell Sci*, 117(Pt 5):689–700.

Schechter, L. M., Vencato, M., Jordan, K. L., Schneider, S. E., Schneider, D. J., and Collmer, A. (2006). Multiple approaches to a complete inventory of *Pseudomonas syringae* pv. *tomato* DC3000 type III secretion system effector proteins. *Mol Plant Microbe Interact*, 19(11):1180–1192.

Scheler, B., Schnepf, V., Galgenmuller, C., Ranf, S., and Hückelhoven, R. (2016). Barley disease susceptibility factor RACB acts in epidermal cell polarity and positioning of the nucleus. *Journal of Experimental Botany*, 67(11):3263–3275.

Schultheiss, H., Dechert, C., Kogel, K. H., and Hückelhoven, R. (2002). A small GTP-binding host protein is required for entry of powdery mildew fungus into epidermal cells of barley. *Plant Physiol*, 128(4):1447–1454.

Schultheiss, H., Dechert, C., Kogel, K. H., and Hückelhoven, R. (2003). Functional analysis of barley RAC/ROP G-protein family members in susceptibility to the powdery mildew fungus. *Plant Journal*, 36(5):589–601.

Schultheiss, H., Preuss, J., Pircher, T., Eichmann, R., and Hückelhoven, R. (2008). Barley RIC171 interacts with RACB in planta and supports entry of the powdery mildew fungus. *Cell Microbiol*, 10(9):1815–1826.

Schultz, J., Milpetz, F., Bork, P., and Ponting, C. P. (1998). SMART, a simple modular architecture research tool: identification of signaling domains. *Proc Natl Acad Sci U S A*, 95(11):5857–5864.

Schwartz, S. L., Cao, C., Pylypenko, O., Rak, A., and Wandinger-Ness, A. (2007). Rab GTPases at a glance. *J Cell Sci*, 120(Pt 22):3905–3910.

Schweizer, P., Christoffel, A., and Dudler, R. (1999). Transient expression of members of the germin-like gene family in epidermal cells of wheat confers disease resistance. *Plant J*, 20(5):541–552.

Seybold, H., Trempel, F., Ranf, S., Scheel, D., Romeis, T., and Lee, J. (2014). Ca^{2+} signalling in plant immune response: from pattern recognition receptors to Ca^{2+} decoding mechanisms. *New Phytol*, 204(4):782–790.

Shimada, C., Lipka, V., O'Connell, R., Okuno, T., Schulze-Lefert, P., and Takano, Y. (2006). Nonhost resistance in Arabidopsis-Colletotrichum interactions acts at the cell periphery and requires actin filament function. *Mol Plant Microbe Interact*, 19(3):270–279.

Shimizu, T., Nakano, T., Takamizawa, D., Desaki, Y., Ishii-Minami, N., Nishizawa, Y., Minami, E., Okada, K., Yamane, H., Kaku, H., and Shibuya, N. (2010). Two LysM receptor molecules, CEBiP and OsCERK1, cooperatively regulate chitin elicitor signaling in rice. *Plant J*, 64(2):204–214.

Shinya, T., Yamaguchi, K., Desaki, Y., Yamada, K., Narisawa, T., Kobayashi, Y., Maeda, K., Suzuki, M., Tanimoto, T., Takeda, J., Nakashima, M., Funama, R., Narusaka, M., Narusaka, Y., Kaku, H., Kawasaki, T., and Shibuya, N. (2014). Selective regulation of the chitin-induced defense response by the Arabidopsis receptor-like cytoplasmic kinase PBL27. *Plant J*, 79(1):56–66.

Singh, A., Lim, G. H., and Kachroo, P. (2017). Transport of chemical signals in systemic acquired resistance. *J Integr Plant Biol*, 59(5):336–344.

Sit, S. T. and Manser, E. (2011). Rho GTPases and their role in organizing the actin cytoskeleton. *J Cell Sci*, 124(Pt 5):679–683.

Skalamera, D. and Heath, M. C. (1998). Changes in the cytoskeleton accompanying infection-induced nuclear movements and the hypersensitive response in plant cells invaded by rust fungi. *Plant Journal*, 16(2):191–200.

Sorek, N., Poraty, L., Sternberg, H., Buriakovsky, E., Bar, E., Lewinsohn, E., and Yalovsky, S. (2017). Corrected and Republished from: Activation Status-Coupled Transient S-Acylation Determines Membrane Partitioning of a Plant Rho-Related GTPase. *Mol Cell Biol*, 37(23).

Spanu, P. D., Abbott, J. C., Amselem, J., Burgis, T. A., Soanes, D. M., Stüber, K., Loren van Themaat, E. V., Brown, J. K. M., Butcher, S. A., Gurr, S. J., Lebrun, M.-H., Ridout, C. J., Schulze-Lefert, P., Talbot, N. J., Ahmadinejad, N., Ametz, C., Barton, G. R., Benjdia, M., Bidzinski, P., Bindschedler, L. V., Both, M., Brewer, M. T., Cadle-Davidson, L., Cadle-Davidson, M. M., Collemare, J., Cramer, R., Frenkel, O., Godfrey, D., Harriman, J., Hoede, C., King, B. C., Klages, S., Kleemann, J., Knoll, D., Koti, P. S., Kreplak, J., López-Ruiz, F. J., Lu, X., Maekawa, T., Mahanil, S., Micali, C., Milgroom, M. G., Montana, G., Noir, S., O'Connell, R. J., Oberhaensli, S., Parlange, F., Pedersen, C., Quesneville, H., Reinhardt, R., Rott, M., Sacristán, S., Schmidt, S. M., Schön, M., Skamnioti, P., Sommer, H., Stephens, A., Takahara, H., Thordal-Christensen, H., Vigouroux, M., Weßling, R., Wicker, T., and Panstruga, R. (2010). Genome Expansion and Gene Loss in Powdery Mildew Fungi Reveal Tradeoffs in Extreme Parasitism. *Science*, 330(6010):1543–1546.

Stam, R., Munsterkotter, M., Pophaly, S. D., Fokkens, L., Sghyer, H., Guldener, U., Hückelhoven, R., and Hess, M. (2018). A New Reference Genome Shows the One-Speed Genome Structure of the Barley Pathogen *Ramularia collo-cygni*. *Genome Biol Evol*, 10(12):3243–3249.

Stecher, B., Robbiani, R., Walker, A. W., Westendorf, A. M., Barthel, M., Kremer, M., Chaffron, S., Macpherson, A. J., Buer, J., Parkhill, J., Dougan, G., von Mering, C., and Hardt, W. D. (2007). *Salmonella enterica* Serovar Typhimurium Exploits Inflammation to Compete with the Intestinal Microbiota. *PLoS Biol*, 5(10):2177–2189.

Stender, S., Friebel, A., Linder, S., Rohde, M., Mirold, S., and Hardt, W. D. (2000). Identification of SopE2 from *Salmonella typhimurium*, a conserved guanine nucleotide exchange factor for Cdc42 of the host cell. *Mol Microbiol*, 36(6):1206–1221.

Stolzenburg, M. C., Aist, J. R., and Israel, H. W. (1984). The role of papillae in re-

sistance to powdery mildew conditioned by the *ml-o* gene in barley. i correlative evidence. *Physiological Plant Pathology*, 25(3):337–346.

Sugiyama, Y., Wakazaki, M., Toyooka, K., Fukuda, H., and Oda, Y. (2017). A Novel Plasma Membrane-Anchored Protein Regulates Xylem Cell-Wall Deposition through Microtubule-Dependent Lateral Inhibition of Rho GTPase Domains. *Curr Biol*, 27(16):2522–2528 e4.

Sun, Y., Li, L., Macho, A. P., Han, Z., Hu, Z., Zipfel, C., Zhou, J.-M., and Chai, J. (2013). Structural Basis for flg22-Induced Activation of the Arabidopsis FLS2-BAK1 Immune Complex. *Science*, 342(6158):624–628.

Syrovatkina, V., Alegre, K. O., Dey, R., and Huang, X.-Y. (2016). Regulation, signaling, and physiological functions of g-proteins. *Journal of Molecular Biology*, 428(19):3850–3868. Molecular Basis of Signal Transduction.

Takahashi, H., Kawahara, A., and Inoue, Y. (2003). Ethylene Promotes the Induction by Auxin of the Cortical Microtubule Randomization Required for Low-pH-Induced Root Hair Initiation in Lettuce (*Lactuca sativa* L.) seedlings. *Plant Cell Physiol*, 44(9):932–940.

Takemoto, D., Jones, D. A., and Hardham, A. R. (2003). GFP-tagging of cell components reveals the dynamics of subcellular re-organization in response to infection of arabidopsis by oomycete pathogens. *Plant J*, 33(4):775–792.

Takeuchi, H. and Higashiyama, T. (2012). A species-specific cluster of defensin-like genes encodes diffusible pollen tube attractants in arabidopsis. *PLoS Biol*, 10(12):e1001449.

Takeuchi, H. and Higashiyama, T. (2016). Tip-localized receptors control pollen tube growth and LURE sensing in Arabidopsis. *Nature*, 531(7593):245–248.

Tasset, C., Bernoux, M., Jauneau, A., Pouzet, C., Brière, C., Kieffer-Jacquinod, S., Rivas, S., Marco, Y., and Deslandes, L. (2010). Autoacetylation of the *Ralstonia solanacearum* Effector PopP2 Targets a Lysine Residue Essential for RRS1-R-Mediated Immunity in Arabidopsis. *PLOS Pathogens*, 6(11):1–14.

Tay, Y. D., Leda, M., Goryachev, A. B., and Sawin, K. E. (2018). Local and global Cdc42 guanine nucleotide exchange factors for fission yeast cell polarity are coordinated by microtubules and the Tea1-Tea4-Pom1 axis. *J Cell Sci*, 131(14).

Thordal-Christensen, H., Zhang, Z., Wei, Y., and Collinge, D. B. (1997). Subcellular localization of H_2O_2 in plants. H_2O_2 accumulation in papillae and hypersensitive response during the barley-powdery mildew interaction. *Plant J*, 11(6):1187–1194.

UN, Food and Agriculture Organization (2004). Barley, post-harvest operations 2004.

USDA, Foreign Agricultural Service (2020). World Agricultural Production 2020.

Van Bruaene, N., Joss, G., and Van Oostveldt, P. (2004). Reorganization and in vivo dynamics of microtubules during arabidopsis root hair development. *Plant Physiol*, 136(4):3905–3919.

van Schie, C. C. and Takken, F. L. (2014). Susceptibility Genes 101: How to Be a Good Host. *Annu Rev Phytopathol*, 52:551–581.

Waadt, R., Schmidt, L. K., Lohse, M., Hashimoto, K., Bock, R., and Kudla, J. (2008). Multicolor bimolecular fluorescence complementation reveals simultaneous formation of alternative CBL/CIPK complexes *in planta*. *Plant J*, 56(3):505–516.

Walter, M., Chaban, C., Schütze, K., Batistic, O., Weckermann, K., Näke, C., Blazevic, D., Grefen, C., Schumacher, K., Oecking, C., Harter, K., and Kudla, J. (2004). Visualization of protein interactions in living plant cells using bimolecular fluorescence complementation. *The Plant Journal*, 40(3):428–438.

Wang, D., Yang, S., Tang, F., and Zhu, H. (2012). Symbiosis specificity in the legume: rhizobial mutualism. *Cell Microbiol*, 14(3):334–342.

Wang, G., Roux, B., Feng, F., Guy, E., Li, L., Li, N., Zhang, X., Lautier, M., Jardinaud, M. F., Chabannes, M., Arlat, M., Chen, S., He, C., Noel, L. D., and Zhou, J. M. (2015). The Decoy Substrate of a Pathogen Effector and a Pseudokinase Specify Pathogen-Induced Modified-Self Recognition and Immunity in Plants. *Cell Host Microbe*, 18(3):285–295.

Wang, J., Hu, M., Wang, J., Qi, J., Han, Z., Wang, G., Qi, Y., Wang, H. W., Zhou, J. M., and Chai, J. (2019). Reconstitution and structure of a plant NLR resistosome conferring immunity. *Science*, 364(6435).

Wang, W., Wen, Y., Berkey, R., and Xiao, S. (2009). Specific targeting of the arabidopsis resistance protein RPW8.2 to the interfacial membrane encasing the fungal Haustorium renders broad-spectrum resistance to powdery mildew. *Plant Cell*, 21(9):2898–2913.

Waterhouse, A. M., Procter, J. B., Martin, D. M. A., Clamp, M., and Barton, G. J. (2009). Jalview Version 2—a multiple sequence alignment editor and analysis workbench. *Bioinformatics*, 25(9):1189–1191.

Weis, C., Hückelhoven, R., and Eichmann, R. (2013). LIFEGUARD proteins support plant colonization by biotrophic powdery mildew fungi. *Journal of Experimental Botany*, 64(12):3855–3867.

Weiss, E., Wetterstrom, W., Nadel, D., and Bar-Yosef, O. (2004). The broad spectrum revisited: Evidence from plant remains. *Proc Natl Acad Sci U S A*, 101(26):9551–9555.

Wicker, T., Oberhaensli, S., Parlange, F., Buchmann, J. P., Shatalina, M., Roffler, S., Ben-David, R., Doležel, J., Šimková, H., Schulze-Lefert, P., Spanu, P. D., Bruggmann, R., Amselem, J., Quesneville, H., Ver Loren van Themaat, E., Paape, T., Shimizu, K. K., and Keller, B. (2013). The wheat powdery mildew genome shows the unique evolution of an obligate biotroph. *Nature Genetics*, 45(9):1092–1096.

Williams, S. J., Sohn, K. H., Wan, L., Bernoux, M., Sarris, P. F., Segonzac, C., Ve, T., Ma, Y., Saucet, S. B., Ericsson, D. J., Casey, L. W., Lonhienne, T., Winzor, D. J., Zhang, X., Coerdt, A., Parker, J. E., Dodds, P. N., Kobe, B., and Jones, J. D. (2014). Structural basis for assembly and function of a heterodimeric plant immune receptor. *Science*, 344(6181):299–303.

Wilton, M., Subramaniam, R., Elmore, J., Felsensteiner, C., Coaker, G., and Desveaux, D. (2010). The type III effector HopF2Pto targets Arabidopsis RIN4 protein to promote *Pseudomonas syringae* virulence. *Proc Natl Acad Sci U S A*, 107(5):2349–2354.

Wong, H. L., Pinontoan, R., Hayashi, K., Tabata, R., Yaeno, T., Hasegawa, K., Kojima, C., Yoshioka, H., Iba, K., Kawasaki, T., and Shimamoto, K. (2007). Regulation of rice NADPH oxidase by binding of Rac GTPase to its N-terminal extension. *Plant Cell*, 19(12):4022–4034.

Wright, A. J., Thomas, B. J., and Carver, T. L. (2002). Early adhesion of *Blumeria graminis* to plant and artificial surfaces demonstrated by centrifugation. *Physiological and Molecular Plant Pathology*, 61(4):217 – 226.

Wu, G., Gu, Y., Li, S., and Yang, Z. (2001). A genome-wide analysis of Arabidopsis Rop-interactive CRIB motif-containing proteins that act as Rop GTPase targets. *Plant Cell*, 13(12):2841–2856.

Wu, S. Z. and Bezanilla, M. (2018). Actin and microtubule cross talk mediates persistent polarized growth. *J Cell Biol*, 217(10):3531–3544.

Wymer, C. L., Bibikova, T. N., and Gilroy, S. (1997). Cytoplasmic free calcium distributions during the development of root hairs of *Arabidopsis thaliana*. *Plant J*, 12(2):427–439.

Xu, R. X., Pawelczyk, T., Xia, T. H., and Brown, S. C. (1997). NMR structure of a protein kinase C-gamma phorbol-binding domain and study of protein-lipid micelle interactions. *Biochemistry*, 36(35):10709–10717.

Yamada, A., Shibuya, N., Kodama, O., and Akatsuka, T. (1993). Induction of Phytoalexin Formation in Suspension-cultured Rice Cells by N-Acetylchitooligosaccharides. *Bioscience, Biotechnology, and Biochemistry*, 57(3):405–409. PMID: 27300216.

Yamada, K., Yamaguchi, K., Shirakawa, T., Nakagami, H., Mine, A., Ishikawa, K., Fujiwara, M., Narusaka, M., Narusaka, Y., Ichimura, K., Kobayashi, Y., Matsui, H., Nomura, Y., Nomoto, M., Tada, Y., Fukao, Y., Fukamizo, T., Tsuda, K., Shirasu, K., Shibuya, N., and Kawasaki, T. (2016). The Arabidopsis CERK1-associated kinase PBL27 connects chitin perception to MAPK activation. *EMBO J*, 35(22):2468–2483.

Yang, G., Gao, P., Zhang, H., Huang, S., and Zheng, Z. L. (2007). A mutation in MRH2 kinesin enhances the root hair tip growth defect caused by constitutively activated ROP2 small GTPase in Arabidopsis. *PLoS One*, 2(10):e1074.

Yu, G. L., Katagiri, F., and Ausubel, F. M. (1993). Arabidopsis mutations at the *RPS2* locus result in loss of resistance to *Pseudomonas syringae* strains expressing the avirulence gene *avrRpt2*. *Mol Plant Microbe Interact*, 6(4):434–443.

Yu, X., Breitman, M., and Goldberg, J. (2012). A structure-based mechanism for Arf1-dependent recruitment of coatomer to membranes. *Cell*, 148(3):530–542.

Zabka, V., Stangl, M., Bringmann, G., Vogg, G., Riederer, M., and Hildebrandt, U. (2008). Host surface properties affect prepenetration processes in the barley powdery mildew fungus. *New Phytol*, 177(1):251–263.

Zhang, D., Wengier, D., Shuai, B., Gui, C. P., Muschietti, J., McCormick, S., and Tang, W. H. (2008). The pollen receptor kinase LePRK2 mediates growth-promoting signals and positively regulates pollen germination and tube growth. *Plant Physiol*, 148(3):1368–1379.

Zhang, Q., Zhang, X., Zhuang, R., Wei, Z., Shu, W., Wang, X., and Kang, Z. (2020). *TaRac6* Is a Potential Susceptibility Factor by Regulating the ROS Burst Negatively in the Wheat-*Puccinia striiformis* f. sp. *tritici* Interaction. *Front Plant Sci*, 11:716.

Zhang, S., Pan, Y., Tian, W., Dong, M., Zhu, H., Luan, S., and Li, L. (2017). Arabidopsis CNGC14 Mediates Calcium Influx Required for Tip Growth in Root Hairs. *Mol Plant*, 10(7):1004–1006.

Zhang, Y. and McCormick, S. (2007). A distinct mechanism regulating a pollen-specific guanine nucleotide exchange factor for the small GTPase Rop in *Arabidopsis thaliana*. *Proc Natl Acad Sci U S A*, 104(47):18830–18835.

Zhang, Y., Su, J., Duan, S., Ao, Y., Dai, J., Liu, J., Wang, P., Li, Y., Liu, B., Feng, D., Wang, J., and Wang, H. (2011). A highly efficient rice green tissue protoplast system for transient gene expression and studying light/chloroplast-related processes. *Plant Methods*, 7(1):30.

Zhao, C., Nie, H., Shen, Q., Zhang, S., Lukowitz, W., and Tang, D. (2014). EDR1 physically interacts with MKK4/MKK5 and negatively regulates a MAP kinase cascade to modulate plant innate immunity. *PLoS Genet*, 10(5):e1004389.

Zhong, R. and Ye, Z. H. (2015). Secondary Cell Walls: Biosynthesis, Patterned Deposition and Transcriptional Regulation. *Plant Cell Physiol*, 56(2):195–214.

Zhou, Z., Shi, H., Chen, B., Zhang, R., Huang, S., and Fu, Y. (2015). Arabidopsis RIC1 Severs Actin Filaments at the Apex to Regulate Pollen Tube Growth. *Plant Cell*, 27(4):1140–1161.

8 Supplements

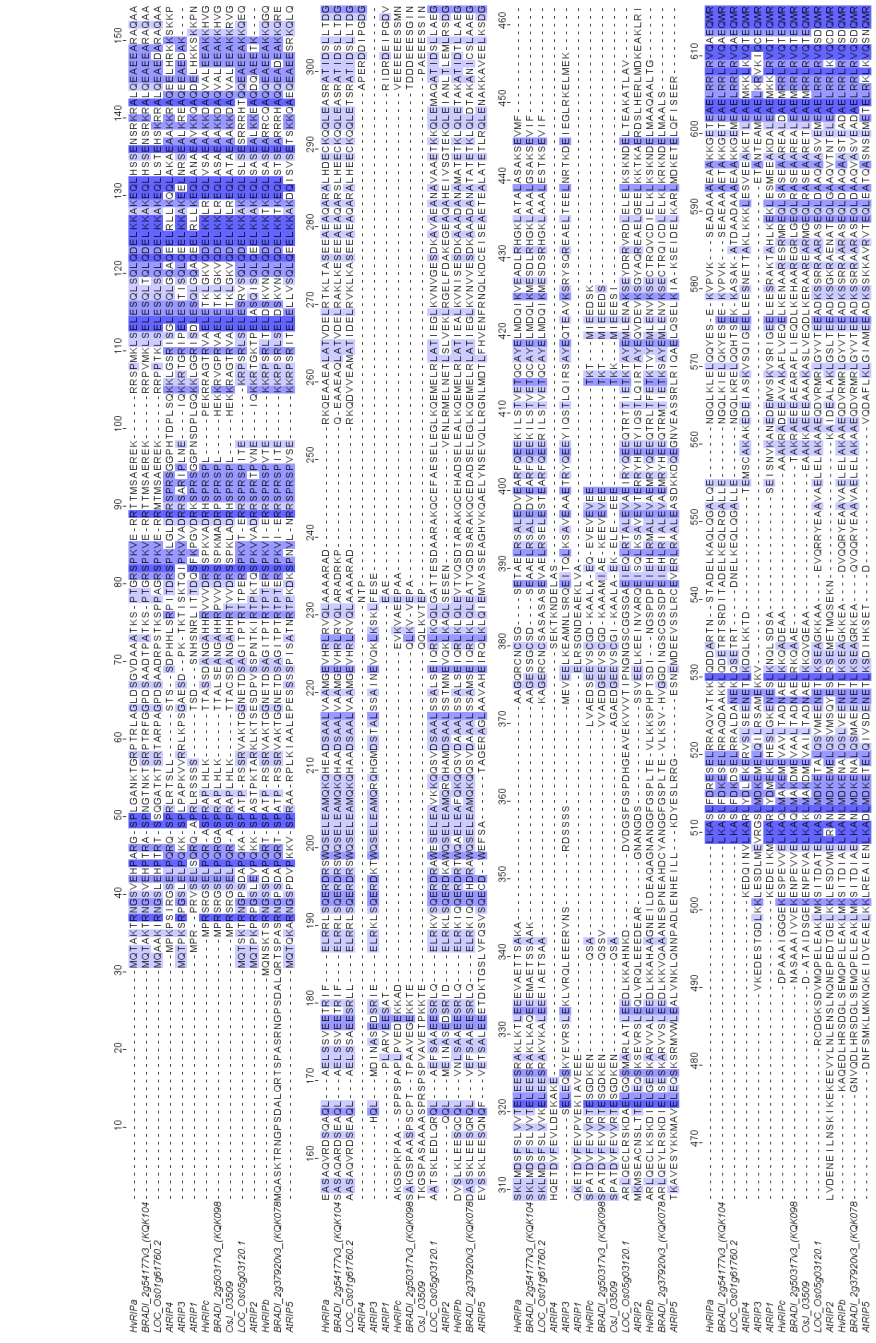

Figure S1: Alignment of barley RIPa, RIPb, RIPc with five RIP proteins of Arabidopsis (AtRIP1, AtRIP2, AtRIP3, AtRIP4, AtRIP5), three RIPs from rice (LOC_Os01g61760.2, LOC_Os05g03120.1, OsJ_03509) as well as three identified RIPs from Brachipodium (BRADI_2g54177v3, BRADI_2g50317v3, BRADI_2g37920v3).

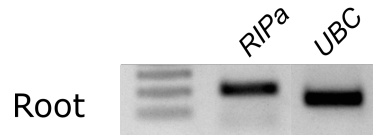

Figure S2: *RIPa* transcription in roots. Semiquantitative PCR shows transcription levels of *HvRIPa* in barley roots. As control, the constitutively expressed housekeeping gene *HvUBC* was used. Same amounts of cDNA were used for sqPCR reactions and an identical amount of PCR product was used for electrophoretic separation. Expected amplicon sizes are 209bp for *RIPa* and 156bp for *UBC*. The lowest band of the ladder corresponds to 100bp, the second lowest band corresponds to 200bp.

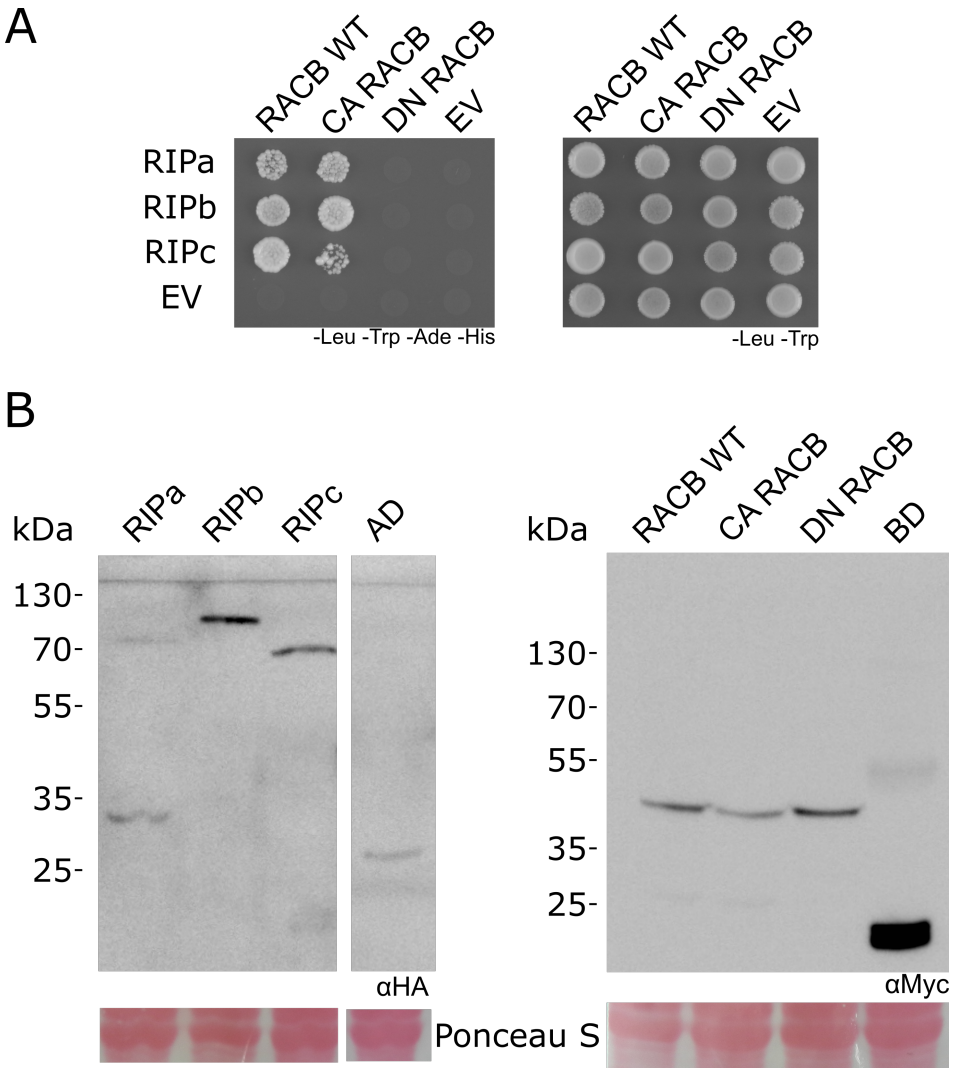

Figure S3: All RIP proteins can interact with RACB in yeast. RIPa, RIPb, and RIPc were tested in a yeast-two-hybrid assay for their interaction with wild-type (WT), constitutively activated (CA) and dominant negative (DN) HvRACB. RIP proteins were expressed from prey plasmids and RACB was expressed from the bait plasmid. As control, all constructs were tested against the respective empty vector (EV) (A). For transformation control, yeast was dropped on SD medium without leucine (-Leu) and tryptophan (-Trp). For the selection of positive interactions, SD medium was used additionally lacking adenine (-Ade) and histidine (-His). Protein expression was analyzed by western blot (B). RIP proteins had a HA fusion from expression with the pGADT7 plasmid, while RACB versions had a 4xMyc tag from expression with the pGBKT7 plasmid and were detected with the respective anti-Myc or anti-HA antibody. Next to the tested proteins, the activation domain (AD) of the GAL4 transcription factor from the pGADT7 plasmid, and the DNA binding domain of the GAL4 transcription factor from expression from the pGBKT7 plasmid, were detected. Lower images in B) show Ponceau S staining of the whole protein extraction. Expected protein molecular weights: AD-RIPa, 73kDa; AD-RIPb, 85kDa; AD-RIPc, 59kDa; AD, 20kDa; BD-RACB, all variants 42kDa; BD, 22kDa.

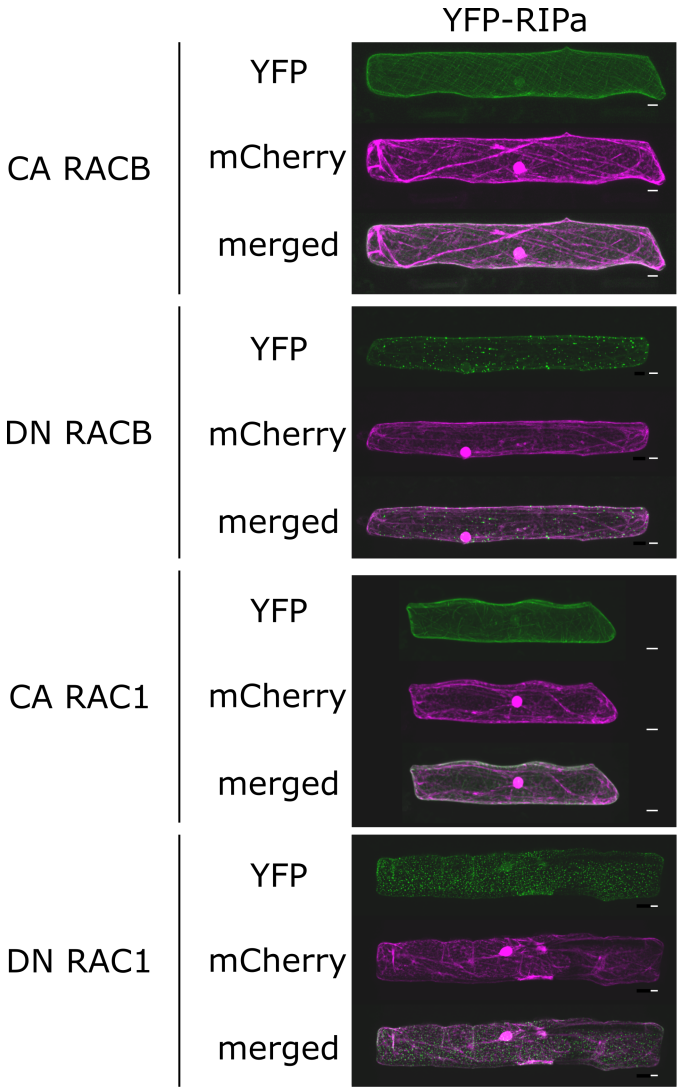

Figure S4: Intracellular recruitment of RIPa by barley ROPs. YFP-tagged RIPa fusion proteins were introduced into single epidermal cells of barley leaves by biolistic transformation and co-expressed with RACB or RAC1 in different states of activity (CA, WT, DN). mCherry was used as a transformation marker. Images were taken 24-48 hab and show z-stacks of XY optical sections of upper half of the cells. Scaling bars represent 20µm. Image brightness was increased for displaying purposes. Experiments performed by Dr. Caroline Höfle.

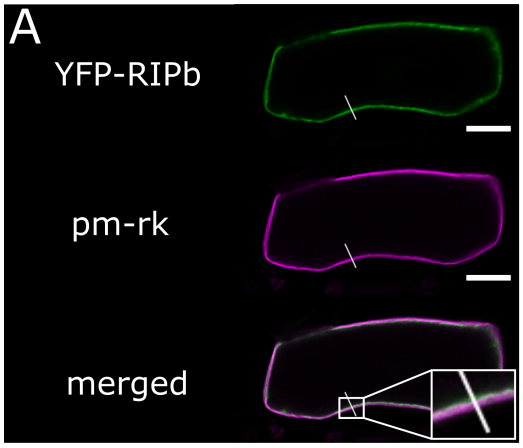
A
YFP-RIPb
pm-rk
merged

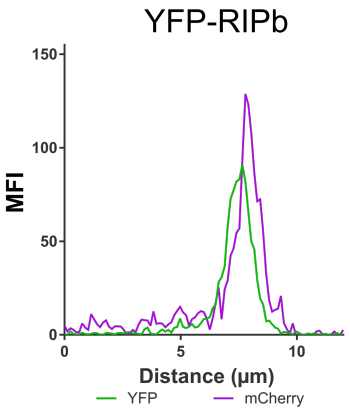
YFP-RIPb
MFI
150
100
50
0
0
5
10
Distance (µm)
YFP
mCherry

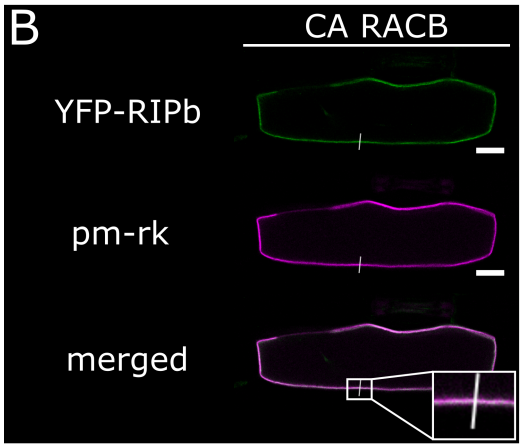
B
CA RACB
YFP-RIPb
pm-rk
merged

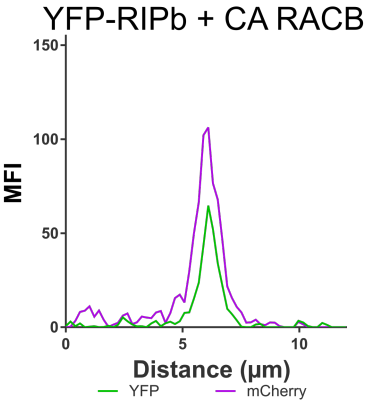
YFP-RIPb + CA RACB
MFI
150
100
50
0
0
5
10
Distance (µm)
YFP
mCherry

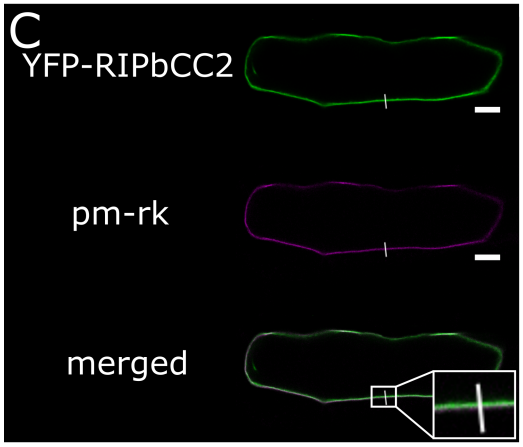
C
YFP-RIPbCC2
pm-rk
merged

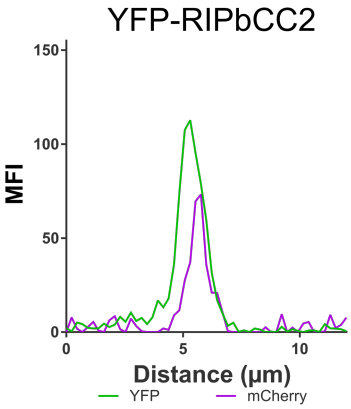
YFP-RIPbCC2
MFI
150
100
50
0
0
5
10
Distance (µm)
YFP
mCherry

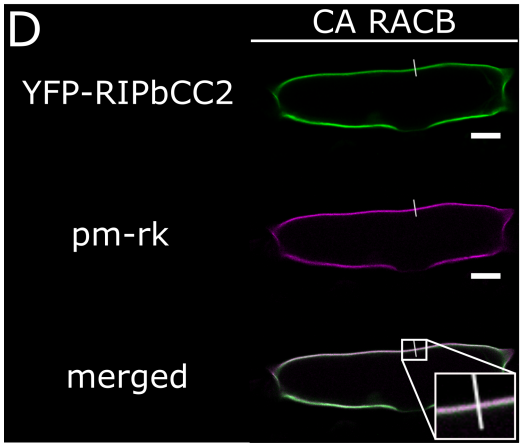
D
CA RACB
YFP-RIPbCC2
pm-rk
merged

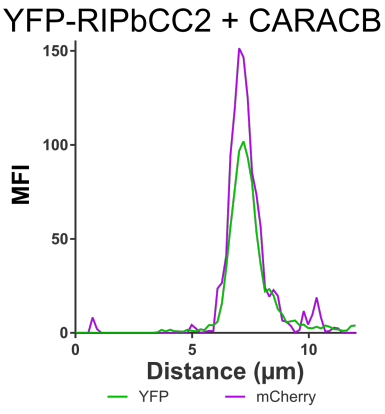
YFP-RIPbCC2 + CARACB
MFI
150
100
50
0
0
5
10
Distance (µm)
YFP
mCherry

Figure S5: RIPb gets recruited to the plasma membrane by RACB. Co-expression of YFP-RIPb and YFP-RIPbCC2 with the plasma membrane marker pm-rk. YFP-RIPb (A, B) and YFP-RIPbCC2 (C, D) were transiently expressed in barley epidermal cells together with the plasma membrane marker pm-rk. Additionally, YFP-RIPb and YFP-RIPbCC2 were co-expressed with CA RACB (B, D). Signal profile was measured over a linear ROI (white line) and displayed in the respective graph on the right hand side. Scaling bars correspond to 20µm. Images on in the bottom right corner are magnifications of the respective white square. Experiments performed by Dr. Stefan Engelhardt.

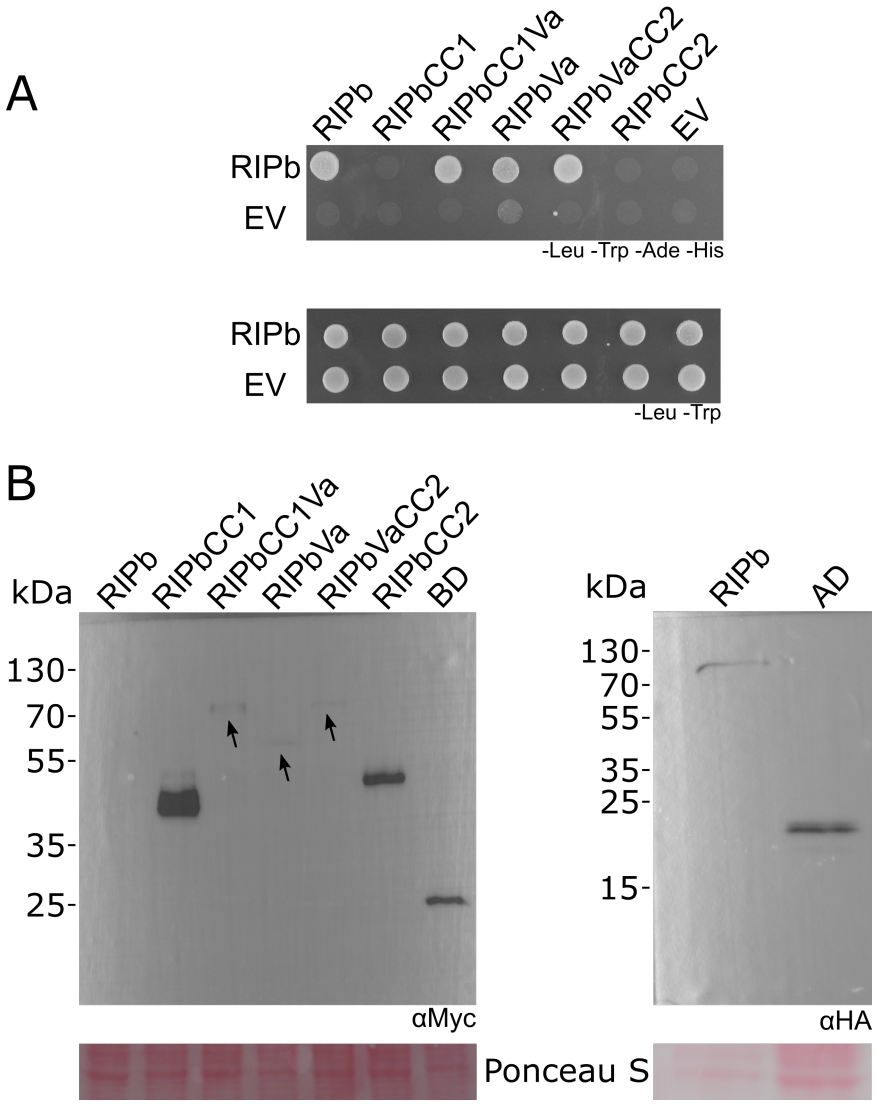

Figure S6: RIPb auto-interaction in yeast. Ripb truncations were tested in a yeast-two-hybrid assay for their interaction with full length Ripb. RIPb truncations were expressed from the bait plasmid. As control, all constructs were tested against the respective empty vector (EV) (A). For transformation control, yeast was dropped on SD medium without leucine (-Leu) and tryptophan (-Trp). For the selection of positive interactions, SD medium was used additionally lacking adenine (-Ade) and histidine (-His). Protein expression was analyzed by western blot (B). RIPb truncations and full length RIPb had a 4xMyc-tag from expression with the pGBKT7 plasmid and were hence detected with a anti-Myc antibody. Full length RIPb as the interaction partner had an HA tag from expression with the pGADT7 plasmid and detected with the anti-HA antibody. Arrows highlight the bands of interest. Next to the truncations, the activation domain (AD) of the GAL4 transcription factor from the pGADT7 plasmid and the DNA binding domain of the GAL4 transcription factor from expression of the pGBKT7 plasmid were detected. Lower images in B) show Ponceau S staining of the whole protein extraction. Expected protein molecular weights: BD-RIPb, 88kDa; BD-RIPbCC1, 35kDA; BD-RIPbCC1Va, 67kDa; BD-RIPbVa, 53kDa; BD-RIPbCC2Va, 73kDa; BD-RIPbCC2, 42kDa; BD, 22kDa; AD-RIPb, 85KDa; AD, 20kDa.

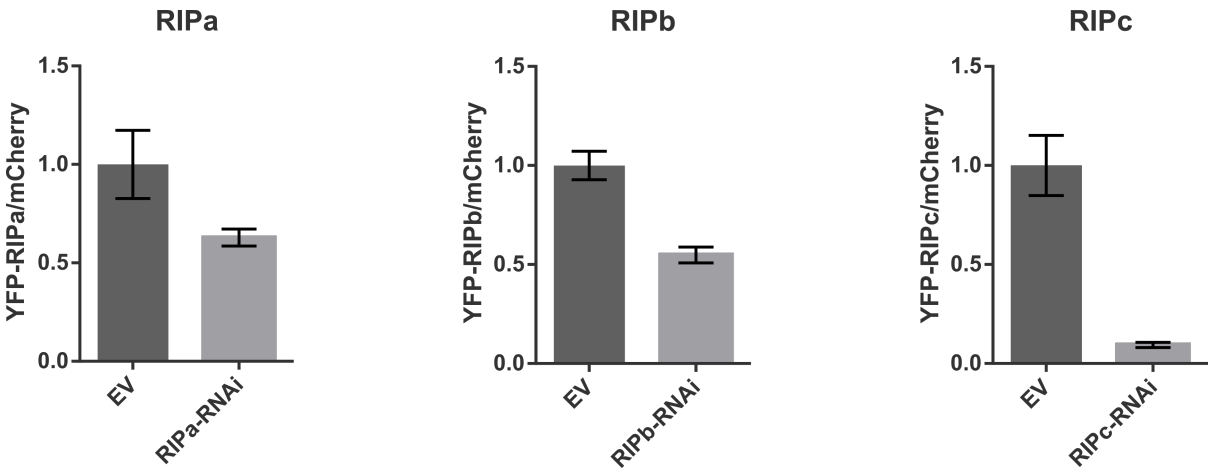

Figure S7: Silencing efficiency of RIP-RNAi constructs. RNAi constructs in the pIPKTA30N plasmid were co-expressed with YFP-tagged fusion proteins for RIPa, RIPb, and RIPc, respectively. Constructs were introduced into single epidermal cells of barley leaves by biolistic transformation. Free mCherry was also co-expressed as transformation marker and internal reference. Signal intensities were measured as MFI by CLSM. For each cell, the signal ratio between YFP and mCherry was calculated. As control, the signal ratio was calculated when the empty RNAi vector (pIPKTA30N) was co-expressed with the YFP-tagged fusion proteins and mCherry. The average signal ratio for the control was set as 1 and all ratios were calculated relative to that. For each construct in each experiment, at least 30 cells were measured.

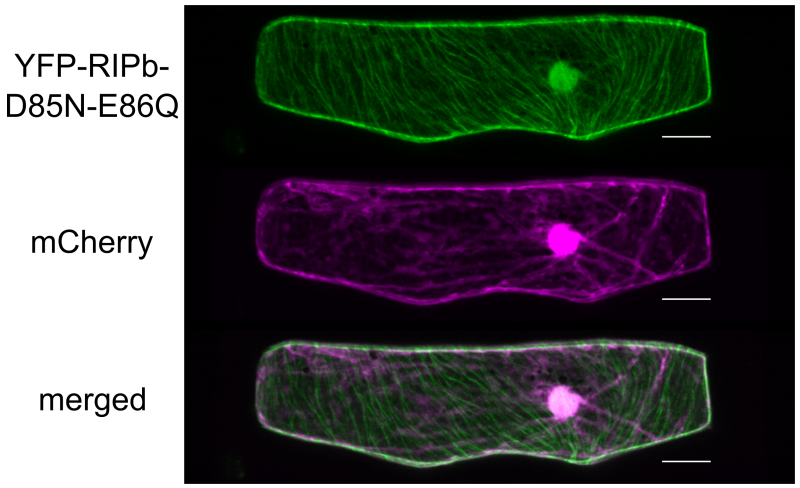

Figure S8: Mutation of the QDEL motif of RIPb. Aspartate 85 and glutamate 86 of RIPb were exchanged, by side-directed mutagenesis to asparagine and glutamine, respectively. A YFP fusion of this mutant was introduced into single epidermal cells of barley leaves by biolistic transformation and detected by CLSM 24 hab. Scaling bars represent 20µm.

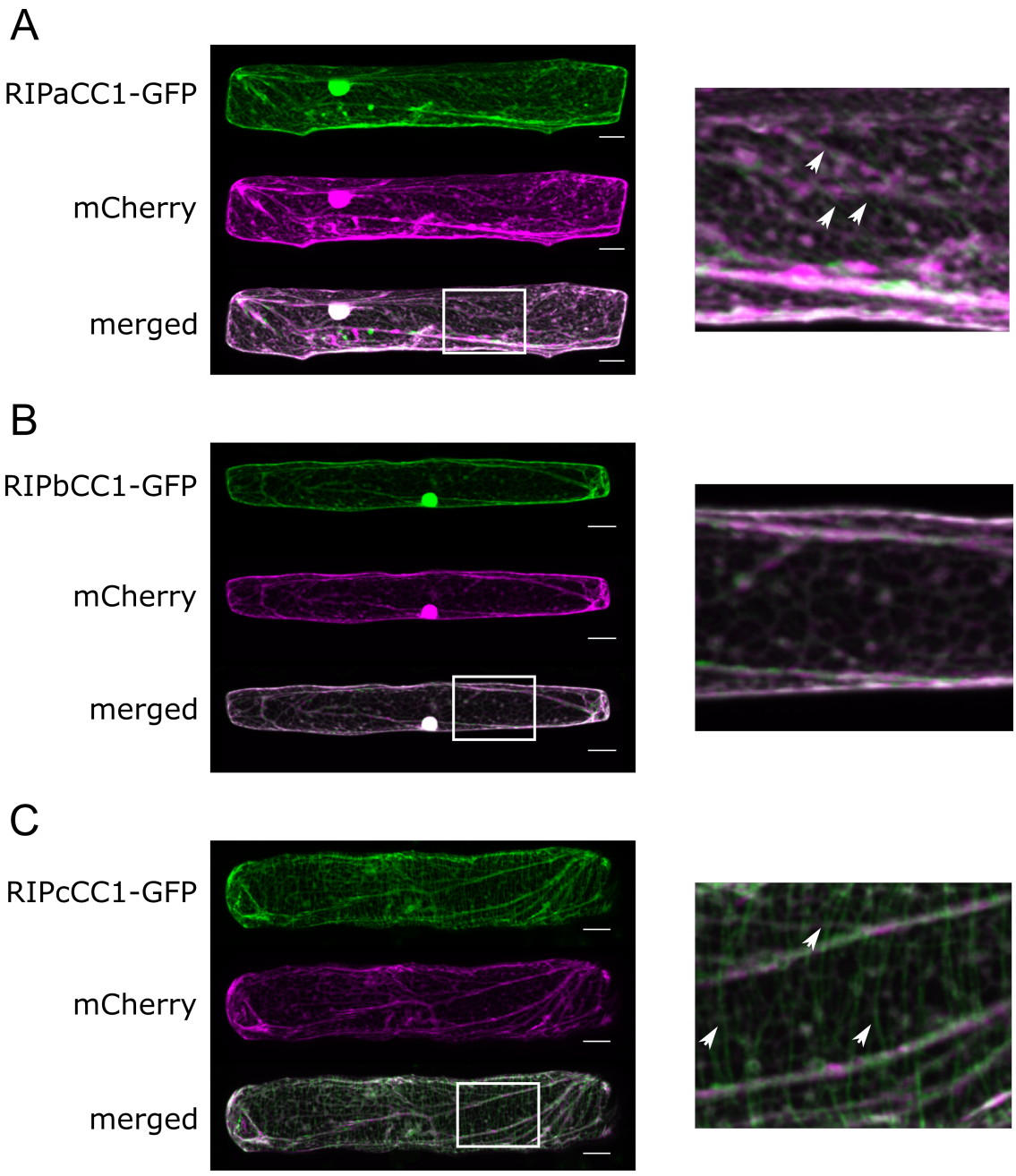

Figure S9: Localization of the CC1 domain of RIP proteins. The CC1 domain of RIPa (A, AA1-136), RIPb (B, AA1-132), and RIPc (C, AA1-109) were C-terminally fused to GFP and transiently expressed in barley epidermal cells by biolistic transformation. Cytosolic mCherry served as a transformation marker. Images show z-stacks of XY optical sections of the upper half of the cell acquired by CLSM. Images on the right hand side show magnifications of the area in the white boxes of the images on the left hand side. Arrows highlight microtubules. Scaling bars represent 20µm.

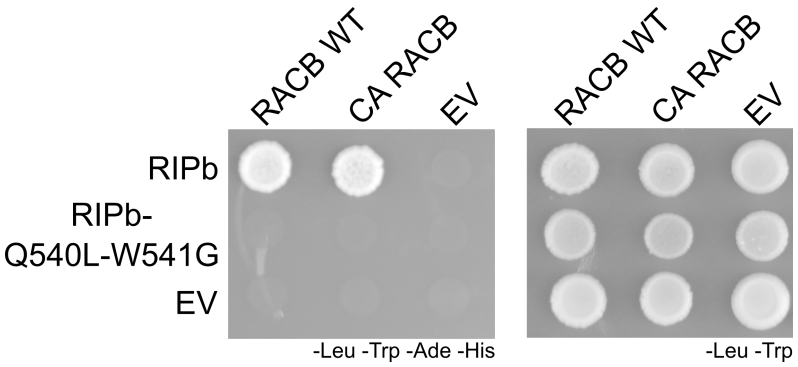

Figure S10: Mutations in the QWRKAA motif of RIPb in yeast. Amino acids glutamine 540 and tryptophan 541 of RIPb were exchanged by side-directed mutagenesis to leucine and gylcine, respectively. The mutant and wild-type RIPb were expressed in prey plasmids and tested in yeast-two-hybird against wild-type RACB and CA RACB expressed in bait plasmids. As negative control, all constructs were tested against the respective empty vector (EV). For transformation control, yeast was dropped on SD medium without leucine (-Leu) and tryptophan (-Trp). For the selection of positive interactions, SD medium was used additionally lacking adenine (-Ade) and histidine (-His).

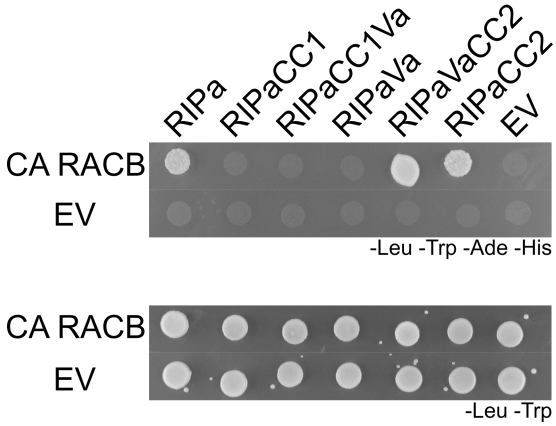

Figure S11: Yeast-two-hybrid of RIPa truncations against CA RACB. Full length RIPa and the RIPa truncations RIPaCC1 (AA1-132), RIPaCC1Va (AA1-375), RIPaVa (AA137-375), RIPaVaCC2 (AA137-510), and RIPaCC2 (AA375-510) were tested in yeast-two-hybrid against CA RACB. As negative control all constructs were tested against the respective empty vector (EV). For transformation control, yeast was dropped on SD medium without leucine (-Leu) and tryptophan (-Trp). For the selection of positive interactions, SD medium was used additionally lacking adenine (-Ade) and histidine (-His).

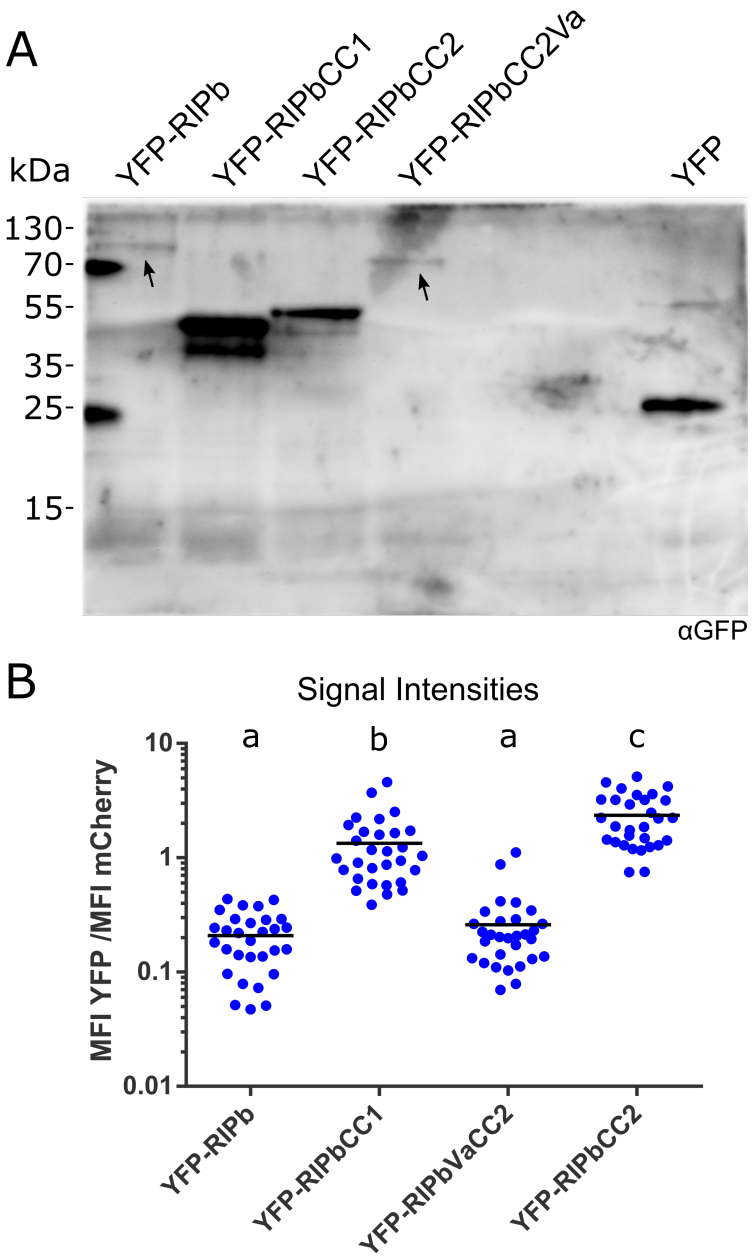

Figure S12: Expression of RIPb and RIPb truncations *in planta*. YFP-RIPb (95kDa), YFP-RIPbCC1 (42kDa), YFP-RIPbCC2 (48kDa), and YFP-RIPbCC2Va (80kDa) were expressed in protoplasts from epidermal cells of barley leaves (A). As control free YFP (26.98kDa) was also expressed. The proteins were then extracted from protoplasts and purified by immunoprecipitation with an anti-GFP-trap. Arrows highlight bands of interest. Additionally, YFP fusion proteins were transiently expressed in single barley epidermal cells together with mCherry as an internal reference in order to measure expression levels (B). Transformed cells were imaged by CLSM. MFI was measured for the upper half of the cells and calculated relative to the internal mCherry reference. For each construct at least 30 cells were measured. Letters indicated significance calculated by one-way ANOVA (Tukey's multiple comparison test). Experiments performed by Lukas Weiss.

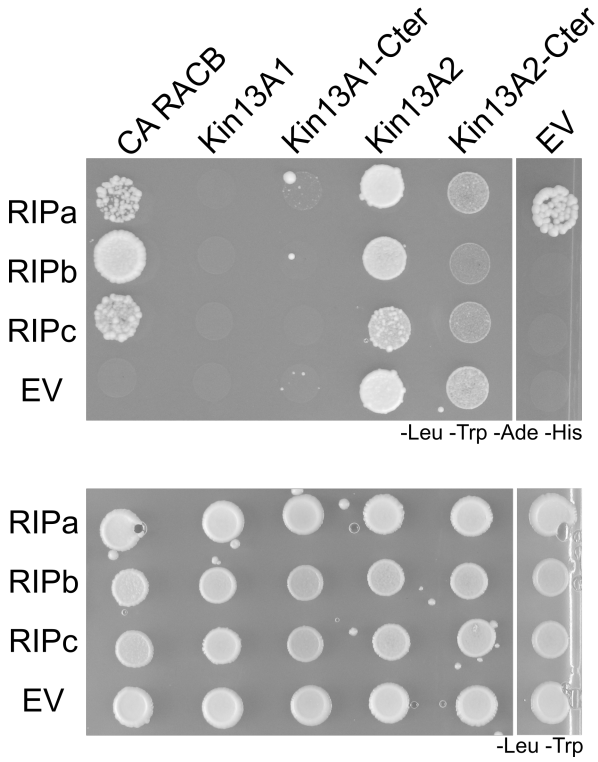

Figure S13: RIP proteins did not interact with KIN13A isoforms of barley. RIPa, RIPb, and RIPc were tested in a yeast-two-hybrid assay for their interaction with HvKin13A1 and HvKin13A2 as well as their respective C-termini. RIP proteins were expressed from the prey plasmid, while Kinesins were expressed from the bait plasmid. As positive control, all constructs were tested against CA RACB and as negative control against the respective empty vector (EV). For transformation control, yeast was dropped on SD medium without leucine (-Leu) and tryptophan (-Trp). For the selection of positive interactions, SD medium was used additionally lacking adenine (-Ade) and histidine (-His).

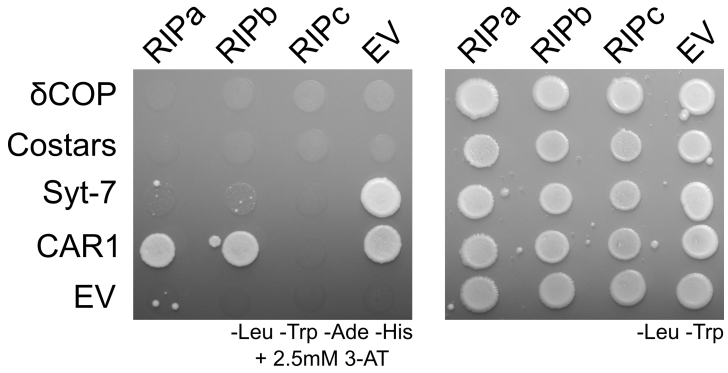

Figure S14: Targeted yeast-two-hybrid with RIPs against the potential interactors from the yeast screening. RIPa, RIPb, and RIPc were tested in yeast-two-hybrid against potential downstream interactors from the yeast screening δCOP, Costats, Syt7, and CAR1. RIPs were expressed in bait plasmids, while downstream interactors were expressed in prey plasmids. As negative control all plasmid were tested against the respective empty vector (EV). For transformation control yeast was dropped on SD medium without leucine (-Leu) and tryptophan (-Trp). For the selection of positive interactions SD medium was used additionally lacking adenine (-Ade) and histidine (-His). 2.5mM 3-AT was added to the medium for interaction selection to get rid of unspecific interactions.

Danksagung

Mein Dank gilt Prof. Dr. Ralph Hückelhoven für das entgegengebrachte Vertrauen, die generelle Unterstützung und den intellektuellen Input.

Ich danke Prof. Dr. Kay Schneitz für die Übernahme des Prüfungsvorsitzes.

Prof. Dr. Jörg Durner danke ich für die Übernahme der Rolle des Zweitprüfers.

Danke an Milena Schäffer und Lars Raasch für das Korrekturlesen der Arbeit.

Danke an Dr. Caroline Höfle für die Vorarbeit und die Einarbeitung in das Projekt.

Ich danke Dr. Stefan Engelhardt für die Betreuung und der gesamten Arbeitsgruppe für die tolle Stimmung und unterstützende Arbeitsatmosphäre. Ich bin jeden Tag gerne zur Arbeit gegangen. Desweiteren möchte ich mich bei Johanna Hofer, Carolin Hutter und Lena Forstner für die praktische Hilfe im Labor bedanken. Ebenso danke ich Katja Probst, Clara Igisch und Annemarie Siebert für die hervorragende Arbeit an Teilprojekten im Zuge von Abschlussarbeiten und Praktika. Ein besonderer Dank gilt Milena Schäffer, Lars Raasch und Alexander Kutschera für viele legendäre Abende und die schönen Zeiten auf der Hütte. Danke an alle Kollegen am Lehrstuhl für die Hilfsbereitschaft und unterhaltsamen Mittagspausen.

Ich danke Dr. Stefan Engelhardt und Lukas Weiss für die Durchführung verschiedener Experimente nach meiner Zeit am Lehrstuhl.

Ich möchte mich außerdem von ganzem Herzen bei all meinen Freunden und meiner Familie für die Unterstützung über die Jahre bedanken. Es war eine lange und anstrengende Reise vom Elektroinstallateur zum Doktortitel und ich hätte es ohne euch nicht geschafft.